CONSTRUCTION OF A NUMERICAL PLATFORM FOR ENZYMATIC SACCHARIFICATION AND MULTI-SUGARS FERMENTATION FOR SIMULATION OF WHOLE SLURRY BIOREFINERY

CHAN KA LAI

PhD

The Hong Kong Polytechnic University

2022

The Hong Kong Polytechnic University

Department of Civil and Environmental Engineering

Construction of A Numerical Platform for Enzymatic Saccharification and Multi-Sugars Fermentation for Simulation of Whole Slurry Biorefinery

Chan Ka Lai

A thesis submitted in partial fulfilment of the requirements for the degree of Doctor of Philosophy

May 2021

CERTIFICATE OF ORIGINALITY

I hereby declare that this thesis is my own work and that, to the best of my knowledge and belief, it reproduces no material previously published or written, nor material that has been accepted for the award of any other degree or diploma, except where due acknowledgement has been made in the text.

_____(Signed)

CHAN KA LAI (Name of student)

Abstract

This dissertation constructed a numerical platform to incorporate the dynamic interaction among enzyme adsorption, cellulose hydrolysis, cell growth and utilization in bioconversion processes of lignocellulosic biomass in biorefinery. Enzymatic hydrolysis is a heterogeneous reaction involving the dynamic interaction between enzyme complex and solid substrates. The dynamic enzyme adsorption was modeled based on the Langmuir isotherm and first order kinetic reaction of to simulate the equilibrium enzyme concentration during the hydrolysis process. A first order model with fractal kinetic and product inhibition was applied to describe cellulose hydrolysis for various pretreated substrates. Cell growth of microorganism was defined by Monod kinetic with both substrates and product inhibition terms. Utilization rate of both single and mixed sugars in batch and continues fermentation was described by the cell growth and product formation.

To quantify the impacts of lignin properties to enzymatic hydrolysis, various types of lignin were isolated from the pretreated substrates of the single/two-staged organosolv pretreatments using 1,4-butanediol and dilute sulfuric acid. The impacts of condensed lignin and high phenolic hydroxyl group generated after acid-first process; the

beneficial structures of organosolv associated functional groups to effective adsorption of cellulase to cellulose, were simulated. Suspended pretreated by-products or functional additives are common impurities in the hydrolysate, causing different effects to hydrolysis that need to be quantified by mathematical model. Bovine Serum Albumin (BSA) and lysozyme were applied as model additives to enzyme adsorption and cellulose hydrolysis. Addition of BSA and lysozyme improved the hydrolysis performance by reducing the non-productive adsorption of enzyme onto the surface of lignin and other impurities. The kinetic model revealed that the hydrolysis rate coefficient increased but the fractal exponent decreased with the addition of BSA and lysozyme. Addition of lysozyme exhibited a better hydrolysis performance, which confirmed by the larger hydrolysis rate coefficient and the smaller fractal exponent.

The feasibility of co-fermentation process featuring with a cell recycling unit (CF/CR) was studied for mixed sugar utilization to produce lactic acid. The fermentation model was applied clarify the cell metabolism through kinetic analysis under the carbon catabolite repression (CCR) in co-fermentation. The model successfully simulated the transition of sugar consumption, cell growth, and lactic acid production among the batch, continuous process, and the continuous process with cell recycling. Cell retention time played a critical role in the pentose and hexose consumption, cell decay,

and lactic acid production in the whole process, which was characterized by stead-state expression of the model parameters.

Publication arising from the thesis

Published journal articles/book chapter

1. **Chan, K.-L.**, Ko, C.-H., Chang, K.-L., Leu, S.-Y. (2021) Construction of a Structural Enzyme Adsorption/Kinetics Model to Elucidate Additives Associated Lignin-Cellulase Interactions in Complex Bio-conversion System. Biotechnology and Bioengineering, 118, 4065-4075.
2. Wang, Y., **Chan, K.-L. (co-first author)**, Abdel-Rahman, M. A., Sonomoto, K., and Leu, S.-Y.* (2020). Dynamic Simulation of Continuous Mixed Sugars Fermentation with Increasing Cell Retention Time for Lactic Acid Production using *Enterococcus mundtii* QU 25. *Biotechnology for Biofeuls*, 13(1), 1-16.
3. **Chan, K.-L.**, Dong, C., Wong, M.S., Kim, L.-H., Leu, S.-Y. (2018) Plant Chemistry Associated Dynamic Modelling to Enhance Urban Vegetation Carbon Sequestration Potential via Bioenergy Harvesting, *Journal of Cleaner Production*, 197, 1084-1094.
4. Tang, X.J., **Chan, K.-L.**, Farzana, S., Wai, W.H.O., and Leu, S.-Y. (2021) Strategic Planting for Watershed Restoration in Coastal Urban Environment – Toward Carbon Sequestration by Stormwater Improvement, *Journal of Cleaner Production*, 295, 126116.
5. Dong, C., Wang, Y., **Chan, K.-L.**, Bhatia, A., Leu, S.-Y.* (2018) Temperature Profiling to Maximize Energy Yield with Reduced Water Input in a Lignocellulosic Ethanol Biorefinery, *Applied Energy*, 214, 63-72.

Conference Paper/Presentation

6. **Chan, K.-L.** and Leu, S.-Y. (2019) Incorporating Pretreatments in Reducing the Recalcitrant of Wastes derived Organic Resources Conversion Processes, International Conference on Cleaner Production and Sustainability, Hong Kong, 30 Oct.– 2 Nov.
7. **Chan, K.-L.**, Wong M. S., Lan P., Wu Z., Kim L., and Leu S.-Y. (2017) Optimizing bioenergy harvesting activities towards best carbon sequestration managements of urban rain garden. Oral presentation at 12th SDEWES Conference, Dubrovnik, Croatia, 4-8, Oct.
8. **Chan, K.-L.**, Pan, L., Leu, S.-Y. (2017) A New Structure Model to Optimize the Whole Slurry Simultaneous Saccharification and Fermentation Processes to Convert Softwood into Biofuel, the 4th GIG-PolyU Workshop on Environ. Engineering and Sci., Guangzhou Institute of Geochemistry, Chinese Academy of Sciences, Guanzhou, China, 2 June.
9. **Chan, K.-L.**, Pan, L., Leu, S.-Y. (2016) New Plant Growth Model to Simulate Carbon Sequestration Potential of Urban Vegetation Systems, 2016 Annual Conference of Korean Wetland Society, Seoul, South Korea, 26 Aug.

Manuscript to be submitted upon this dissertation

10. **Chan, K.-L.**, Islam, K.M., Leu, S.-Y. (*in preparation*) Solvent Induced Lignin-Cellulase Interaction on Enzymatic Kinetics for Organosolv Pretreated Lignocellulosic Substrate.

Acknowledgments

I would like to express my deepest and sincere gratitude to my supervisor, Dr. Leu Shao-Yuan, for his patience, motivation, encouragement, guidance, advice and continuous support throughout entire period of doctoral study. This dissertation would have never been accomplished without his assistance and involvement throughout the study. My sincere thank also goes to the lab technicians, especially Mr. Lam Wai-Shung, for their technical support and help in the lab experiments. I was grateful for my teammates from Dr. Leu Shao-Yuan's group, for their valuable comments and helps.

Table of contents

Abstract I
Publication arising from the thesis IV
Acknowledgments VI
Table of contents VII
List of figures X
List of tables XIII
Nomenclature and Abbreviation XIV
Chapter 1 Introduction 1
1.1 Background 1
1.2 Aim and objectives 3
1.3 Outline 4
Chapter 2 Literature review 8
2.1 Characteristics of lignocellulosic biomass 8
2.2 Lignocellulosic biomass in Hong Kong 11
2.2.1 Physical properties 13
2.2.2 Chemical composition analysis 14
2.2.3 Carbon credit of energy harvesting 15
2.2.4 Morphological characterization 17
2.2.5 Properties of selected plant species 18
2.3 Lignocellulosic conversion process 22
2.3.1 Pretreatment 23
2.3.2 Hydrolysis 26
2.3.3 Fermentation 29
2.3.4 Distillation 30
2.4 Inhibitory compounds 31
2.5 Modes of operation 35
2.5.1 SSF 35
2.5.2 Batch and fed-batch 37
Chapter 3 Model development 39

3.1 System boundary 41
3.2 Selection of model principles 45
3.3 Model structure of hydrolysis 47
3.4 Fermentation model 51
3.5 Validation of parameters 59
Chapter 4 Solvent Induced Lignin-Cellulase Interaction on Enzymatic Kinetics for Organosolv Pretreated Lignocellulosic Substrate Interaction on Enzymatic Kinetics for Organosolv Pretreated Lignocellulosic Substrate 61
4.1 Background 61
4.2 Experiments 63
4.2.1 Materials 63
4.3 Pretreatment 63
4.3.1 Lignin preparation 65
4.3.2 Enzyme adsorption 65
4.3.3 Enzymatic hydrolysis 66
4.3.4 Analytical analysis 66
4.4 Result and discussion 67
4.4.1 Characteristic of pretreated substrate 67
4.4.2 Adsorption isotherm of substrates and lignins 68
4.4.3 Impact of lignin on adsorption and hydrolysis 72
4.4.4 Kinetic simulation of pretreated substrates 78
4.5 Conclusion 79
Chapter 5 Construction of a Structural Model to Elucidate Additive Associated Lignin-Cellulase Interactions in Complex Bioconversion System 81
5.1 Background 81
5.2 Experiments 84
5.2.1 Materials/pretreatment of lignocellulosic materials 85
5.2.2 Adsorption of cellulase 87
5.2.3 Enzymatic hydrolysis of lignocellulose biomass 88
5.2.4 Adsorption and hydrolysis with additives 88
5.3 Results and discussion 89
5.3.1 Lignin induced influence on adsorption isotherm 89

5.3.2 Enzyme loadings and hydrolysis 93
5.3.3 Impact of additives on adsorption and hydrolysis 99
5.3.4 Adsorption capacity and hydrolysis 102
5.3.5 Sensitivity and validation of kinetic coefficients 103
5.4 Conclusion 107
Chapter 6 Dynamic Simulation of Continuous Mixed Sugar Fermentation with Increasing Cell Retention Time 109
6.1 Background 109
6.2 Methods 114
6.2.1 Microorganism and medium 114
6.2.2 Hollow fibre microfiltration module 115
6.2.3 Set-up of experiments 116
6.2.4 Batch and continuous fermentation 117
6.2.5 Continuous co-fermentation with cell recycling (CF/CR) 118
6.2.6 Analytical methods 119
6.2.7 Parameter determination and model validation 120
6.3 Results and Discussion 121
6.3.1 Batch fermentation 121
6.3.2 Continuous co-fermentation 128
6.3.3 Effects of dilution rates on continuous co-fermentation 131
6.3.4 Continuous fermentation with cell recycling (CF/CR) 137
6.3.5 Importance of cell retention time (CRT) 144
6.4 Conclusion 147
Chapter 7 Conclusion 149
References 151

List of figures

Figure 2.1 Schematic illustration of the structure and major polymers of plant cell wall (Zhao et al., 2019) 9
Figure 2.2 Geographical distribution of the collected samples in The Hong Kong Polytechnic University 12
Figure 2.3 Morphological characterization of *Tradescantia pallida, Camellia japonica, Ginkgo biloba* Linn. 18
Figure 2.4 Schematic procsesses of lignocellulosic ethanol production 23
Figure 2.5 Schematic illustration of enzyme and lignocellulosic biomass interaction during enzymatic hydrolysis (Liu et al., 2016). 28
Figure 2.6 Formation pathways of by-products of lignocellulosic biomass during pretreatment (Palmqvist & Hahn-Hägerdal, 2000) 33
Figure 2.7 Conversion pathways of furfural and HMF in yeast fermentation (Liu, 2011) 34
Figure 3.1 Schematic diagram of the dynamic model with concerned parameters for simulation of enzymatic hydrolysis of three scenarios: (a) pure cellulosic substrate; (b) lignocellulosic substrate; and (c) lignocellulose with additives. 42
Figure 3.2 Tested and simulated systems with key model parameters; (a) batch reactor; (b) continuous flow; and (c) continuous flow with cell recycling (dilution ratio (*D*) is the inverse of cell retention time). Controlled parameters described the experimental design; growth kinetics is given after references or model validation; outputs are simulated data. 52
Figure 3.3 CF/CR system 56
Figure 4.1 Enzyme adsorption kinetics at 4°C with 2% (w/v) solid content and enzyme loading of 5-50 mg/g substrate for pretreated substrate DA_{20}, BDO_{60} and $DA_{20}BDO_{40}$ and $BDO_{40}DA_{20}$. Solid lines fit with Langmuir adsorption isotherm. 70
Figure 4.2 Effect of additional lignin of the pretreated substrates on the cellulose hydrolysis rate of the MCC with a 2% (w/v) solid loading and 15 mg/g substrate enzyme loading. 73
Figure 4.3 Enzymatic hydrolysis of MCC with 10 to 50% of additional lignin prepared from pretreated substrates with a 2% solid loading and 15 mg/g substrate enzyme loading incubated at 50°C. 74
Figure 4.4 2D HSQC NMR spectra of residual lignin isolated of raw biomass of *Acacia confuse*. 75
Figure 4.5 2D HSQC NMR spectra of residual lignin isolated after dilute acid

pretreatment 76
Figure 4.6 2D HSQC NMR spectra of residual lignin isolated after BDO_{60} pretreatment. 77
Figure 4.7 Model simulation and experimental results (symbols) of a) dynamic enzyme adsorption and b) glucose release at 50˚C with 2% (w/v) solid loading and 15 mg/g substrate enzyme loading for the pretreated substrate of DA_{20}, BDO_{60}, $DA_{20}BDO_{40}$, and $BDO_{40}DA_{20}$. 79
Figure 5.1 Workflow for kinetic modeling of enzymatic hydrolysis. 85
Figure 5.2 Enzyme adsorption isotherm at 4˚C with 1% (w/v) solid content. Enzyme loadings 5-60 mg/g-substrate for (a) BEK; (b) UEK; and (c) SEP with no additives (control); with BSA; and with lysozyme. Dashed lines fit with Langmuir isotherms. 91
Figure 5.3 Relationships of maximun adsorption capacity (δ_{Max}) and Langmuir equilibrium constant (k_d) for three substrates at different hydrolysis conditions. Lignin and additives both play critical roles in enzymatic adsorption. 92
Figure 5.4 Simulation (dash lines) and experiment results (symbols) of dynamic enzyme adsorption and glucose release at 40˚C with 1% (w/v) solid content for (a) & (d) BEK, (b) & (e)UEK and (c) & (f) SEP with enzyme loadings of 0.5 mg/g, 5 mg/g, and 50 mg/g. 97
Figure 5.5 Simulation (dash lines) and experiment results (symbols) of dynamic enzyme adsorption and glucose release at 40˚C with 1% (w/v) solid content for (a) & (d) BEK, (b) & (e)UEK and (c) & (f) SEP with/without the addition of BSA/lysozyme at the enzyme loading of 5mg/g. 98
Figure 5.6 Sensitivity analysis of the kinetic parameters for the simulation model: (a-e) BEK; (f-i) UEK; (j-o) SEP with the enzyme loadings of 0.5 mg/g (a, f, & j), 5 mg/g (b, g, & k), and 50 mg/g (c, h, & m); and with the addition of BSA (d, I, & n) and lysozyme (e, j, & o) at the enzyme loading of 5mg/g. 105
Figure 5.7 Relationship between substrate lignin contents and (a) fractal exponent and (b) hydrolysis rate coefficients. 107
Figure 6.1 Conceptual diagram and model structure of the continuous lactic acid co-fermentation process with membrane separation and selected enzyme combination for preventing carbon catabolite repression; (a) hydrolysis system; (b) fermentation; (c) membrane separation; and (d) pathway to be cut-off to prevent carbon catabolite repression (CCR). 112
Figure 6.2 Simulation results (curves) and measurement data (symbols) for lactic acid fermentation by *E. mundtii* QU 25 with different carbon sources, *i.e.*, glucose (left), cellobiose (middle) and xylose (right). The data presented from top to

bottom are residual sugars, lactic acid (*LA*), and dry cell weight (*X*). The data points represent the mean values of three independent experiments. 124
Figure 6.3 Experiment and simulation results of co-fermentation using various sugar combinations in a batch reactor; carbon catabolite repression was not observed when cellobiose with xylose was mixed. The data points represent the mean values of three independent experiments. 126
Figure 6.4 Continuous fermentation to produce lactic acid using *E. mundtii* QU 25 with combined cellobiose and xylose. The designed feeding sugar combinations were: cellobiose 100 g/L and xylose 60 g/L (C100X60, left); and cellobiose 50 g/L and xylose 30 g/L (C50X30, right). Both reactors started with batch mode and then transferred to continuous mode after achieving state-state. The color coded curves show the simulation results and the symbols indicate the experimental results. At least three analyses were carried out before the transition of different operational conditions in the process. 134
Figure 6.5 Continuous fermentation with cell recycling to produce lactic acid using *E. mundtii* QU 25 with a combination of cellobiose and xylose. The designed feeding sugar combination was cellobiose 50 g/L and xylose 30 g/L. The reactor started with batch mode and then transferred to continuous mode after achieving steady-state. The cells were concentrated before transfer. The color coded curves show the simulation results and the points show the averages of three measurements. 139
Figure 6.6 Performances of co-fermentation over different cell retention times (in hours) and two attempted numerical fits: (a) linear regressions; and (b) steady state expression based on the proposed simulation model. 145

List of tables

Table 2.1 Measured physical trails and chemical compositions of the selected rain garden species. 21
Table 3.1 Summary of reported and proposed adsorption models 43
Table 3.2 Summary of hydrolysis models associated with the adsorption kinetics 44
Table 4.1 Pretreatment operation conditions for the lignocellulosic biomass 64
Table 4.2 Chemical composition of the pretreated biomass 67
Table 4.3 Enzyme adsorption parameters of adsorption isotherm at 4˚C 68
Table 4.4 Kinetic parameters of enzymatic hydrolysis of the pretreated substrates 79
Table 5.1 Chemical compositions of pretreated substrates (wt.%) 89
Table 5.2 Enzyme adsorption parameters of adsorption isotherm at 4˚C and 40˚C 89
Table 5.3 Kinetic parameters of fractal hydrolysis model with various enzyme loadings 94
Table 5.4 Kinetic parameters of fractal hydrolysis model with BSA and lysozyme 95
Table 6.1 Kinetic parameters from different batch studies and this work (*E. mundtii* QU 25) 123
Table 6.2 Validation of mathematical models for sugar consumption, product formation and cell growth. 130
Table 6.3 Continuous L-lactic acid production by *E. mundtii* QU 25 using different sugar mixtures in feeding media (G100X60 or C100X60) at dilution rate of 0.2 1/h 130
Table 6.4 Effect of dilution rates on lactic acid production in CSFTR 132
Table 6.5 Comparison of lactic acid production by different continuous fermentation systems. 140

Nomenclature and Abbreviation

C50X30	50 g/L cellobiose and 30 g/L xylose
CFSTR	continuous flow stirring tank reactor
CF/CR	co-fermentation process featured with cell recycle unit
CRT	cell retention time
D	dilution rate or the inverse of hydraulic retention time (1/h)
E_B	enzyme adsorption, mg/g
E_B^C	enzyme adsorption on cellulose, mg/g
E_B^L	enzyme adsorption on lignin, mg/g
E_B^S	enzyme adsorption on solid, mg/g
E_{eq}	equilibrium enzyme adsorption, mg/g
E_F	free enzyme concentration in the solution, mg/L
E_T	total enzyme concentration, mg/g
G100X50	100 g/L glucose and 50 g/L xylose
h	fractal exponent
HRT	hydraulic retention time (h)
k_{ad}	adsorption rate constant, 1/h
k_d	Langmuir equilibrium constant, mg/L
k_h	time-dependent hydrolysis rate coefficient, g/g-h
k	hydrolysis rate constant, g/g-h
K_{iG}	glucose inhibition coefficient, g/L
K_D	first order decay coefficient (1/h)
K_I^{sug}	inhibition coefficient of sugar, g/L
K_I^{LA}	inhibition coefficient of lactic acid, g/L
K_S	half saturation concentrations, g/
r_C	rate of cellulose hydrolysis, g/L-h
S_i	dissolved substrate i, g/L
S_{glu}	glucose concentration, g/L
X	cell concentration, g/L
X_C	cellulose concentration, g/L
X_H	hemicellulose concentration, g/L
X_L	lignin concentration, g/L
X_S	solid concentration, g/L
X/G	the ratio of consumed xylose to consumed glucose (by mass)
X/C	the ratio of consumed xylose to consumed cellobiose (by mass)
Y_i	molar yield of cell production to the respective consumed substrate i
Y_i^j	Mass yields of product j per unit mass subject i consumed (wt.%)

$_{cel}$	cellobiose
$_{glu}$	glucose
$_{la}$	lactic acid
$_{xyl}$	xylose
$_{C}$	cellulose
$_{H}$	hemicellulose
$_{L}$	lignin
$_{S}$	solid
μ_{max}	Maximum specific growth rate of cell (1/h)
σ_{Max}	maximum adsorption capacity, mg/g substrate

Chapter 1 Introduction

1.1 Background

With the increasing population and industrial development, energy demand increases, but conventional non-renewable fossil fuels are finite resources and might be depleted soon. Lignocellulosic biomass is one of the renewable and reliable resource that could be converted into biofuel and used as an alternative of fossil fuel for promoting sustainable development and protecting the environment (Robak & Balcerek, 2018). Compared to conventional fossil-fuel system, the lignocellulosic-based biorefinery process could reduce greenhouse gas emission and energy input (Bilal & Iqbal, 2020). Lignocellulosic biomass is a reliable natural resource and has a great supply potential for a long term and high titer biofuel production while avoiding the competition for crops between biorefinery and food supply. However, this type of feedstock is treated as waste and more than 380 tonnes of woody biomass is disposed to the landfill every day in Hong Kong (HKEPD, 2020), which includes gardening residuals, timber, bamboo, and wooden pallet from the commercial and construction industries. Development of urban biorefinery using woody waste as feedstock is a possible solution for waste management and production of biofuel and value-added chemicals with proper treatments.

Lignocellulosic biomass is mainly composed of cellulose, hemicelluloses and lignin, interlinked in a matrix structure (Shahzadi et al., 2014). Various physical and/or chemical pretreatment methods have been developed to overcome the recalcitrance of lignocellulosic biomass and make cellulose and reducing sugars accessible to the enzyme and microorganisms (Kim & Holtzapple, 2006; Mosier et al., 2005; Shafiei, Kumar, & Karimi, 2015). Simultaneous saccharification and fermentation (SSF) is a commonly adapted process for converting woody biomass into bioethanol by using cellulase and *Saccharomyces cerevisiae* (Olofsson et al., 2008; Wang et al., 2014c; Wingren et al., 2003). However, degradation products generated during pretreatment and SSF processes are inhibitory to sugar release and/or product formation.(Wang et al., 2014c)

During the SSF process, the actual sugar release is difficult to measure due to the simultaneous uptake of fermentable sugars by the fermenting microorganisms. Therefore, a validated kinetic model of SSF is necessary to optimize the feeding profile of fed-batch and continuous modes of SSF operation and thus to increase the product yield and productivity. Various kinetic models have been proposed for enzymatic hydrolysis and fermentation of cellulose (Mutturi & Lidén, 2014; Philippidis & Hatzis, 1997; Wang et al., 2014c; Zhang et al., 2009). Most of the above established models for SSF consider the effects of substrate and products inhibitions on cellulose hydrolysis and cell growth, but only a few consider

the influences of inhibitory compounds formed in pretreatment and non-soluble lignin. It might be due to the substrate used for SSF process. The pretreated softwood contains a high level of non-soluble lignin that might interfere with the enzyme activity and fermentation.

1.2 Aim and objectives

This study aims at establishing a kinetic model of SSF of whole slurry pretreated lignocellulosic biomass that simulates dynamics and interactions of enzymatic hydrolysis of cellulose, cell growth, fermentable sugar consumptions, product formation, and inhibitor metabolisms. To realize this aim, three objectives are established as follows:

1) To review the published kinetic models of enzyme adsorption, cellulose hydrolysis and the key kinetic parameters of dynamic statues of enzyme adsorption, cellulose hydrolysis, sugar utilization by microorganisms, cell growth and product formation in a whole slurry SSF processes;
2) To investigate the effects of lignin and surfactants to improve the hydrolysis performance of different pretreated substrates and simulate the dynamic interaction of enzyme adsorption and cellulose hydrolysis through the proposed model structure;

3) To investigate the feasibility of co-fermentation with mixed-sugar and optimize the biological process of fed-batch and continuous fermentation system through kinetic analysis.

1.3 Outline

Chapter 1 provides the background information of overall bioconversion process of lignocellulosic biomass and identify0020the aim and objective of this study.

Chapter 2 begins with the overall properties of the lignocellulosic biomass and the general processes of bioethanol production. The modes of process operation and mathematical models of the related processes are reviewed to provide a clear understanding of the previous studies in this area. Biomass recalcitrant is a key factor directly impact the capacity of the substrate in the biorefinery processes, of which the compositions of building block chemicals (i.e., lignin, hemicelluloses, and cellulose) plays a significant role in the numerical platform. Meanwhile, pretreatment and the related byproducts, *i.e.*, both solid and liquid, can also affect the reaction kinetics. This chapter provided an overview of enzymatic hydrolysis and the substrate-related mechanisms used in the perspective model. Experimental results of chemical composition analysis for 27 different plant species and

wastes were provided to elucidate the structure.

Chapter 3 aims to construct a comprehensive numerical platform with appropriate simplicity for enzymatic hydrolysis and fermentation simulation. Seven model structures were developed based on literature and/or basic theories while validated with experimental results. A kinetic model and parameters were determined with dynamic enzyme adsorption, cellulose hydrolysis with product inhibition. The Langmuir adsorption and a first order kinetic reaction were used to model dynamic enzyme adsorption to simulate the equilibrium enzyme concentration during the hydrolysis process. The single/mixed sugar utilization by the fermenting microorganism was described by the cell growth and product formation. Monod kinetic with substrate and production inhibition was used to defined cell growth.

Chapter 4 aims to quantify the impacts of lignin properties to enzymatic hydrolysis, staged organosolv pretreatments using 1,4-butanediol and dilute sulfuric acid were applied to fractionate the woody biomass with different orders of solvent and acid treatment. Various types of lignin were isolated from the pretreatment substrates. The adsorption isotherm of pretreated substrates and isolated lignin were simulated and the impacts of lignin on pretreated cellulose hydrolysis performance was quantify. The

acid/acid-first pretreatment accounted for a serious condensation of substrate lignin and inhibit the cellulase accessibility. Adsorption isotherm was integrated into cellulose hydrolysis model to simulate the hydrolysis process, which defined the desirable pretreatment methods for cellulose digestion.

Chapter 5 investigate the addition of Bovine Serum Albumin (BSA) and lysozyme to improve hydrolysis efficiency. Non-productive adsorption of enzyme onto the surface of lignin and other impurities were reduced by the addition of BSA and lysozyme. The model was applied to simulate enzyme adsorption on cellulose and glucose releasing with a hydrolysis rate coefficient increased but the fractal exponent decreased with the addition of BSA and lysozyme. Compared to BSA, addition of lysozyme exhibited a better hydrolysis performance, which confirmed by the larger hydrolysis rate coefficient and the smaller fractal exponent.

Chapter 6 focus on the dynamic simulation of multi-substrate co-fermentation system. The simultaneous and effective conversion of both pentose and hexose in the fermentation is a critical and challenging task in a biorefinery. Mixed sugar co-fermentation process featuring with a cell recycling unit (CF/CR) was studied for production of lactic acid. Carbon catabolite repression in co-fermentation was identified

and the cell metabolism was clarified and analyzed through kinetic models of cell growth and utilization of single/mixed sugars. The transition of sugar consumption, cell growth, and lactic acid production among the batch, continuous process and the continuous process with cell recycling were successfully simulated by the proposed model structure.

Chapter 2 Literature review

This chapter provides a literature review and preliminary study from recently accomplished projects on bioconversion processes from lignocellulosic biomass in Hong Kong. The general chemical compositions and structure of lignocellulosic biomass were reviewed. The lignocellulosic biomass collected from local wastes were investigated. The chemical and physical properties were investigated by both laboratory analysis and filed measurement. The four major steps of the bioconversion process of biomass were summarized. This is then followed by the modes of operation. Inhibition factors of the processes are discussed. The purpose of this review is to provide an understanding of the previous studies in this area.

2.1 Characteristics of lignocellulosic biomass

Lignocellulosic biomass, such as residues from agricultural, forestry, urban gardening and municipal and energy crops, is an abundant organic material for bioethanol production and a potential substitute to fossil fuel. The major compounds of lignocellulosic biomass are cellulose (30-55%), hemicelluloses (25-50%) and lignin (10-35%). The carbohydrate components (cellulose and hemicellulose) are fermentable after hydrolyzing into reducing sugars. The contents and distribution of these three compounds are different in various

plants. Figure 2.1 illustrates the structure of typical plant cell wall and the chemical structure of the three major components of cellulose, hemicellulose and lignin. The inherent characteristics of native lignocellulosic biomass, such as structural and chemical properties, make it resistant to biodegradation by enzyme and microorganisms.

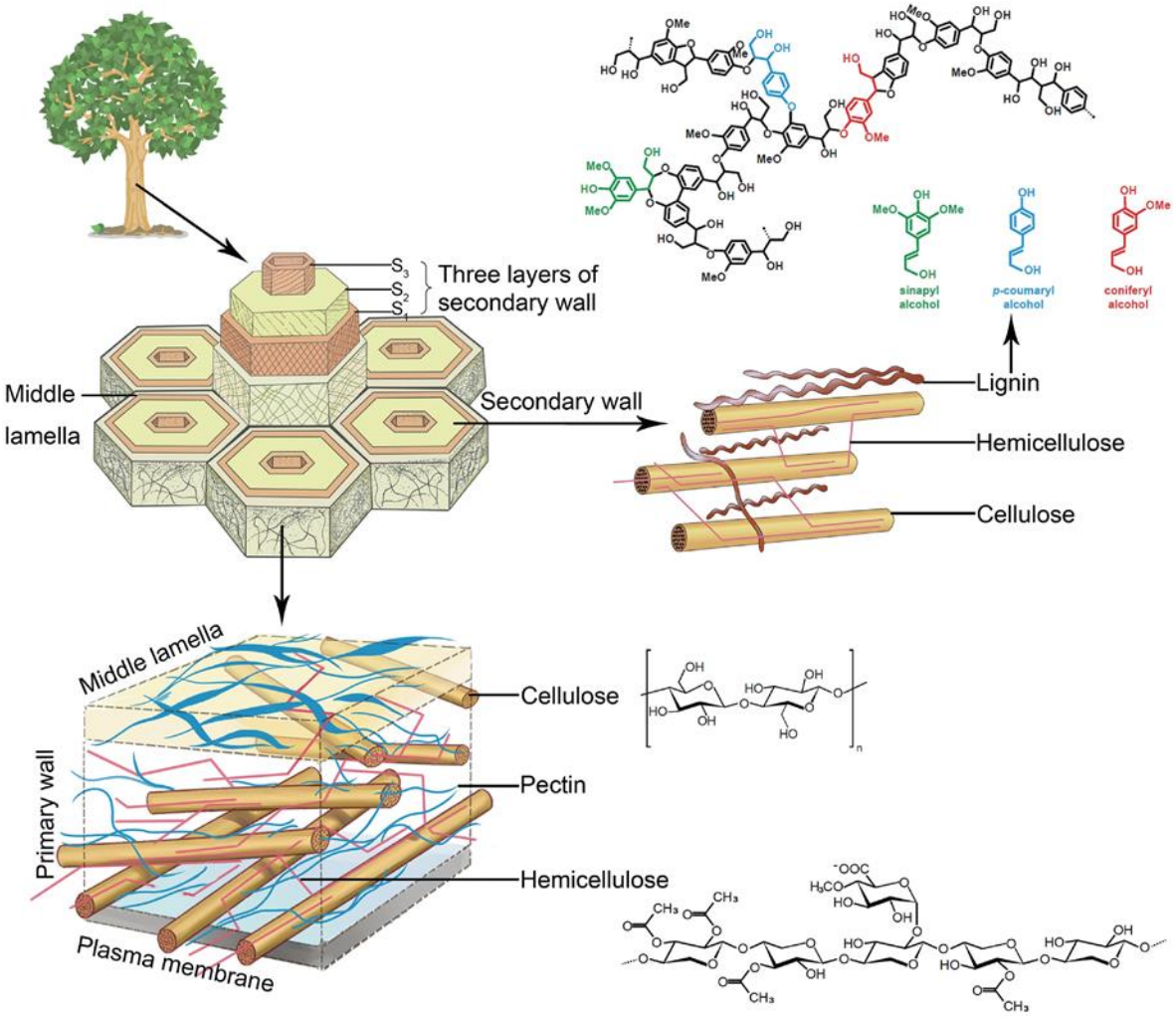

Figure 2.1 Schematic illustration of the structure and major polymers of plant cell wall (Zhao et al., 2019)

Cellulose is the most abundant polymer and constitutes 30 – 55% of plant cell wall

depended on plant spcies (Bajpai, 2016). Cellulose is a linear polysaccharide polymer of D-glucose, which is strongly linked via a β-1,4 glycosidic bonds. Cellulose chains have different orientations throughout the structure, leading different level of crystallinity. Cellulose consist of two region: amorphous (low crystallinity) and crystalline (high crystallinity) regions ((Atalla & VanderHart, 1984). Cellulose chains are attached to each other by hemicellulose and/or pectin, and covered by lignin. Such a complicated structure provides cellulose resistant to biological and chemical attack.

Hemicellulose is composed of short-chained and branched polysaccharides including xylan, xyloglucan, glucomannan, mannan, galactomannan, callose and others (Chen, 2014). The short and branched chains of hemicellulose link cellulose and lignin, building a rigid cellulose-hemicellulose-lignin matrix to render cellulose difficult for chemical and biological attacks (Kumar et al., 2009). Hemicellulose is more easily hydrolyzed in acidic condition than cellulose due to its lower degree of polymerization and less crystalline structure. Therefore, most of the hemicellulose is degraded to reducing sugars and dissolved in solution after pretreatment.

Lignin is a complex of organic polymers composed of complicated phenylpropane units linked randomly (Chen, 2014). It is the second abundant organic compound in

lignocellulose. Coniferyl alcohol, p-coumaryl alcohol and sinapyl alcohol are the three main monomers (Chen, 2014). Lignin is insoluble in water and most solvents due to strong hydrogen bonds formed by the hydroxyl and polar groups in the lignin structure. Lignin provides the rigid and three-dimensional structure of plant cell wall and protects the cellulose form attack. These properties of lignin render the lignocellulosic biomass resistant to degradation, leading to the higher the lignin content, the greater difficulty of degrading the material. It is one of the major barriers to utilize the lignocellulosic biomass. In general, woody biomass has a relatively higher content of lignin compared to herbaceous plants, particularly softwood (such as pine and spruce).

2.2 Lignocellulosic biomass in Hong Kong

Hong Kong shows a great potential for bioconversion of lignocellulosic biomass from the urban vegetation. The plant species growing in this study area has shown high diversity and growth rates. More than 3,300 native and exotic plant species have been recorded by the Hong Kong Herbarium (HKHCSBG, 2009). The details of field procedures were described in our previous study (Sarker & Rahman, 2010). All sampling sites are located in Hong Kong, including a secondary forest near Tai Lam Country Park (Site 1, 22°23'15.8"N 114°03'00.9"E) and rain gardens located on the main campus of the Hong Kong Polytechnic University, Hung Hom (Site 2, 22°18'15.1"N; 114°10'46.5"E). Hong Kong

shows a great capacity for urban vegetation and rain garden development. The plant species growing in this study area has shown high diversity and growth rates.

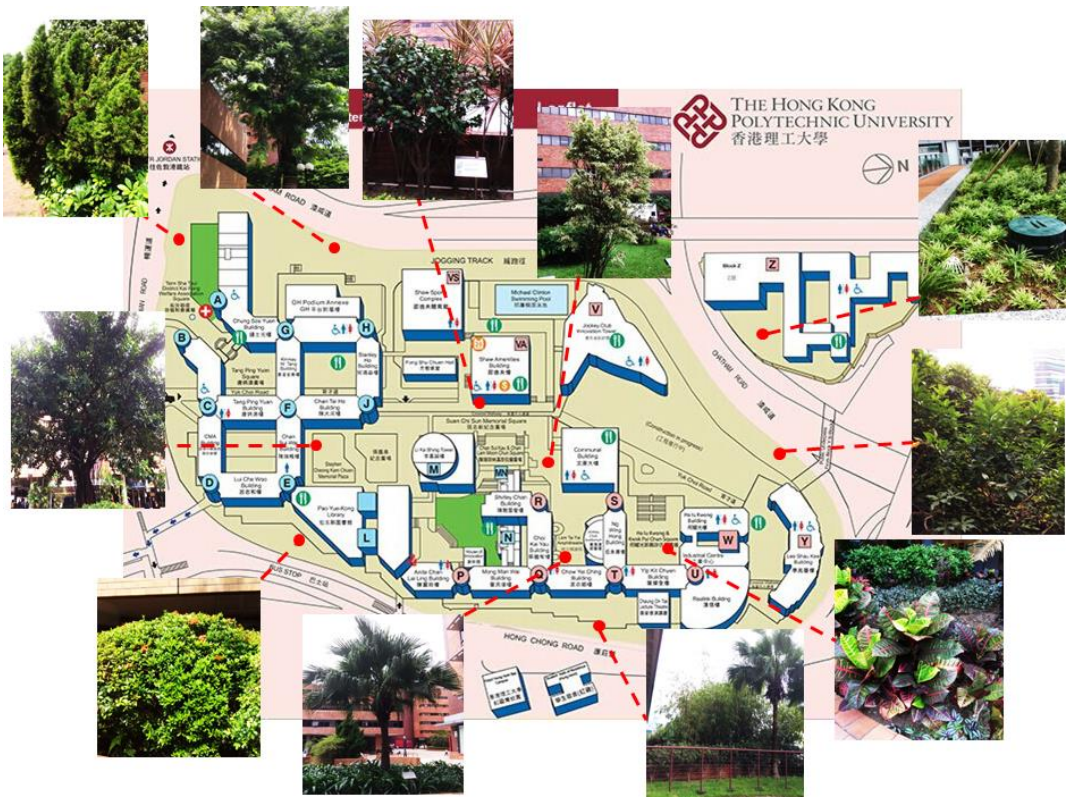

Figure 2.2 Geographical distribution of the collected samples in The Hong Kong Polytechnic University

More than 3,300 native and exotic plant species have been recorded by the Hong Kong Herbarium (HKHCSBG, 2009). The details of field procedures were described in our previous study (Sarker & Rahman, 2010). Seventy-five trees with a wide range of trunk were selected from 14 different tree species in Site 1. Diameters at breast height (DBH), basal diameter of trunk (D), tree height (H), and above-ground biomass (AGB) were

measured on-site and after tree harvesting, respectively. The representative tree species in Site 1 included *Acacia auricubcformis*, *Acacia confusa*, *Acacia mangium*, *Acacia torelligua*, *Aquilaria sinensis*, *Castonopisis fissa*, *Eucalyptus torelligua*, *Lophostemon confertus*, *Machilus breviflora*, *Machilus chekiangensis*, *Machilus gamblei*, *Machilus pauhoi*, and *Pinus elliottii*. In addition, twenty plant species (including 7 herbs, 7 shrubs, and 6 trees) were collected from the rain gardens (Site 2). These selected plant species are listed **Table 2.1** and are represented by H1-6 (herbs), S1-6 (shrubs) and T1-7 (trees). Biomass production per area (kg/m^2) of the herbal species were measured based on a five-point sampling methods (Brower et al., 1998), in which plant biomass samples in a 0.5×0.5 m^2 square were collected from the four corners and the middle of the selected area. The shrub and tree biomass were directly determined for each independent plant.

2.2.1 Physical properties

Bioenergy potentials of plants are related to the physical and chemical properties of each species. In order to obtain the related information two measurements were carried out on-site and in the laboratory, to evaluate the physical properties of living trees and harvested urban vegetation residues, respectively. Trunk diameter (DBH and/or D) and height were measured before harvesting a selected tree and tree height was then measured again with a measuring tape after harvesting. The harvested tree was then segregated into

five fractions: leaves, twigs (diameter less than 3.2 cm), small branches (diameter between 3.2 cm and 6.4 cm), large branches (diameter greater than 6.4 cm), and stems (Ketterings et al., 2001). The fresh biomass (*M*) of each part of the tree was estimated separately immediately after segregation using a digital weight scale (0.05 g precision) at the site. After taking fresh biomass measurements, representative samples from every part of the tree were taken for dry weight measurements. The samples were oven-dried at 80℃ until constant weights reached to determine the moisture content and total dry mass. The dried samples were homogenized using a laboratory blender (8010S, Waring Commercial, USA) for further analysis. The total dry mass of each plant was calculated by summation of the weight of all the samples.

2.2.2 Chemical composition analysis

Plant cell wall was composed of cellulose, hemicellulose, lignin, water, extractives and ash (Liu et al., 2016). If those chemicals can be separated properly two basic types of biofuels can be generated. The rapidly degradable sugars derived from cellulose and hemicellulose are proper carbon sources for bioethanol conversion, and lignin is a biopolymer with a high heating value for direct combustion. Bioethanol and solid biofuel are thus selected to be the simulated bioenergy outputs in our study. As the contents of sugars and lignin vary significantly among plant species the productivity of the two biofuels are plant-specific.

The chemical compositions of each plant species need to be measured individually. The chemical composition of the biomass was determined according to the standard analytical methods of the National Renewable Energy Laboratory (NREL, Golden, CO, USA) (Sluiter et al., 2008). A two-step acid hydrolysis procedure was applied to fractionate the biomass. The cellulose and hemicellulose contents were determined by High Performance Liquid Chromatography (HPLC) equipped with an Aminex HPX-87P column (BioRad, Hercules, CA, USA) and a refractive index detector (Lab Alliance, State College, PA, USA). The column was operated at 85°C and 0.2-μm filtered deionized water was used as mobile phase with a flow rate of 0.6 mL/min. The solid residue was considered to be acid-insoluble lignin (AIL) and ash, which was measured as the weight of insoluble residue remaining at 105°C and 575°C, respectively. The acid-soluble lignin was measured by UV-Vis spectroscopy (Milton Roy Company, Ivyland, PA, USA) at 205 nm. The total lignin content was the summation of acid-insoluble lignin and acid-soluble lignin.

2.2.3 Carbon credit of energy harvesting

Two biorefinery techniques to convert biomass into cellulosic ethanol and pelletized fuels were considered in the model for plant biomass management. Bioethanol can be generated by fermenting the rapidly-degradable carbohydrates (such as hemicelluloses and glucose) in a biorefinery process (Dong et al., 2018a). The remaining solids contain large amount of

lignin and can be as a solid biofuel after pelletization (Ko et al., 2017). Based on the mass contents of carbohydrate monomers and aromatic compounds, conversion parameters were given to calculate the carbon sequestration potentials. The carbon sequestration potentials of bioethanol (to partially substitute gasoline) and direct combustion (to replace coal) were quantified in a similar fashion to in the previous study (Ko et al., 2017). The total sequestrated carbon (*TC*) was calculated as follows:

$$TC_{Biofuel} = \left[C_{EtOH}^{Gasoline} \cdot Y_{Sugars}^{EtOH} \cdot \left(f_{cl} + f_h \right) + C_{Pellet}^{Coal} \cdot f_l \right] \cdot M \qquad (3\text{-}3)$$

where *C* (*i.e.*, $C_{EtOH}^{Gasoline}$ and C_{Pellet}^{Coal}) represents the mass ratios of carbon content to be emitted from biofuels and fossil fuels at the same unit energy consumption (kg/kg); *Y* represents the yield of conversion from the substrate to the products (%); and *EtOH* represents ethanol. The ethanol yield from the carbohydrates $\left(Y_{Sugars}^{EtOH}\right)$ was assumed to be 80% and energy density of ethanol was assumed to be 72% of one provided by the same unit mass of gasoline (Peres et al., 2013). Combusting 1 L gasoline produces 2.12 kg CO_2. The heat value of coal and was assumed to be 32 MJ/kg and the emission of CO_2 was 2.86 kg/kg (Ko et al., 2017). The heat value of pelletize biofuel was 20 MJ/kg. In summary $C_{EtOH}^{Gasoline}$ of ethanol is 1.53 kg/kg and C_{Pellet}^{Coal} is 1.78 kg/kg.

2.2.4 Morphological characterization

Optical microscopy was applied to reveal the morphology of the transverse section and outer surface of the herb, shrub, and tree stem as showed in

Figure 2.3. Among those plants, *Tradescantia pallida* (H3), *Camellia japonica* (S3), *Ginkgo biloba* Linn (T2)., were observed by optical microscopy at 10×20 magnification. Significant difference can be observed among these selected plants. For the herb *Tradescantia pallida* (H3), the parenchyma cells predominated the inner region of the plant leaves, with some vascular bundles each containing xylem and phloem. The vascular bundles (xylem, and phloem) dominated the inner region for tree cell (*i.e., Ginkgo biloba* Linn) *a*rranged slightly more closely than shrub's (*Camellia japonica)* from the image of transverse section.

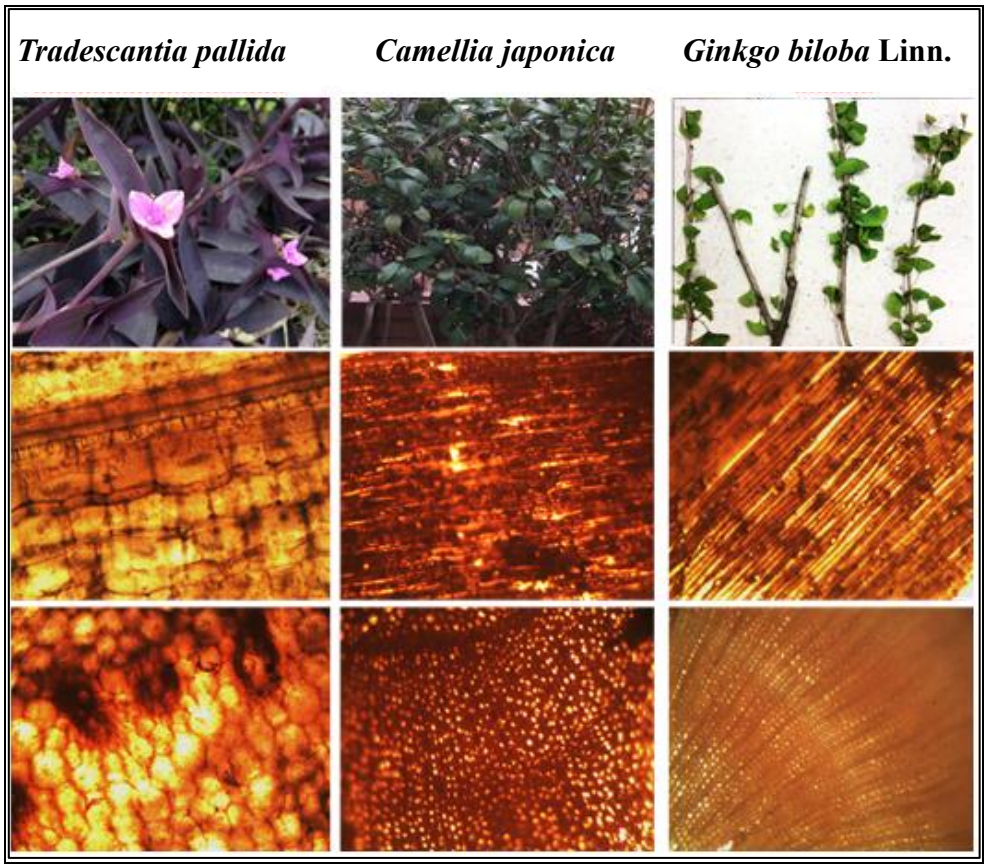

Figure 2.3 Morphological characterization of *Tradescantia pallida, Camellia japonica, Ginkgo biloba* Linn.

2.2.5 Properties of selected plant species

Physical and chemical properties of the plants obtained from the rain garden are presented in **Table 2.1**. Population densities are defined by the maximum heights and canopy sizes of the individual plant to ensure proper a spatial arrangement for sufficient water and nutrient uptakes (Kohyama, 1993). Height at maturity, trunk diameter (DBH or D), and minimum root depth were defined based on the morphology of the plants. Moisture contents of the collected samples ranged from 41-95%. Herbs and shrubs showed higher

moisture contents than the trees, implying higher carbon stored in a unit mass of trees. Moisture contents showed a wide variation in herbs (*e.g.*, *Tradescantia pallida* (H3) and *Axonopus compressus* (H1) contained approximately 95% and 51% water, respectively) but were more consistent among trees (43-66%). The chemical compositions of different plants varied significantly (*i.e.*, 16.8-40.2% for cellulose, 3.2-19.1% for hemicellulose, and 8.0-36.7% for lignin), but generally followed the normal distribution. The cellulose contents of most of the plants were approximately 20% although *Allamanda cathartica* (S4) contained more than 40% of cellulose. The average hemicellulose content was approximately 10%, but *Axonopus compressus* (H1, 17.9%), *Miscanthus floridulus* (H6, 16.2%), and *Ficus benjamina* (T1, 17.3%) showed much higher hemicellulose content than that by most of the other plant species. The average lignin content was approximately 20%, the highest values of which were obtained from the samples of shrubs (*i.e. Camellia japonica* (S3), *Dwarf ixora* (S5), and *Rhododendron pulchrum* Sweet (S6), 31.1-32.5%) and trees (*Ficus benjamina* (T1), 36.7%; and *Sabina Chinensis* cv. Kaizuca (T4), 34.1%). Plant biomass with high cellulose/hemicellulose contents and low lignin content are optimal feedstock for bioethanol production. Lignin-rich biomass shows higher recalcitrance to enzymatic saccharification, and therefore results in a lower product yield compared with lignin-free substrates (Liu et al., 2016). High-lignin biomass is more suitable for use as woody pellets due to its high energy value. The average ± standard error

carbon contents of herbs, shrubs, and trees were 22.6±6.9%, 31.3±4.0%, and 32.4±7.7%, respectively, and the specific plant species with the highest carbon contents in each category were the herb *Miscanthus floridulu* (H6, 35%), shrub *Rhododendron pulchrum* Sweet (S6, 37%), and tree *Ficus benjamina* (T1, 47%).

Table 2.1 Measured physical trails and chemical compositions of the selected rain garden species.

No.	Plant species	Population density, ρ	Height at mature, H	DBH/D^*	Minimum root depth	Moisture content	Chemical composition			Carbon content, f_c
							Cellulose, f_{cl}	Hemicellulose, f_h	Lignin, f_l	
		Stand/m^2	m	cm	m	%	%	%	%	%
H1	*Axonopus compressus*	-	-	-	0.1	51.1	20.7	17.9	11.9	25
H2	*Parathelypteris glanduligera*	-	-	-	0.3	63.3	23.5	4.6	14.9	22
H3	*Tradescantia pallida*	-	-	-	0.2	95.1	17.3	4.9	8	15
H4	*Liriope spicata* var. Variegata	-	-	-	0.2	79.7	21.6	3.2	9.8	18
H5	*Ophiopogon japonicus*	-	-	-	0.1	65.0	27	6.4	9.8	21
H6	*Miscanthus floridulus*	-	-	-	0.4	58.2	35.3	16.2	18.4	35
S1	*Codiaeum variegatum*	10	0.6	5	0.5	66.6	30.7	7	15.2	27
S2	*Schefflera arboricola*	8	1	5	1.0	82.7	27.4	11.6	14.9	27
S3	*Camellia japonica*	4	2	10	1.0	40.9	16.8	11.4	31.1	33
S4	*Allamanda cathartica*	8	2	5	1.0	72.4	40.2	9.7	11.3	30
S5	*Dwarf ixora*	10	2	5	0.5	62.9	18.9	7.6	32.5	34
S6	*Rhododendron pulchrum* Sweet	10	1	5	1.0	65.1	24.1	10.1	32.4	37
T1	*Ficus benjamina*	0.02	30	40	5.0	43.1	32.7	17.3	36.7	47
T2	*Ginkgo biloba* Linn	0.05	35	35	5.0	65.2	19.5	6.8	29.5	31
T3	*Ficus elastica*	0.05	30	40	2.0	51.9	21	6.9	23.1	28
T4	*Sabina Chinensis* cv. Kaizuca	0.1	8	20	2.5	65.6	18.1	11.2	34.1	36
T5	*Cassia siamea*	0.05	12	30	4.0	62.0	21.8	10.4	17.5	26
T6	*Livistona chinensis*	0.05	10	30	1.0	51.9	35.7	12.7	11.5	29
T7	*Roystonea regia*	0.05	30	30	2.0	54.7	31.9	13.3	14.2	30

* Based on the height at mature for trees and shrubs the two different indexes were presented. *DBH* is the trunk diameter measured at breast height (1.3 m) and *D* is measured approximately 10 cm above the ground.

2.3 Lignocellulosic conversion process

Bioconversion of lignocellulosic biomass can be generally categorized into two classes based on the feedstock used in the process. The first-generation ethanol generally uses food crops (e.g. sugar cane, wheat and corn) as the feedstock. Lignocellulosic biomass (such as wood, straw and grass) is used as a feedstock in the second-generation ethanol production. Although the ethanol production from food crops is highly efficient and well established, there is an urge to promoting and improving bioethanol production from cheaper and more abundant lignocellulosic biomass.

The process of bioconversion can be divided into four major steps including 1) pretreatment, 2) hydrolysis, 3) fermentation, and 4) distillation (**Figure 2.4**). The processes of enzymatic hydrolysis and fermentation are commonly combined and performed at the same time for production of lignocellulosic ethanol. This process is also known as simultaneous saccharification and fermentation (SSF). Pretreatment of the lignocellulosic biomass is an additional and essential step required in the second-generation ethanol production compared to the first generation due to its complicated and rigid structure.

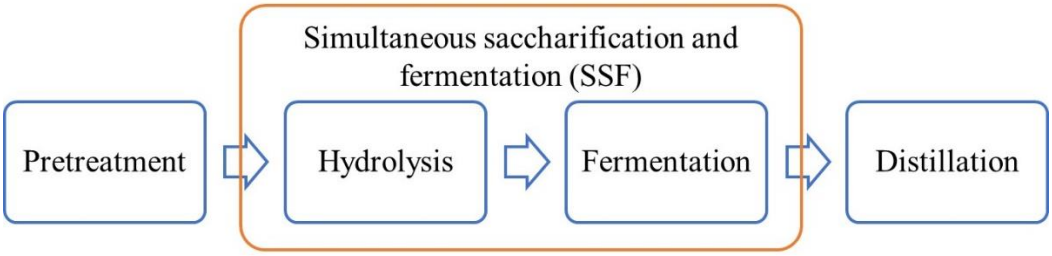

Figure 2.4 Schematic procsesses of lignocellulosic ethanol production

1) Pretreatment is the process that breaks down the robust structure of lignocellulosic biomass facilitating the downstream processes.
2) Hydrolysis is the process that converts polysaccharide into fermentable reducing sugars by breaking the chemical bonds between polymers.
3) The reducing sugars are metabolized and converted to ethanol by fermenting microorganisms.
4) Distillation is the step that separate final product from the fermentation broth to obtain high concentrated or pure ethanol.

2.3.1 Pretreatment

In order to improve the rate of hydrolysis and increase the yield of fermentable sugars from lignocellulosic biomass, pretreatment process is essential to disrupt the naturally recalcitrant carbohydrate shield and/or remove structural and compositional barriers that hinder the accessibility of enzymes and microorganisms to cellulose and

hemicellulose (Mosier et al., 2005). The pretreatment process lead to chemical and/or physical changes in the biomass to achieve this results. The major contributions to the resistance of lignocellulosic biomass are crystallinity of cellulose, accessible surface area, lignin protection and cellulose sheathing by hemicellulose (Kim & Holtzapple, 2006; Mosier et al., 2005; Shafiei et al., 2015). An effective pretreatment should consider the following criteria: 1) preservation of the greater part of fermentable sugars; 2) minimum formation of inhibitory co-products that hinder enzyme activity and microorganism growth in the downstream processes; 3) minimum cost, energy and chemical demands; 4) generation of high value co-products; 5) cost and recyclability of chemical catalyst for pretreatment (Jørgensen et al., 2007; Shafiei et al., 2015).

The pretreatment methods can be classified into four categories: 1) physical, 2) chemical, 3) biological, and 4) physiochemical treatments. Various pretreatment processes have been studied and achieved varying results. The optimal process and conditions of pretreatment is depended on the type of lignocellulosic biomass due to various compositions and complex chemical structure of the feedstock.

The physical treatment is the process that altering the properties of the feedstock without using any chemicals or microorganisms. Steam and water are not considered as

chemicals. The well-established physical treatments involve comminution (mechanical size reduction e.g., milling and grinding), steam explosion, hydrothermolysis (liquid hot water), extrusion and irradiation (microwave and ultrasound).

In contrast, chemical treatment refers to the process that altering the physical and chemical structures of the feedstock by using chemicals, such as acids, bases and ionic liquids. Sulfuric acid (H_2SO_4) and sodium hydroxide (NaOH) are the most commonly used acid and base in chemical pretreatment (Mosier et al., 2005). Acid pretreatment is able to hydrolyze hemicellulose to xylose, arabinose, galactose and other monomers, facilitating the enzyme to access the cellulose in the next stage. However, inhibiting compounds, such as furfural and hydroxymethylfurfural (HMF, might be formed during the processes. Dilute acid is more favorable than strong acid due to the lower risk on the formation of inhibiting compounds. Apart from sulfuric acid, hydrochloric acid, nitric acid, acetic acid, and phosphoric acid have been studied in pretreatment with varying results. Alkaline pretreatment can be carried out in lower temperature and pressure (even at ambient conditions) compared to acid and other pretreatments. Bases used in alkaline pretreatment involve sodium hydroxide, calcium hydroxide, potassium hydroxide and ammonium. Solvation and saphonication caused the bases make the swollen cellulose more accessible for enzymes. However, the dissolved

polysaccharides might loss to degradation products and solubilized lignin causes inhibitory effects in the following processes of hydrolysis and fermentation.

Biological pretreatment refers to the method that uses fungi and microorganisms to enhance digestibility of cellulose and improve fermentation products. It requires lower energy inputs and no chemicals but longer processing time compared to physical and chemical pretreatments. In addition, fewer inhibiting compounds are formed. However, carbohydrates are competed between pretreatment and downstream fermentation as growth of fungi and/or microorganisms requires certain amount of carbohydrates in biological pretreatment. Therefore, fungi and microorganisms used are selectively break down hemicellulose and lignin while using limit cellulose in fungal and microbial pretreatments.

2.3.2 Hydrolysis

Hydrolysis is a process of converting complex carbohydrates (such as cellulose and hemicellulose) into component sugars (such as glucose and xylose) by cleavage of chemical bonds between the polymers. The hydrolysis of polysaccharides to simple sugars is also known as saccharification. Hydrolysis is mainly divided into two types, chemical and enzymatic hydrolysis.

Chemical hydrolysis is primarily acid based. The pretreatment and hydrolysis can be combined by using acid-based hydrolysis. Both concentrated and dilute acid are studied and used for hydrolysis. Concentrated acid process yields a higher sugar concentration and can be operated at lower temperature (Taherzadeh & Karimi, 2007). Diluted acid process is more favorable and economically feasible since concentrated acids are corrosive and hazardous (Sun & Cheng, 2002). Diluted acid process requires a high temperature (greater than 160ºC) and pressure to break down the cellulose and hemicellulose. However, several of degradation by-products are formed, which severely inhibit the fermentation in the downstream process.

Enzymatic hydrolysis is the process that using enzymes to convert lignocellulosic biomass to fermentable sugar for ethanol production. The major enzymes involved in cellulose conversion cellulase complex are endoglucanases (EGs), cellobiohydrolases (CBHs, also known as exoglucanases) and beta-glucosidases (βGs). **Figure 2.5** illustrates the interactions among these enzymes and lignocellulosic biomass. EGs and CBHs adsorb to the surface of cellulose and lignin, while most of the hemicellulose are degraded in the pretreatment process. EGs randomly attack the cellulose at amorphous regions and cleave β-1-4-glycosidic bonds to create reactive ends. CBHs act 'processively' at the reactive ends and covert the cellulose including crystalline

cellulose, to produce cellobiose. βGs float around and convert the resulting dissolved cellobiose into two glucose molecules. βGs are critical during the hydrolysis of cellulose as cellobiose is severely inhibiting the activities of CBHs and EGs (Philippidis et al., 1993). The presence of lignin greatly interferes with the enzyme complex during cellulose hydrolysis.

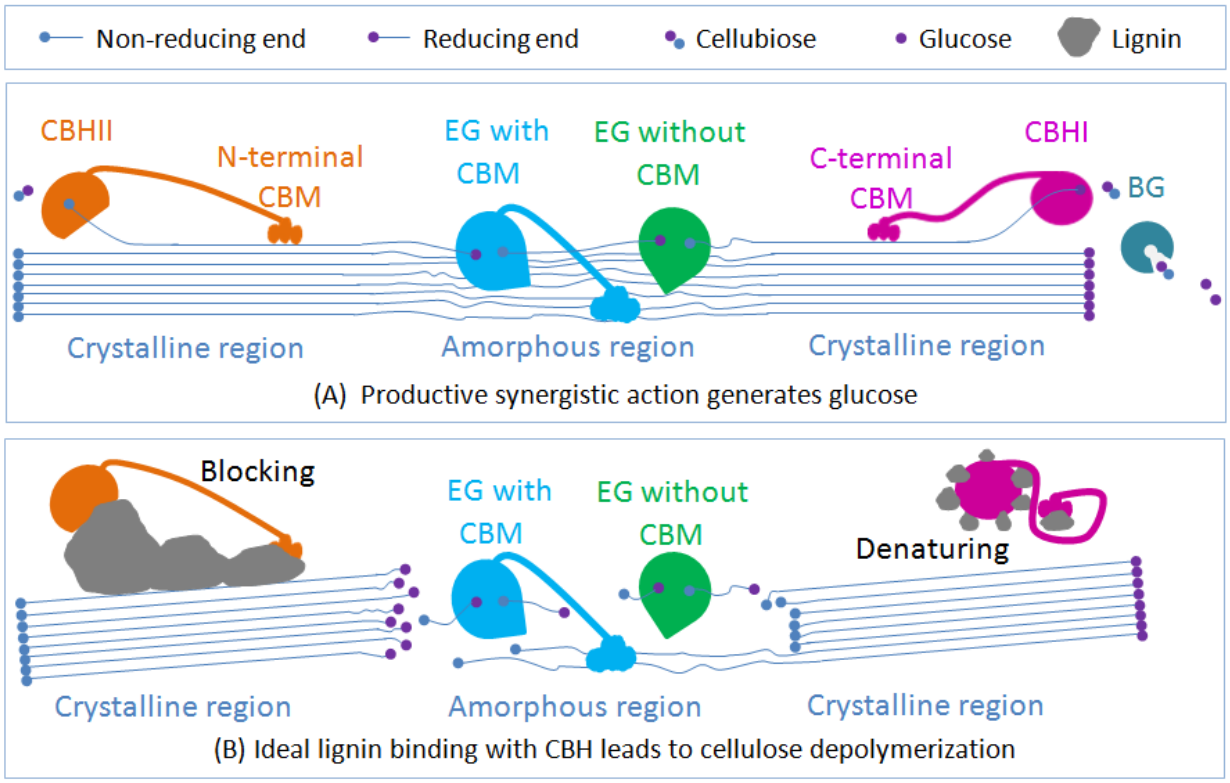

Figure 2.5 Schematic illustration of enzyme and lignocellulosic biomass interaction during enzymatic hydrolysis (Liu et al., 2016).

Chemical hydrolysis is relatively cheap and easily controlled and operated, but

enzymatic hydrolysis was adopted in this study. To achieve economic feasibility, a high dosage of enzyme is needed, typically 15 FPU/g cellulose (Yang et al., 2011). This process is capable to achieve a higher yield, a variety of selection and a lower energy inputs compared to the processes that using chemicals to hydrolyze lignocellulosic materials(Yang et al., 2011). Ballesteros (2010) agrees that enzymatic hydrolysis has a greater potential for advancement than chemical hydrolysis.

Cellulase production bacteria, such as *Clostridium thermocellum* can grow in solid state fermentation and used on site for enzymatic hydrolysis to lower the operation cost of the bioconversion process (Sadhu & Maiti, 2013). However, commercial enzyme was adopted in this study due to the high efficiency, high enzyme stability and ease of storage and application in the downstream processes. More investigations are needed to be conducted to overcome the technical barriers for the enzymatic process to achieve economic feasibility.

2.3.3 Fermentation

Fermenting microorganisms, such as yeast, bacteria and fungi, are used to convert the simple sugars into biofuels or biochemicals, such as ethanol, butanol and lactic acid. The microorganisms should produce a high product yield and productivity and tolerate

high product concentration to minimize the distillation cost. High temperature tolerance, inhibitors tolerance and utilization of diverse pentoses and hexoses are also required for lignocellulosic ethanol production. The Bakers' yeast, *Saccharomyces cerevisiae* is most commonly used microorganisms in starch and cellulose-based ethanol production. It is a facultative anaerobic organism, which can grow with and without oxygen because it can metabolize energy aerobically or anaerobically. Most strains of *S. cerevisiae* can utilize glucose and mannose for fermentation, while galactose fermentation is strain dependence. It is reported that some of the genetically modified strains are able to ferment xylose (Li et al., 2016a). Apart from yeast, bacteria strains, such as *Zymomonas mobilis* and genetically engineered *Escherichia coli*, are used for fermenting a variety of substrates.

2.3.4 Distillation

Distillation is the process of separating the fermenting products (*e.g.* ethanol, lactic acid) from water and solids after fermentation. The fermentation broth is preheated from the fermentation temperature in multiple stages. Ethanol is recovered at the top of a distillation column, where separating the ethanol with most of the water and solid biomass. It is then concentrated in a rectifying column. The concentration of ethanol in the fermentation broth before distillation should exceed 4% w/w to achieve

economically viable (Horn & Eijsink, 2010). A higher productivity should be achieved in order to lower the production cost of lignocellulosic ethanol. To make the lignocellulosic ethanol production process more economically feasible, several improvements needed to be considered as follows:

1) to improve the performance of pretreatment and minimize the inhibitors generated;
2) to improve the efficiency of hydrolysis;
3) to utilize all the fermentable sugars released from the upstream processes; and
4) to improve the process integration to minimize the demand of water, energy and chemical, and recycle the used materials.

2.4 Inhibitory compounds

Pretreatment of lignocellulose biomass for ethanol production generates inhibitory compounds that suppress microbial growth and subsequent fermentation. The types and amounts of inhibitory compounds depend on the type of raw material and the pretreatment methods. Detoxifications of the pretreated substrates have been developed in order to improve the efficiency of the downstream processes. However, due to the

additional cost and waste productions of inhibitors removal and potential loss of fermentation sugars, additional detoxification should be avoided if possible (Olofsson et al., 2008). The typical degradation by-products of the lignocellulosic biomass after pretreatment include furaldehydes (i.e., furfural and Hydroxymethylfurfural (HMF)), carboxylic acids (i.e., formic acid, acetic acid, and levulinic acid), ketones, phenols, and other aromatic compounds, and the reaction pathway of inhibitory compounds in the pretreatment of a Spruce wood are illustrated in **Figure 2.6** (Palmqvist & Hahn-Hägerdal, 2000). HMF and furfural are formed from the degradation of hexoses and pentose respectively; weak acids are formed when HMF and furfural further degraded; and phenolic compounds are formed by lignin degradation (Chandel et al., 2011; Palmqvist & Hahn-Hägerdal, 2000; Parawira & Tekere, 2011).

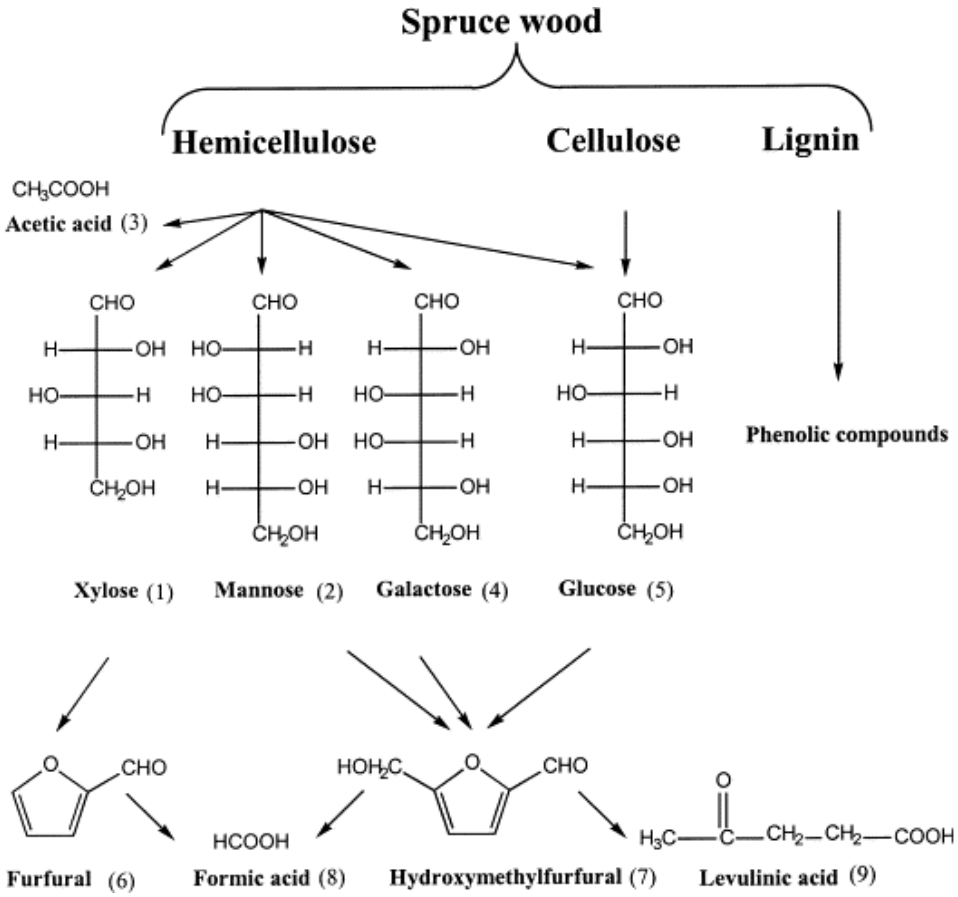

Figure 2.6 Formation pathways of by-products of lignocellulosic biomass during pretreatment (Palmqvist & Hahn-Hägerdal, 2000)

The commercial yeast are more susceptible to inhibition by furfural than HMF and the presence of furfural and HMF synergistically suppressed cell growth. The yeast strains showed a prolonged lag phase at the presences of more than 1 g/L of HMF and furfural, respectively (Liu et al., 2004). Liu et al. (2004) identified a metabolite of 2,5-bis-hydroxymethylfuran transformed from HMF degradation**. Figure 2.7**

illustrates the conversion pathway of furfural and HMF transformation to a less toxic degradation product. Liu et al. (2005) reported that the adapted strains of *S. cerevisiae* showed enhanced ability of transformation to reduce the concentration of HMF and furfural up to 7.5 and 2.8 g/L, respectively. The accumulation of these metabolites are less toxic to the yeast cell and suggests the potential for in situ detoxification of these inhibitory compounds.

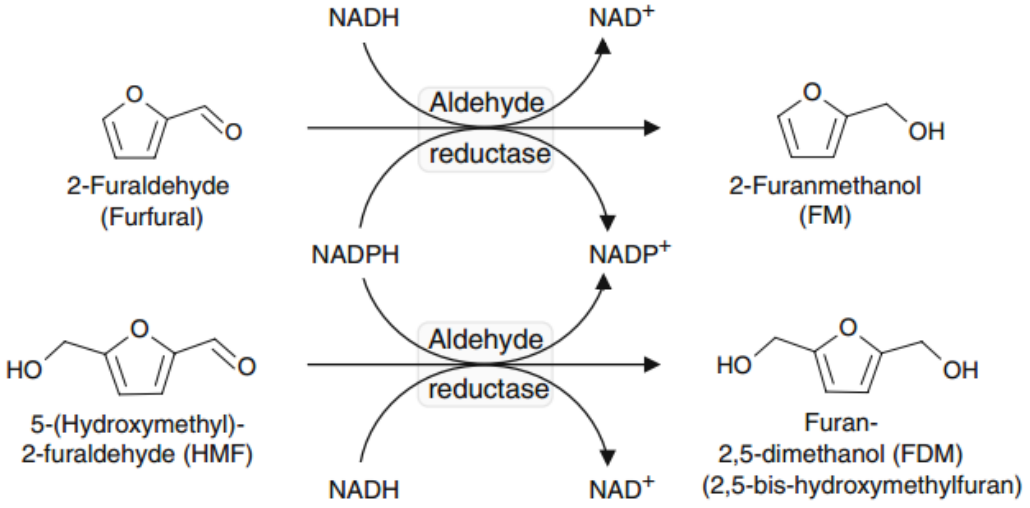

Figure 2.7 Conversion pathways of furfural and HMF in yeast fermentation (Liu, 2011)

A long lag phase of microbial growth due to the change of environment from cultivation medium to fermentation conditions can be solved by adaptation of microorganisms to inhibitors prior fermentation. Adapting the microorganisms to the inhibitory compounds by cultivating the microorganism in pretreatment hydrolysate. A combination of inhibitor-tolerant yeast strain with effective feed strategies possibly

improves the efficiency of lignocellulosic biomass conversion.

2.5 Modes of operation

2.5.1 SSF

The bioethanol conversion from lignocellulosic biomass occurs in the main steps – hydrolysis and fermentation, which are in close collaboration. The cellulose is first hydrolyzed into monosaccharide, glucose, which is then converted to ethanol by yeast or bacteria. The processes can be conducted into two ways, which are separate hydrolysis and fermentation (SHF) and simultaneous Saccharification and fermentation (SSF).

The optimum temperature for enzyme complex to effectively hydrolyze the cellulose ranges from 45°C to 50°C at a pH of 4.8. In contract, the optimum temperature for the fermentation of glucose to product ethanol by the commercial yeast, *Sacchoromyces cerevisiae*, is 30°C to 35°C. SHF process involves a change in operation conditions and reaction unit from the hydrolysis to fermentation stage. The major advantage of SHF is both enzymatic hydrolysis and yeast growth operate in its own optimal conditions. Furthermore, lignin residue can be removed after hydrolysis and thus it is possible to recycle yeast cell in a continuous mode of operation. However, the cellobiose and

glucose produced in cellulose hydrolysis strongly inhibit the activity of enzymes complex (Philippidis et al., 1993).

SSF is the strategic process that combines and performs enzymatic hydrolysis and fermentation to produce biofuels and/or biochemicals. The glucose produced can be rapidly converted to ethanol by the fermenting microorganisms. The continuous removal of glucose from the reaction medium minimizes the depression of enzymatic activity. Another advantage of SSF is the reduction in overall operation time and therefore increase in productivity. However, the operation conditions are needed to be compromised between the optimal condition of hydrolysis and fermentation. The operation temperature of SSF ranges from 35°C to 42 °C (Olofsson et al., 2008). Compared to SHF process, inhibition effects caused by the produced ethanol on the enzyme activity and synergic effects of inhibitors and high temperature might lead to high death rate of yeast and hinder cell recyclability should be taken into consideration in SSF processes. The inhibition caused by ethanol produced in SSF is relatively moderate to the enzyme complex compared to the inhibitory effects of glucose and cellobiose (Philippidis et al., 1993).

Numerous studies were conducted to compare the SHF and SSF processes with various

substrates at different operation conditions. Alfani et al. (2000) reported that SHF process achieved a relatively higher ethanol yield (81%) than SSF process (68%) but the productivity of SSF process (0.837 g/L-h) was much higher than SHF process (0.313 g/L-h). Wingren et al. (2003) reported that the total cost of bioethanol production of SSF process was 0.57 USD/L, which was lower than the SFH process (0.63 USD/L). Higher ethanol yield was the main reason of lower capital cost of SSF process.

The major disadvantage of SSF is the enzymatic hydrolysis and fermentation is needed to be performed in a compromised operation temperature. In other words, both enzyme complex and microorganism are not working in their optimal condition. Non-isothermal SSF process, in which temperature is changed during the process. Mutturi and Lidén (2014) reported that the process time could be significantly shortened by adopting the non-isothermal SSF to achieve the same final product yield.

2.5.2 Batch and fed-batch

Based on the feeding profile of the substrate, the operation of SSF process may be classified into three modes: 1) batch; 2) fed-batch; and 3) continuous. The pretreated substrate, enzyme and yeast are added at the beginning of the batch process. However,

the batch culture becomes difficult to mix with the increasing solid content, especially for the solid content higher than 15%. For the high solid SSF (more than 15% solid content), fed-batch is a promising mode of operation to solve the problem of mixing and inhibition, and thus increase the ethanol yield. Solid substrate and/or pretreatment liquor are fed discretely into the reactors at designed time points in the fed-batch process. With the increased accumulation of inhibitory compounds, inert materials and loss of enzyme activity, the ethanol concentration become steady. Continuous feeding of substrate into the system enables higher productivity of ethanol and steady process. However, the slow reaction rate and heterogeneous nature of the substrate in a solid-liquid reaction system hinder the hydrolysis process for continuous reaction systems.

Chapter 3 Model development

As mentioned in the previous section, a synergistic reaction of three different enzymes is needed for cellulose hydrolysis in a heterogeneous system. These features determine the highly complexity of enzymatic hydrolysis and fermentation, which render it difficult for mathematical modelling with complicated input parameters, such as kinetic, physical properties (e.g. specific surface area, crystalline index) and mass transfer. The final yield of enzymatic hydrolysis and fermentation is influenced by the dynamic interaction among substrate, reducing sugars, enzymes, microorganism, product and other inhibitors.

Extensive studies of cellulose hydrolysis and fermentation kinetics have been conducted in the past several decades (Kadam et al., 2004; Liao et al., 2008; Philippidis & Hatzis, 1997; South et al., 1995; Wang et al., 2014a), however, the kinetic of dynamic interaction and continuous process remain incomplete. Numerous hydrolysis kinetic models are established for predicting the initial reaction rate of cellulose hydrolysis based on the Michaelis-Menten reaction kinetic. However, these models have encounter difficulties and discrepancies in predicting reducing sugars over extended batch and fed-batch system, mainly caused by changing structure and composition of

biomass and loss of enzyme activity. The Michaelis-Menten equation is based on mass action law that applied for homogenous reaction and hence it is not appropriate to use to simulate the enzymatic hydrolysis of a heterogeneous substrate.

South et al. (1995) developed a typical SSF model by using a Langmuir adsorption model and a conversion dependent rate to describe enzymatic hydrolysis, and Monod kinetics with substrate and product inhibition to describe fermentation processes including cell growth, glucose consumption and ethanol production. Philippidis et al. (1993) proposed a cellulose hydrolysis rate model consist of cellulose to cellobiose conversion and cellobiose to glucose conversion. The enzyme – substrate absorption equilibrium was not included in this model and the enzyme concentration was considered to be independent to the conversion of cellobiose to glucose. Philippidis and Hatzis (1997) modified the enzymatic hydrolysis model according to the mechanism that cellulose is simultaneously convert to cellobiose by cellulase and glucose as well as released cellobiose is converted to glucose by β-glucosidases. Kadam et al. (2004) modeled the three hydrolysis reactions of lignocellulosic biomass, including two heterogeneous reactions for converting cellulose to cellobiose and glucose and one homogeneous reaction for converting cellobiose to glucose. Langmuir adsorption isotherm was adopted to describe the enzyme adsorption on the surface of substrate. For the adsorption of cellulase to cellulose, the following equation describes the adsorption

of cellulase to cellulose and lignin respectively as adsorbed enzyme = rate constant × free enzyme × substrate.

3.1 System boundary

The proposed model structure is depicted in **Figure 3.1**. The model was validated under three designed conditions with specific order (from simple to complex) of experiments. In the first system (**Figure 3.1a**), cellulase was introduced to break down the cellulose (X_C) into reducing glucose without the interference of lignin on the substrate. The enzyme adsorbed on the surface of cellulose is the active enzyme ($E_B{}^C$), which can be quantified by the total enzyme deducted by the measured free protein concentration (mg/g) in the supernatant (or the free enzyme, E_F). Further in the second system (**Figure 3.1b**), enzyme could be adsorbed by both cellulose and lignin (X_L) with various tendencies. The enzyme adsorbed on the surface of lignin is defined as ineffective enzyme-substrate or enzyme-lignin complex ($E_B{}^L$). In the final system (**Figure 3.1c**), additives were introduced in the hydrolyzate, which may offer various forms of beneficial effects to saccharification, such as selectively attach on the surface of lignin (X_{ad}), and/or prevent the non-productive adsorption of cellulase to lignin.

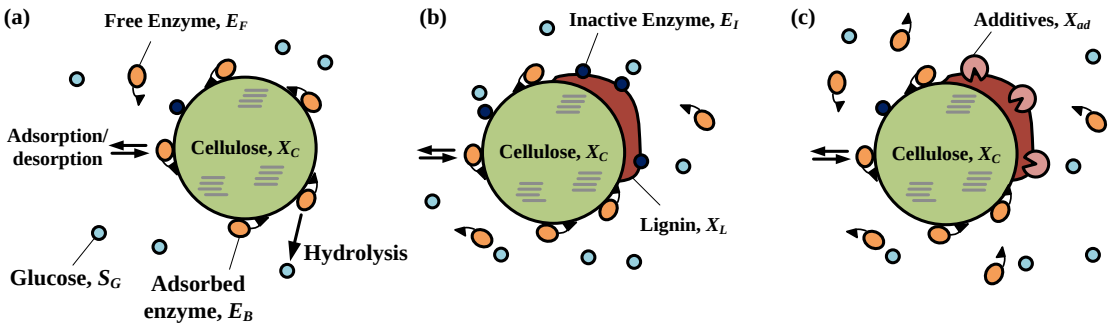

Figure 3.1 Schematic diagram of the dynamic model with concerned parameters for simulation of enzymatic hydrolysis of three scenarios: (a) pure cellulosic substrate; (b) lignocellulosic substrate; and (c) lignocellulose with additives.

Several key assumptions have been made to simplify the model. The structure of substrate is assumed to be uniform for enzyme adsorption. The three major working enzymes involved in cellulose hydrolysis are considered as one enzyme with multiple functions as described by Liao et al. (2008). Although the hydrolysis reaction could be inhibited by the final products, such as cellobiose, glucose and xylose, those influences were considered insignificant in this study. The β-glucosidase activity of the applied enzyme complex was high and the measured concentrations of cellobiose were negligible during the experiments. The conversion of cellobiose to glucose is not a rate limiting factor to cellulose hydrolysis and is not described in the model. Also, since the xylose concentration was very low, inhibition caused by xylose was neglected. Thus, glucose inhibition was the only limiting factor consider for the enzymatic hydrolysis.

Table 3.1 Summary of reported and proposed adsorption models

#	Description	Equilibrium enzyme adsorption	Adsorption kinetic	Comment	Ref.
1	Michaelis kinetic equation at steady-state	$E_B = \frac{E_F \cdot X_S}{K_m}$	N/A	Applicable for the basic homogenous enzymatic reaction	(Xu & Ding, 2007)
2	Empirical model with initial solid content, initial enzyme concentration, and initial specific area of cellulose (A^0)	$E_B = \frac{E_B^0}{X_S^0} \cdot X_S$; $E_B^0 = \frac{a \cdot X_S^0 \cdot E_{load}}{K_m + X_S^0} + bA^0$	N/A	The parameters used in the model are with only numerical means but not based on known theory of reaction kinetics	(Fan & Lee, 1983)
3	Langmuir isotherm	$E_B = \frac{\sigma_{Max} \cdot k_{ad} \cdot E_F}{1 + k_{ad} \cdot E_F} \cdot X_S$	N/A	Langmuir adsorption isotherm assumed uniform biding site and no interaction between the adsorbing molecules	(Kadam et al., 2004)
4	Empirical expression simulated the change of adsorption constant	$E_B = \frac{E_{load} \cdot K \cdot X_S}{1 + K \cdot X_S}$; $K = \frac{at}{b+t}$	N/A	*K* reflects enzyme adsorption capability of the substrates, and an empirical equation was developed to describe the dynamic change of *K* value over time	(Liao et al., 2008)
5	First order adsorption and desorption kinetics	N/A	$\frac{dX_{CE}}{dt} = k_{ad} \cdot X_C \cdot E_F - k_{de} X_{CE} - k_p X_{CE}$	Difficult to quantify and distinguish the enzyme adsorption to and desorption from cellulose	(Gan et al., 2003)
6	Second-order adsorption kinetic	$E_{eq} = \frac{E_{load} \cdot X_S^0}{X_S}$	$\frac{dE_B}{dt} = k_{ad} \cdot (E_{eq} - E_B)^2$	The adsorption curve does not converge with experimental results	(Wang et al., 2014a)
7	First order kinetic with adsorption isotherm	$E_{eq} = \frac{\sigma_{Max} \cdot E_F}{k_d + E_F} \cdot X_S$	$\frac{dE_B}{dt} = k_{ad} \cdot (E_{eq} - E_B)$	Combine adsorption isotherm and kinetic to describe the dynamic change of enzyme adsorption during hydrolysis	This study

Table 3.2 Summary of hydrolysis models associated with the adsorption kinetics

#	Reaction kinetics	Additional expression	Comment	Ref.
1	$r_C = \frac{k_h \cdot E_B \cdot R_S \cdot X_S}{1 + S_{glu}/K_{iG} + S_{cel}/K_{iC} + S_{xyl}/K_{iX}}$	$R_S = \frac{X_S}{X_S^0}$	The inhibition by xylose and substrate reactivity (R_S) were considered and simulated in the model,	(Kadam et al., 2004)
2	$r_C = \frac{k_h \cdot E_B^C \cdot X_C^{Eff}}{1 + S_{glu}/K_{iG}}$	$X_C^{Eff} = \left(\frac{X_C}{X_C^0}\right)^{\lambda} \cdot X_C$	X_C^{Eff} is the concentration available for enzyme adsorption	(Liao et al., 2008)
3	$r_C = k_{de} \cdot X_{CE} - k_{ad} \cdot X_C \cdot E_F + \sigma \frac{dC_p}{dt}$	$\frac{dC_p}{dt} = k_p \cdot X_{CE}$	Difficult to quantify and distinguish the enzyme adsorption to and desorption from cellulose	(Gan et al., 2003)
4	$r_C = \frac{k_h \cdot E_B \cdot (X_S - X_S^{\max})}{1 + S_{glu}/K_{iG} + S_{cel}/K_{iC} + S_{xyl}/K_{iX}}$	N/A	The model was modified from Kadam's model with the replacement of substrate reactivity with a substrate saturation constant ($X_S^{\max}$)	(Mutturi & Lidén, 2014)
5	$r_C = \frac{k_h \cdot E_B^C \cdot X_C}{1 + S_{glu}/K_{iG}}$	$E_B^C = E_B \cdot \frac{X_C}{X_S}$	E_B^C is the enzyme adsorbed on celluose	This study

3.2 Selection of model principles

To construct a proper model structure to simulate the interested mechanisms during enzymatic hydrolysis, we reviewed the most applied model structures in the literatures and summarized them in **Table 3.1** and **Table 3.2**. The simulation models were composed of ordinary differential equations (ODEs) associated with different reaction kinetics and sub-functions (to characterize/quantify the relationships among different parameters with physical meanings). The enzyme adsorption functions in the hydrolysis model can be classified into eight major categories (**Table 3.1**). The complexity of the model increased over time, of which the four adsorption functions published between 1983 and 2008 (Fan & Lee, 1983; Kadam et al., 2004; Liao et al., 2008; Xu & Ding, 2007) did not consider the dynamic changes of adsorbed enzyme on the substrates. Gan et al. (2003) applied separated first order adsorption and desorption kinetics to simulate the dynamic changes of adsorbed enzyme on the substrate, but the model cannot quantify the impacts of non-productive adsorption of enzyme to lignin. Finally, Wang et al. (2014a) developed a model structure with the combination of the adsorption parameters and dynamic adsorption of enzyme on the substrate, but the simulation results did not fit well with the experimental data.

The enzyme adsorption kinetics were incorporated into five basic forms of reaction kinetics (**Table 3.2**). Most of the hydrolysis kinetics are constructed based on the well-known Monod function associated with inhibiting coefficients of concerned reagents, products, impurities, and/or additives (Kadam et al., 2004; Liao et al., 2008; Mutturi & Lidén, 2014). The model structure proposed by Gan et al. (2003) described the comprehensive relationships among various forms of celluloses with reasonable fits between the simulated and measured sugars, but the model structure need further development to characterize the hydrolysis of lignocellulosic substrate and the impacts of additives.

The following assumptions are made for the entire model structure of enzymatic hydrolysis and fermentation processes:

1. The enzymatic hydrolysis was a two-step reaction that included enzyme adsorption on the surface of substrate and cellulose hydrolysis induced by the attached enzyme complex.
2. The three major enzymes (endo-β-glucanase, exo-β-glucodiase, and β-glucosidase) involved in the cellulose hydrolysis were regarded as one enzyme with multiple functions, quantified by protein concentration in the systems.
3. The hydrolyzability of the amorphous and crystalline fraction of cellulose are the

same, which agreed with the current understanding of a specific fraction of various enzymes in the commercial enzyme complex for cellulose hydrolysis.

4. The structure of the substrate was uniform for enzyme adsorption and the components of the substrate and products are evenly distributed in the hydrolysis and fermentation system.

3.3 Model structure of hydrolysis

To quantify the impacts of lignin contents to enzyme adsorption, a few modifications were made to combine the equilibrium enzyme adsorption functions with the hydrolysis kinetics. The simulation was first expressed by the adsorption isotherm of solid substrate (real solid biomass with various fraction of carbohydrate and lignin under different pretreatment conditions) and isolated lignin under equilibrant condition (no hydrolysis, at 4°C) to obtain the equilibrium constants. The enzyme adsorption followed by Langmuir isotherm with a first order reaction was descried in Equation (**3-1**) :

$$E_{eq}^{i} = \frac{\sigma_{max}^{S} \cdot X_{S}^{0} \cdot E_{F}}{k_{d} + E_{F}} \tag{3-1}$$

where the subscribe/superscribe *i* represented the solid substrate, and lignin; E_{eq}^{i} is the concentration of enzyme adsorbed on the surface of substrate (mg/L) at the equilibrium state; σ_{max} is maximun adsorption capacity (g/g); k_d is Langmuir equilibrium constant, (g/L); and E_F is the measured free enzyme concentration in the liquid (mg/ L).

The adsorption capacity of cellulose fraction in the pretreated solid can be deduced from the adsorption parameters from Equation (3-1) for solid and lignin that assuming complete accessibility of enzyme to cellulose and lignin in the pretreated solid and adsorption of hemicellulose was negligible (Kumar & Wyman, 2009).

$$\sigma_{max}^{C} = \frac{\sigma_{max}^{S} - \sigma_{max}^{L} \cdot f_L}{f_C} \tag{3-2}$$

With the information of adsorption isotherm, the dynamic status of enzyme adsorption on the overall solid substrate, and lignin can be described by pseudo first order kinetics as:

$$\frac{dE_B}{dt} = k_{ad} \cdot (E_{eq} - E_B) \tag{3-3}$$

where k_{ad} is adsorption rate constant (1/h); E_B and E_{eq} are the actual and equilibrium

enzyme concentration during enzymatic hydrolysis (g/g).

The actual absorbed enzyme on cellulose can be deduced as in Equation (3-4):

$$E_B^C = E_B \cdot \frac{X_C}{X_S} \tag{3-4}$$

The cellulose hydrolysis rate (r_C) was modeled as a first order kinetic reaction in turn of concentration of adsorbed enzyme on cellulose, cellulose concentration, and glucose inhibition as:

$$r_C = \frac{k_h \cdot E_B^C \cdot X_C}{1 + S_{glu} / K_{IG}} \tag{3-5}$$

where S_G and X_C are the concentrations of glucose and cellulose (g/L), respectively; E_T is the total enzyme loading in the system (mg/L); K_{iG} is the glucose inhibition constant (53.16 L/g) (Philippidis et al., 1993).

A fractal kinetic equation was used to describe the hydrolysis rate coefficient k_h (L/g-h), which decays over time with a fractal exponent h as shown in Equation (**3-6**) as follows:

$$k_h = k \cdot t^{-h} \tag{3-6}$$

where k is the hydrolysis rate constant.

Apart from glucose, lignin is the second abundant composition in after pretreatment. The residual lignin presents a chemical and physical barrier to the cellulose hydrolysis under various condition and solvent applied in the pretreatment, which related to the condensation level of the lignin after pretreatment. For the fed-batch and continuous system of hydrolysis and fermentation, the lignin will be accumulated during the process and lead to inhibition to the hydrolysis. A lignin inhibition term was added to the cellulose hydrolysis model as follows:

$$r_C = \frac{k_h \cdot E_B^C \cdot X_C}{1 + S_{glu} / K_{IG}} \cdot \frac{K_{IL}}{K_{IL} + S_L} \tag{3-7}$$

The overall mass balance for the cellulose (solid) and glucose (dissolved) can be expressed as follows:

$$\frac{dS_{glu}}{dt} = 1.11 \cdot r_C \tag{3-8}$$

$$\frac{dX_C}{dt} = -r_C \tag{3-9}$$

$$E_F = E_T - E_B^S \tag{3-10}$$

$$E_B^S = E_B^C + E_B^H + E_B^L \tag{3-11}$$

3.4 Fermentation model

The configuration of the bioreactor operations and model development and validation in various process modes are illustrated in

Figure 3.2. The model parameters, such as the growth kinetics were validated by seeking for the least differentials between the simulation results and experimental data. The model was applied to simulate the biological systems with increased complexity of the process conditions, *i.e.*, from batch reactor with three single sugars; batch reactor with mixed sugars; the continuous flow stirring tank rector (CFSTR); and to the continuous co-fermentation with cell recycling (CF/CR). The following equations for sugar utilization were derived to establish the mass balance in the dynamic situations of the reagents and products in the fermentation systems.

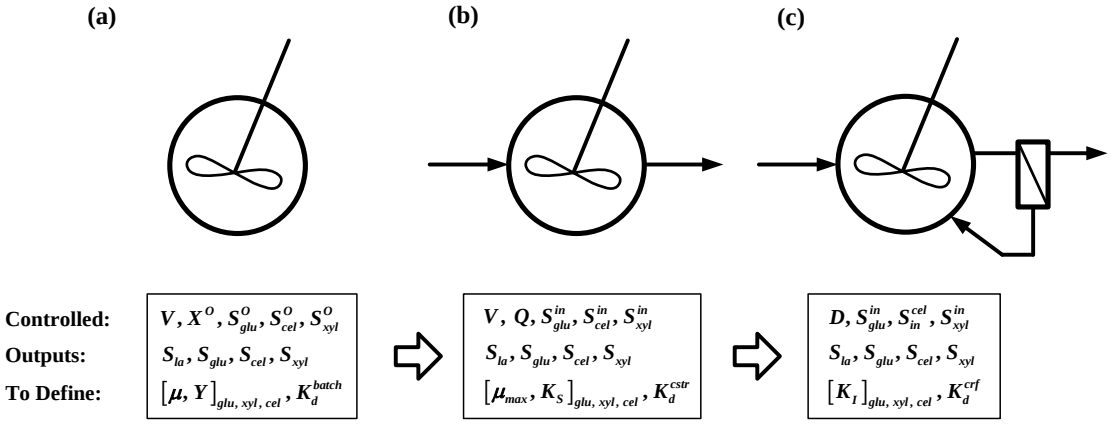

Figure 3.2 Tested and simulated systems with key model parameters; (a) batch reactor; (b) continuous flow; and (c) continuous flow with cell recycling (dilution ratio (*D*) is the inverse of cell retention time). Controlled parameters described the experimental design; growth kinetics is given after references or model validation; outputs are simulated data.

The stoichiometry describing sugar consumption, and productions of cell and lactic acid was derived to clarify the molar yield coefficients of the studied strain. The empirical functions were constructed upon the Embden-Meyerhof-Parnas (EMP) pathway and the pentose phosphate (PP)/glycolic pathway from hexose and pentose, respectively; or the homo-lactic acid metabolism, as detailed by Wang et al. (Wang et al., 2015). Based on this metabolism it was assumed that no respiration (formation of CO_2) occurred from the simulated carbon sources. Meanwhile, the fermentation by-products (*i.e.*, acetic acid and ethanol) through the hetero-lactic acid metabolism (*i.e.*, phosphoketolase, or the PK pathway (Wang et al., 2015)) was negligible as confirmed in our previous study (Wang et al., 2014b). The stoichiometry of the

interested carbon sources were expressed as follows:

Glucose ($C_6H_{12}O_6$ = 180 g/mol):

$$C_6H_{12}O_6 + Y_{glu}NH_4^+ \rightarrow Y_{glu}C_5H_7NO_2 + \left(2 - \frac{5}{3}\cdot Y_{glu}\right)C_3H_6O_3 + 3\cdot Y_{glu}H_2O + Y_{glu}H^+ \quad (3\text{-}12)$$

Cellobiose ($C_{12}H_{22}O_{11}$ = 342 g/mol):

$$C_{12}H_{22}O_{11} + Y_{cel}NH_4^+ \rightarrow Y_{cel}C_5H_7NO_2 + \left(4 - \frac{5}{3}\cdot Y_{cel}\right)C_3H_6O_3 + \left(3\cdot Y_{cel} - 1\right)\cdot H_2O + Y_{cel}H^+ \quad (3\text{-}13)$$

Xylose ($C_5H_{10}O_5$ = 150 g/mol):

$$C_5H_{10}O_5 + Y_{xyl}NH_4^+ \rightarrow Y_{xyl}C_5H_7NO_2 + \frac{5}{3}\cdot\left(1 - Y_{xyl}\right)C_3H_6O_3 + 3\cdot Y_{xyl}H_2O + Y_{xyl}H^+ \quad (3\text{-}14)$$

where Y_{glu}, Y_{cel}, and Y_{xyl} are molar yields of cell production over the respective consumed substrates. It was assumed that all the substrates can be used for cell growth and lactic acid production. The molecular weight of the cell ($C_5H_7NO_2$) is 113 g/mol, and the molecular weight of lactic acid ($C_3H_6O_3$) is 90 g/mol. The mass yields (in wt.%) of cell biomass (X) and lactic acid (S_{la}) were calculated based on the molar ratios as the following expressions using cellobiose as an example. Glucose and xylose were calculated in similar fashions.

$$Y_{cel}^{X} = Y_{cel} \cdot \frac{113}{342} \tag{3-15}$$

$$Y_{cel}^{LA} = \left(3 \cdot Y_{cel} - 1\right) \cdot \frac{90}{342} \tag{3-16}$$

where Y_{cel}^{X} and Y_{cel}^{LA} are the mass yields of cell and lactic acid per unit mass cellobiose consumed (wt.%), respectively.

Cell growth and lactic acid production were described by the utilization of glucose, cellobiose and xylose as substrates during single and mixed sugar fermentation. Substrates and production inhibition were observed in batch fermentation experiments with *E. mundtii* QU 25 (Abdel-Rahman et al., 2013; Abdel-Rahman et al., 2015). Cell growth was defined by Monod kinetics with substrate and production inhibition terms as shown in Equation (**3-17**). The consumptions of glucose, cellobiose and xylose were described by a linear relationship with cell growth. Lactic acid formation was also associated with cell growth.

$$\mu^{sug} = \frac{\mu_{max}^{sug} \cdot S_{sug}}{K_S^{sug} + S_{sug} + \frac{{S_{sug}}^2}{K_I^{sug}}} \cdot \frac{K_I^{LA}}{K_I^{LA} + S_{LA}} \tag{3-17}$$

Where μ_{max} is the maximum specific growth rate of the cell (1/h); K_S is the half saturation concentration (g/L); and K_I^{sug} and K_I^{LA} are the inhibition coefficients of substrate and product (g/L), respectively.

Sugar consumption and lactic acid production are associated with cell growth (Luedeking & Piret, 1959). The following ordinary differential equations (ODEs) were derived to quantify the dynamic changes of the reactants and products:

Sugar (S_{sug}) consumption:

$$\frac{dS_{sug}}{dt} = D \cdot \left(S_{sug}^{in} - S_{sug} \right) - \mu^{sug} \cdot X \cdot \frac{1}{Y_{sug}^{X}} \tag{3-18}$$

Cell growth:

$$\frac{dX}{dt} = D \cdot \left(X^{in} - X \right) + \left[\mu^{glu} + \mu^{cel} + \mu^{xyl} - K_D \right] \cdot X \tag{3-19}$$

Lactic acid production:

$$\frac{dS_{LA}}{dt} = D \cdot \left(S_{LA}^{in} - S_{LA} \right) + \left[\frac{Y_{glu}^{LA}}{Y_{glu}^{X}} \cdot \mu^{glu} + \frac{Y_{cel}^{LA}}{Y_{cel}^{X}} \cdot \mu^{cel} + \frac{Y_{xyl}^{LA}}{Y_{xyl}^{X}} \cdot \mu^{xyl} \right] \cdot X \tag{3-20}$$

where S_{sug} is a general form of glucose (S_{glu}), cellobiose (S_{cel}), and xylose (S_{xyl}), each with independent metabolic kinetics; D is the dilution rate (1/h); and K_D is the decay coefficient (1/h). A total of five ODEs were derived in our calculation.

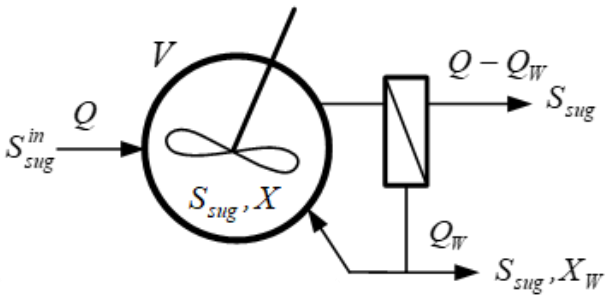

Figure 3.3 CF/CR system

The following section showed the step-by-step procedure that reforming the dynamic bioreactor model into the steady-state expressions in the continuous flow co-fermentation system with cell recycling control (the CF/CR process, **Figure 3.3**). The fermentation cells (X) and sugar (S_{sug}) concentrations were presented in functions of two key control parameters, *i.e.*, the hydraulic retention time (HRT) and the cell retention time (CRT). The calculation was developed in a similar fashion as presented in Leu et al. (Leu et al., 2009), based on the Monod kinetics and Lawrence and McCarty expressions (Lawrence & McCarty, 1970) as follow:

For cells:

$$\frac{dX}{dt} = -\frac{Q_W \cdot X_W}{V} + (\mu - K_D) \cdot X \tag{3-21}$$

For sugars:

$$\frac{dS_{sug}}{dt} = \frac{1}{HRT} \cdot \left(S_{sug}^{in} - S_{sug} \right) - \frac{\mu}{Y_{sug}^{X}} \cdot X \tag{3-22}$$

where Q_W is the wasted flow rate of the discharged cell (L/h); X_E and X_W are effluent and wasted cell concentration (g/L); μ is the growth rate of the cell (1/h). The rest of the nomenclature please refer to the main text.

At steady state, dX/dt and $dS_{sug}/dt = 0$

From Equation (**3-21**)

$$\mu - K_D = \frac{Q_W \cdot X_W}{X \cdot V} \tag{3-23}$$

From Equation (**3-22**)

$$\mu \cdot \frac{X}{Y_{sug}^{X}} = \frac{1}{HRT} \cdot \left(S_{sug}^{in} - S_{sug} \right) \tag{3-24}$$

By definition

$$CRT = \frac{X \cdot V}{Q_W \cdot X_W} \tag{3-25}$$

Therefore,

$$\mu - K_D = \frac{1}{CRT} \tag{3-26}$$

Substitute μ in (**3-24**) with (**3-26**)

$$\frac{1}{Y_{sug}^{X}} \cdot \left(K_D + \frac{1}{CRT} \right) = \frac{1}{HRT} \cdot \frac{\left(S_{sug}^{in} - S_{sug} \right)}{X} \tag{3-27}$$

Therefore,

$$X = Y_{sug}^{X} \cdot \frac{CRT}{HRT} \cdot \left(\frac{S_{sug}^{in} - S_{sug}}{K_D \cdot CRT + 1} \right) \tag{3-28}$$

With Monod kinetics

$$\mu = \frac{\mu_{\max} \cdot S_{sug}}{K_S + S_{sug}} \tag{3-29}$$

Apply Equation (**3-29**) to Equation (**3-26**)

$$\frac{\mu_{\max} \cdot S_{sug}}{K_S + S_{sug}} - K_D = \frac{1}{CRT} \tag{3-30}$$

After rearrangement

$$S_{sug} = \frac{K_S \cdot (1 + CRT \cdot K_D)}{CRT \cdot (\mu_{\max} - K_D) - 1} \tag{3-31}$$

In a short CRT process or CSFTR process operating at high dilution rate, the limiting cell retention time occurred when $CRT \cdot (\mu_{\max} - K_D) - 1 \leq 0$, so the critical CRT will be:

$$CRT = \frac{1}{\mu_{\max} - K_D} \tag{3-32}$$

3.5 Validation of parameters

The model was coded by Matlab R2013a (MathWorks). The dynamic functions were solved by using the 'ODE45' function (Runge-Kutta formula). The simulation results were fit with the experimental data obtained at designed conditions, chemicals, and substrates as detailed in the next section. The optimization function 'lsqnonlin' developed upon Levenberg-Marquardt algorithm was adopted for the non-linear least square (*SSD*) minimization over the residual between model values (X_{pi}) and the

corresponding experiment data (X_{expi}). The objective function to estimate the kinetic parameters follows:

$$SSD = \min \sum_{i=1}^{n} \sqrt{(X_{pi} - X_{expi})^2} \tag{3-33}$$

where X_{pi} and $X_{\exp i}$ are the model predicted value and experimental data, respectively; n is the number of experimental data.

In addition to parameters optimization, sensitivity analysis was also conducted to visualize and identify the importance of different parameters that can more significantly affect the reaction.

Chapter 4 Solvent Induced Lignin-Cellulase Interaction on Enzymatic Kinetics for Organosolv Pretreated Lignocellulosic Substrate Interaction on Enzymatic Kinetics for Organosolv Pretreated Lignocellulosic Substrate

4.1 Background

Lignocellulosic biomass is an abundant and sustainable resource produce biofuels through biorefinery processes to address global energy demand and reduce reliance on fossil fuels. The major components of lignocellulosic biomass are cellulose, hemicellulose and lignin, which form the complicated structure of plant cell wall. Pretreatment and enzymatic hydrolysis are the critical and essential processes for the bioconversion of lignocellulosic biomass. Pretreated biomass with various lignin features is produced after different pretreatment methods, in which chemical composition and structure of the feedstock are changed. In order to efficiently covert biomass into fermentable sugars, it should maximally remove lignin while minimize the modification of polysaccharides by pretreatment (Ding et al., 2012) The pretreated biomass may results in certain amount of residual lignin, which might significantly affected the performance of enzymatic hydrolysis by unproductive adsorption of the cellulase, by forming physical barrier to restrict cellulose accessibility to cellulose, by

inhibiting the enzyme accessibility of cellulose, or by deactivating enzyme (Ximenes et al., 2011).

Removal or modification of lignin through appropriate pretreatments could reduce the lignin inhibition to enzymatic hydrolysis of cellulose. Lignin inhibition on enzymatic hydrolysis of cellulose was widely studied but the dynamic interaction between lignin and enzyme, and relationship between lignin inhibition and physiochemical properties of the pretreated lignin have not been sufficiently investigated. Hydrophobicity and phenolic hydroxyl group of the lignin were highly related to the lignin inhibition to enzymatic hydrolysis of cellulose Yang and Pan (2016). Residual lignin is a critical component that in the enzymatic hydrolysis of cellulose. The dynamic lignin-cellulase interaction and cellulose hydrolysis kinetic were investigated in this study.

This study aims to develop a numerical model platform to simulate the dynamic interactions between enzyme adsorption and cellulose hydrolysis of pretreated substrates with various lignin properties and content. A pseudo-first order adsorption kinetic equation was applied to simulate the dynamic changing properties of the enzyme-cellulase system.

4.2 Experiments

4.2.1 Materials

The lignocellulosic biomass used in this study was *Acacia confusa*, which was collected from the tree removal practice by the Hong Kong Highways Department. The biomass was airdried, milled and screened (mesh size < 2 mm). All the chemicals and reagents used in this study were of reagent grades. The commercial enzyme Ctec2 and Pronase were purchased from Novozymes Investment Co. Ltd (Beijing, China) and Sigma Chemical Company (USA) respectively.

4.3 Pretreatment

Form our previous studies (Dong et al., 2019), 1,4-butanediol (1,4-BDO) was selected to use as organosolv with/without acids in in single step and two-staged pretreatment and the detailed operation conditions was presented in **Table 4.1**. The pretreatment was carried out in the similar way as our previous studies (Islam et al., 2021). The pretreatment processes were conducted in a 15 L rotating digester. For the single step of dilute acid (DA) pretreatment, a batch of 1 kg (oven-dried weight) of wood powder was mixed with 50 mM sulfuric acid (H_2SO_4) at the liquid to solid ratio of 3:1. For the single step acid catalyzed 1,4-BDO pretreatment, 1,4-BDO and 50 mM H_2SO_4 was mixed with biomass at the liquid to solid ratio of 7:1. The biomass and solvents were loaded in

the stainless-steel digester. The digester was heated to 170°C and maintained at this designed temperature for 1 hour. For the two-staged pretreatment, organosolv and acid were added with the substrate for a separated treatment in sequence. For $DA_{20}BDO_{40}$, the biomass was treated with dilute H_2SO_4 for 20 min at a liquid to solid ratio of 3:1 at 170°C; and then the pretreatment liquor and solid were separated by the Buchner filter. The half-pretreated substrate was then treated with 1,4-BDO for 40 min at a liquid to solid ratio of 4:1 at 170°C. The $BDO_{40}DA_{20}$ pretreatment, the biomass was treated in the similar way with the organosolv (1,4-BDO) treatment followed by the dilute acid (H_2SO_4). The pretreated substrates were washed two times with the organosolv after every 1,4-BDO treatment and then washed thoroughly with DI water after the overall pretreatment. The pretreated solids were collected and stored at 4°C.

Table 4.1 Pretreatment operation conditions for the lignocellulosic biomass

Pretreatment	First stage				Second stage			
	Temp. (°C)	Time (min)	Solvent	L/S ratio[a]	Temp. (°C)	Time (min)	Solvent	L/S ratio
DA_{20}[b]	170	20	H_2SO_4	3	-	-	-	-
BDO_{60}[c]	170	60	1,4-BDO + H_2SO_4	4	-	-	-	-
$DA_{20}BDO_{40}$[d]	170	20	H_2SO_4	3	170	40	1,4-BDO	4
$BDO_{40}DA_{20}$[e]	170	40	1,4-BDO	4	170	20	H_2SO_4	3

[a] liquid to solid ratio; [b] DA_{20} – dilute acid pretreatment; [c] BDO_{60} – acid catalyzed 1,4-butanediol pretreatment; [d] $DA_{20}BDO_{40}$ – dilute acid followed by 1,4-butanediol pretreatment; [e] $BDO_{40}DA_{20}$ - 1,4-butanediol followed by dilute acid pretreatment.

4.3.1 Lignin preparation

Lignin was isolated from the pretreated substrates with prolonged incubation of a high enzyme loading (50 FPU/g solid) at 50˚C. After two times of extensive hydrolysis of the pretreated substrates with fresh enzyme for 72 h, the residual lignin was recovered by centrifugation and washed three times by resuspension in 500 mL DI water and sonication for 1 h. The residue was resuspended in a phosphate buffer (pH 7) with Pronase (1 U/mL) and incubated at 37˚C for 24 h to remove the adsorbed enzyme from the residual lignin (Kumar & Wyman, 2009). The protease was deactivated by heating at 90˚C for 1 h. The residual lignin was washed three times with DI water and freeze dried and kept in zipped bag for further analysis and experiment. Chemical composition of the residual lignin was conduced, and the lignin content was 92.2 to 94.3%

4.3.2 Enzyme adsorption

The enzyme adsorption of pretreated substrates and isolated lignins were conducted with solid loading of 2% (w/v) and the enzyme dosage of 5, 10, 15, 20, 30, 40, 50 mg protein/g solid. The pretreated substrates (or isolated lignins) were incubated in sodium acetate buffer (pH4.8) in 15 mL centrifuge tube on an end-over-end rotator (70rpm) for 2 h at 4˚C to avoid hydrolysis of cellulose (Kumar & Wyman, 2009). Samples were taken after achieving adsorption equilibrium and were centrifuged at 5000 rpm. The

protein concentration of the supernatant was determined by the BCA method (Smith et al., 1985) using bovine serum albumin (BSA) as standard. All experiments were conducted in duplication and average values are presented in the discussion section.

4.3.3 Enzymatic hydrolysis

Enzymatic hydrolysis of pretreated substrates was carried out at 2% (w/v) solid loading with an enzyme loading of 15 mg protein/g solid in a 250 mL flask. The working volume was 50 mL and the pretreated substrate was mixed with 50mM acetate buffer (pH 4.8) and incubated in a rotary shaker at 50˚C and 150 rpm. A 1 mL sample of the well-mixed solution was taken at the time point of 0, 3, 6, 9, 12, 24, 48, and 72 h for further chemical analysis. To investigate the effects of lignin on enzymatic hydrolysis, various concentration of lignin (0-50%) were mixed with microcrystalline cellulose (MCC)in the incubation system. A 2% solid loading of mixed isolated lignin and MCC at designated fractions was prepared for enzymatic hydrolysis as described above. All experiments were conducted in duplication and average values are presented in the discussion section.

4.3.4 Analytical analysis

The chemical composition analysis of the pretreated substrate was conducted to

evaluate fraction of major building block chemicals (*i.e.,* cellulose, hemicellulose and lignin) before and after the designated pretreatments according the standard National Renewable Energy Laboratory with the two-step acid hydrolysis (Sluiter et al., 2008). The structure of isolated lignins from pretreated substrates was determined by the two-dimensional heteronuclear single quantum coherence nuclear magnetic resonance (2D-HSQC NMR) to provide quantitative information of the linkages in the lignin. The detailed procedures were described on our previous studies (Dong et al., 2019; Islam et al., 2021)

4.4 Result and discussion

4.4.1 Characteristic of pretreated substrates

Table 4.2 Chemical composition of the pretreated biomass

Pretreatment	Solid yield, %	Cellulose, %	Hemicellulose, %	Lignin, %
Raw [a]	100	37.9	15.9	30.3
DA_{20} [b]	55.2	39.3	ND[f]	52.6
BDO_{60} [c]	58.8	64.2	6.1	27.7
$DA_{20}BDO_{40}$ [d]	53.4	43.0	ND	51.5
$BDO_{40}DA_{20}$ [e]	63.3	59.9	1.6	33.8

[a] raw biomass of *A. confusa*; [b] DA_{20} – dilute acid pretreatment; [c] BDO_{60} – acid catalyzed 1,4-butanediol pretreatment; [d] $DA_{20}BDO_{40}$ – dilute acid followed by 1,4-butanediol pretreatment; [e] $BDO_{40}DA_{20}$ - 1,4-butanediol followed by dilute acid pretreatment; [f] ND - not detected.

4.4.2 Adsorption isotherm of substrates and lignins

The enzyme adsorption of various pretreated solid was conducted at 4˚C to avoid the cellulose hydrolysis of cellulose. The adsorption kinetics parameters of the solid substrate were determined by nonlinear regression adopting the Langmuir adsorption equation (Equation (3-1)) as described in the previous chapter and summarized in **Table 4.3**. The experimental data of cellulase adsorption followed the Langmuir kinetic well as illustrated in **Figure 4.1**. The substrate of BDO_{60} showed a highest maximum adsorption capacity of 93.86 mg/g substrate, and followed by $BDO_{40}DA_{20}$ substrate of 67.98 mg/g substrate. These two substrates had a relatively low lignin content at around 30%. While the maximum enzyme adsorption capacity of substrate by DA_{20} and $DA_{20}BDO_{40}$ showed low values of 55.30 and 36.19 mg/g substrate, respectively, which with a higher lignin content of more than 50%.

Table 4.3 Enzyme adsorption parameters of adsorption isotherm at 4˚C

Sample	σ_{max}^{S} (mg/g substrate)	k_d^S (mg/mL)	σ_{max}^{L} (mg/g lignin)	k_d^L (mg/mL)	σ_{max}^{C} (mg/g cellulose)
DA_{20}[b]	55.30	0.33	62.83	2.86	58.68
BDO_{60}[c]	67.98	0.52	15.66	0.48	99.10
$DA_{20}BDO_{40}$[d]	36.19	0.21	63.26	0.92	8.47
$BDO_{40}DA_{20}$[e]	93.86	1.07	34.87	1.30	137.06

[a] raw biomass of *A. confusa*; [b] DA_{20} – dilute acid pretreatment; [c] BDO_{60} – acid catalyzed 1,4-butanediol pretreatment; [d] $DA_{20}BDO_{40}$ – dilute acid followed by 1,4-butanediol pretreatment; [e] $BDO_{40}DA_{20}$ - 1,4-butanediol followed by dilute acid pretreatment; [f] ND - not detected.

To further investigate the effects of lignin imposed on cellulase adsorption and enzymatic hydrolysis, residual lignin was isolated from the pretreated substrates by prolonged enzymatic hydrolysis with high enzyme loading. The enzyme adsorption of isolated lignins was conducted at 4°C in consistent with the conditions employed for the pretreated substrates. The cellulase adsorption of isolated lignins followed the Langmuir adsorption equation and the adsorption kinetic parameters were summarized in **Table 4.3**. The maximum adsorption capacity of lignins showed an opposite trend with the values obtained from the pretreated substrate. The $DA_{20}BDO_{40}$-L and DA_{20}-L showed higher values of 63.26 and 62.83 mg/g lignin, respectively. The results show that $DA_{20}BDO_{40}$-L reached the lowest adsorption capacity (15.66 g/g lignin) followed by BDO_{60}-L (34.87 g/g lignin). Ko et al. (2015) reported that the maximum cellulase adsorption capacities of isolated lignins of difference severities from liquid hot water pretreated hardwood were 36.6-44.8 mg/g lignin, while showed a significant difference in the maximum adsorption capacity of lignin isolated from different pretreatment strategies. Isolated lignin from sulfur dioxide pretreatment had the highest adsorption capacity (67.5 mg/g lignin) and ammonia fiber expansion (AFEX) had the lowest adsorption capacity (38.7 mg/g lignin). Kumar et al. (2012) showed the lignin restricted cellulose hydrolysis through

unproductive adsorption of cellulase inhibition of swelling of cellulose and therefore the cellulose accessibility. The cellulose accessibility and hydrolysis yield increased with the increasing lignin removal.

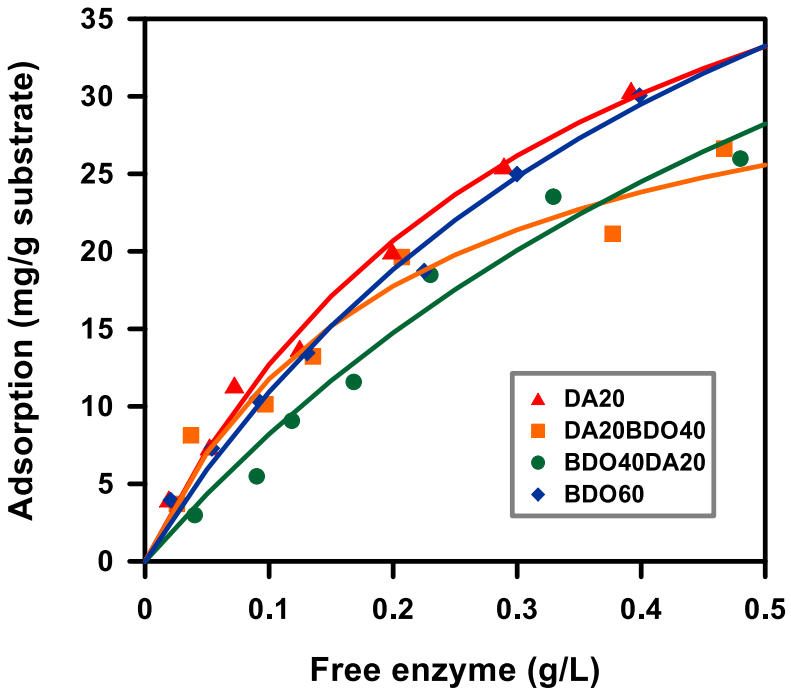

Figure 4.1 Enzyme adsorption kinetics at 4°C with 2% (w/v) solid content and enzyme loading of 5-50 mg/g substrate for pretreated substrate DA_{20}, BDO_{60} and $DA_{20}BDO_{40}$ and $BDO_{40}DA_{20}$. Solid lines fit with Langmuir adsorption isotherm.

The maximum enzyme adsorption capacity of cellulose fraction in the pretreated substrates was determined by the adsorption kinetic parameters of pretreated substrate and the corresponding isolated lignin as described in the chapter of model

development (Equation (3-2)). The values of adsorption capacity of cellulose fraction were listed in **Table 4.3**. Cellulose in $BDO_{40}DA_{20}$ pretreated substrate had the highest adsorption capacity of 137.06 mg/g cellulose followed by the BDO_{60} (99.10 g/g cellulose). Cellulose in the pretreated substrate of $DA_{20}BDO_{40}$ showed the lowest enzyme adsorption capacity of 8.47 mg/g cellulose. The adsorption capacities of cellulose fraction in pretreated substrate showed a same trend with the values calculated from the adsorption isotherm of the corresponding solid substrates.

The substrates of single BDO and BDO first staged pretreatments, had relatively lower values of maximum adsorption capacity of lignin and higher values of cellulose, which were in contract with the single DA and DA first staged pretreatments. The enzyme adsorption of lignin increased with the increasing degree of condensation of lignin during pretreatment process (Yu et al., 2014). Islam et al. (2021) reported that the residual lignin from DA first staged pretreatment contained more than 20% of the condensed structure and organosolv pretreatment prevented lignin condensation by stabilizing lignin. The 2D HSQC NMR spectra of raw substrate, dilute acid and 1,4-BDO pretreated lignin (**Figure 4.4 - Figure 4.6**) showed a structural changed and formation of functional groups after pretreatment. Dong et al. (2019) discovered that lignin deposition was not observed using 1,4-BDO as pretreatment solvent compared

to other conventional pretreatments.

4.4.3 Impact of lignin on adsorption and hydrolysis

To investigate the effect of lignin on cellulose hydrolysis performance and enzyme adsorption, the enzymatic hydrolysis of MCC mixed with various loading of isolated lignin (0-10 g/L) was conducted at 2% solid loading and 15 mg/g substrate. The lignin concentration was ranged from 0 to 50%, which covered the lignin fractions of the pretreated substrates in this study. The initial cellulose conversion rate (t=0) was simplified from the **Equation (3-7)** as following:

$$(r_C)_{t=0} = \text{constant} \cdot \frac{K_{IL}}{K_{IL} + X_L} \tag{4-1}$$

The lignin concentration is the only variable in the equation. The lignin inhibition coefficient (K_{IL}) was obtained by the nonlinear regression of the measured relative initial cellulose conversion rate using **Equation (4-1).** The $DA_{20}BDO_{40}$-L and DA_{20}-L showed lower values of 7.67 g/L and 8.94 g/L, respectively. The $BDO_{40}DA_{20}$-L and BDO_{60}-L had higher values of 16.72 g/L and 15.84 g/L. For lignin concentration of 6 g/L, the cellulose conversion rate was reduced by 40% for $DA_{20}BDO_{40}$-L and DA_{20}-L containing substrate, indicating a serious inhibition. Lignins from the pretreated

substrate of $DA_{20}BDO_{40}$ and BDO_{60} had a moderate inhibition on the cellulose

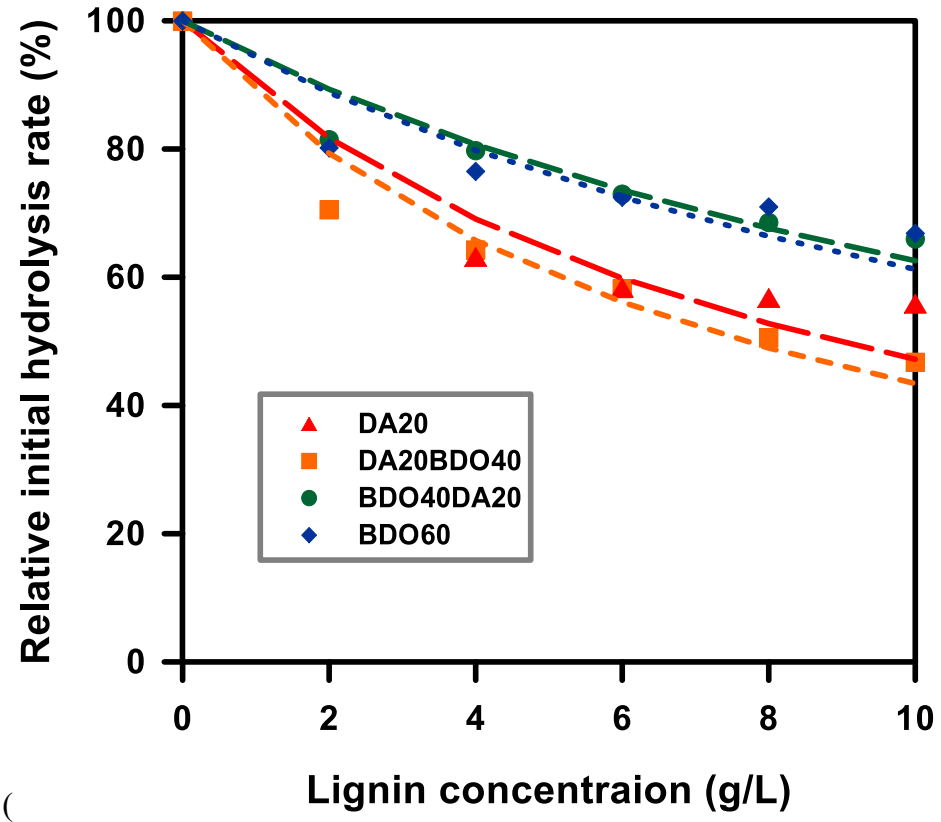

conversion (

Figure 4.2).

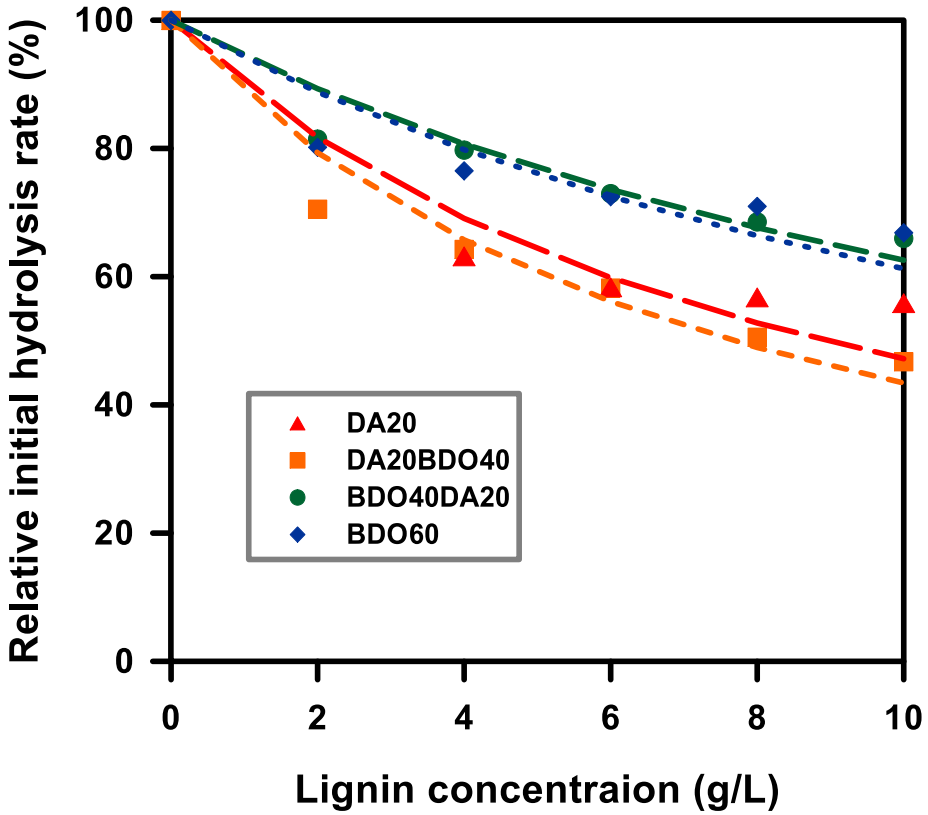

Figure 4.2 Effect of additional lignin of the pretreated substrates on the cellulose hydrolysis rate of the MCC with a 2% (w/v) solid loading and 15 mg/g substrate enzyme loading.

Guo et al. (2014) investigated the functional group and composition of six isolated lignins and found out that guaiacyl (G) lignin have a higher adsorption capacity on enzyme compared to syringyl (S) lignin. A lower S/G ratio was in good correlation with a higher enzyme adsorption capacity on lignin. Dong et al. (2019) reported that the S/G ratio of the lignin prepared from acid catalyzed organosolv pretreated substrate was more than two times lower than the DA pretreated lignin. The 2D HSQC NMR spectra of raw substrate, dilute acid and 1,4-BDO pretreated lignin (**Figure 4.4** - **Figure** 4.6) showed a consistent S/G ratio with the above studies.

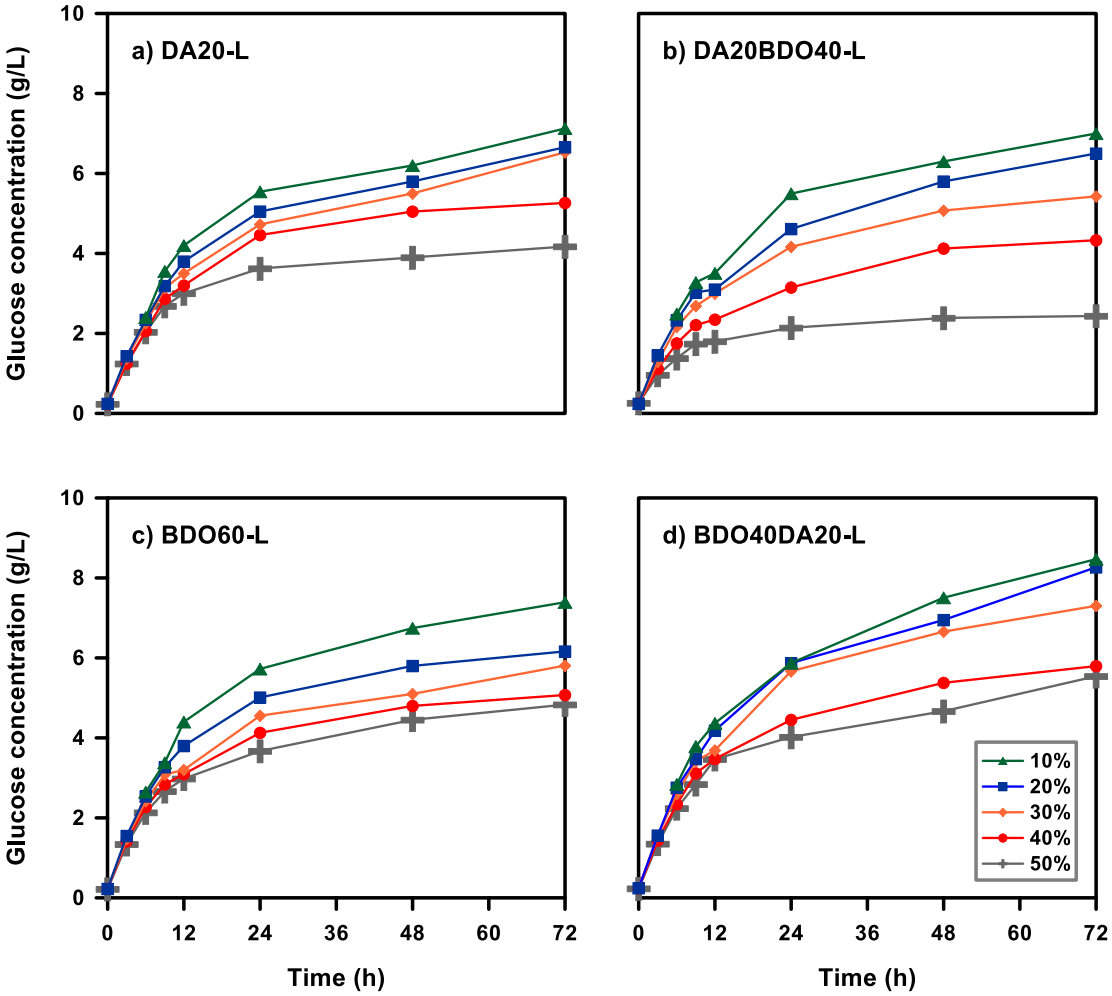

Figure 4.3 Enzymatic hydrolysis of MCC with 10 to 50% of additional lignin prepared from pretreated substrates with a 2% solid loading and 15 mg/g substrate enzyme loading incubated at 50˚C.

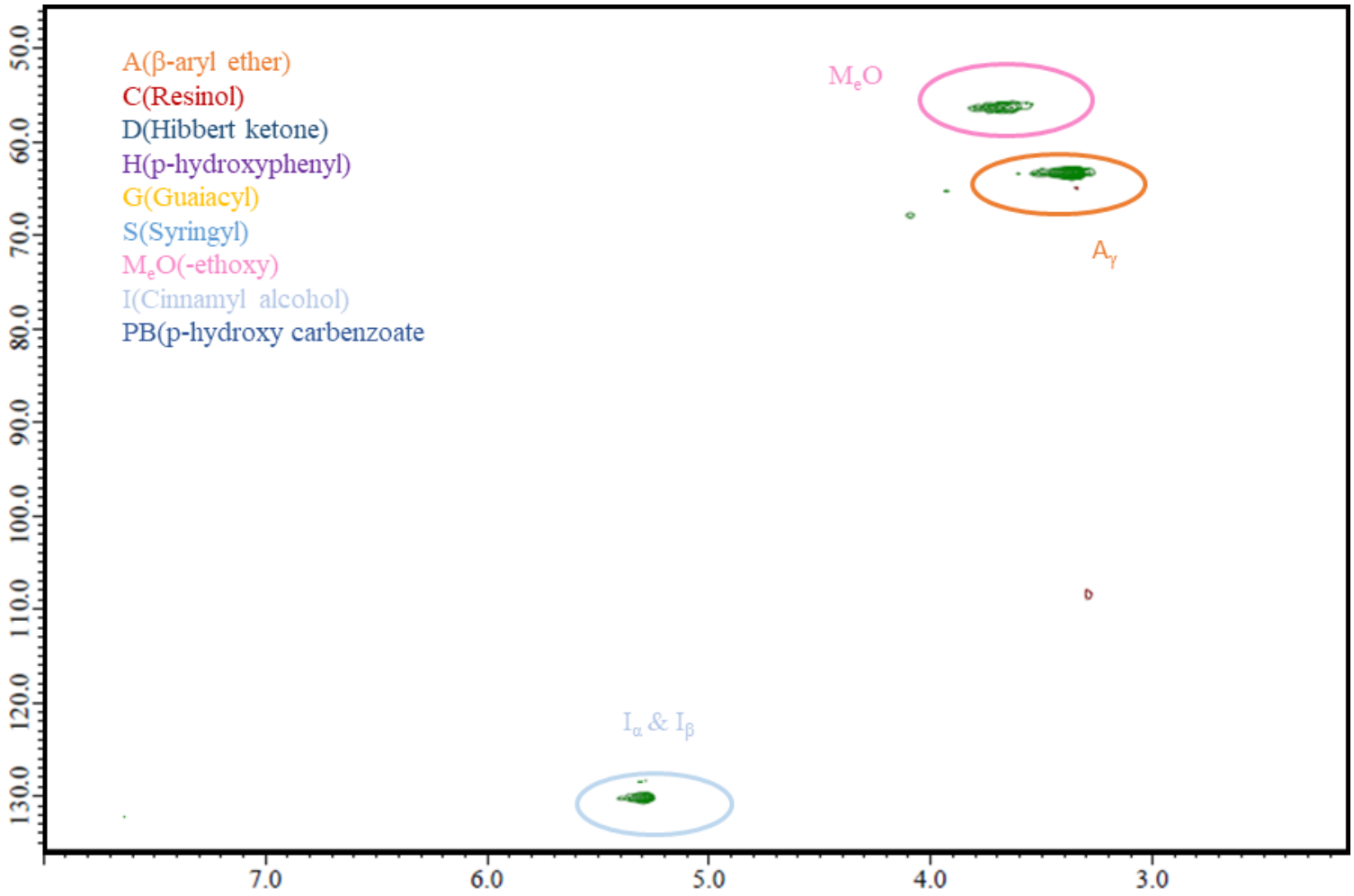

Figure 4.4 2D HSQC NMR spectra of residual lignin isolated of raw biomass of *Acacia confuse*.

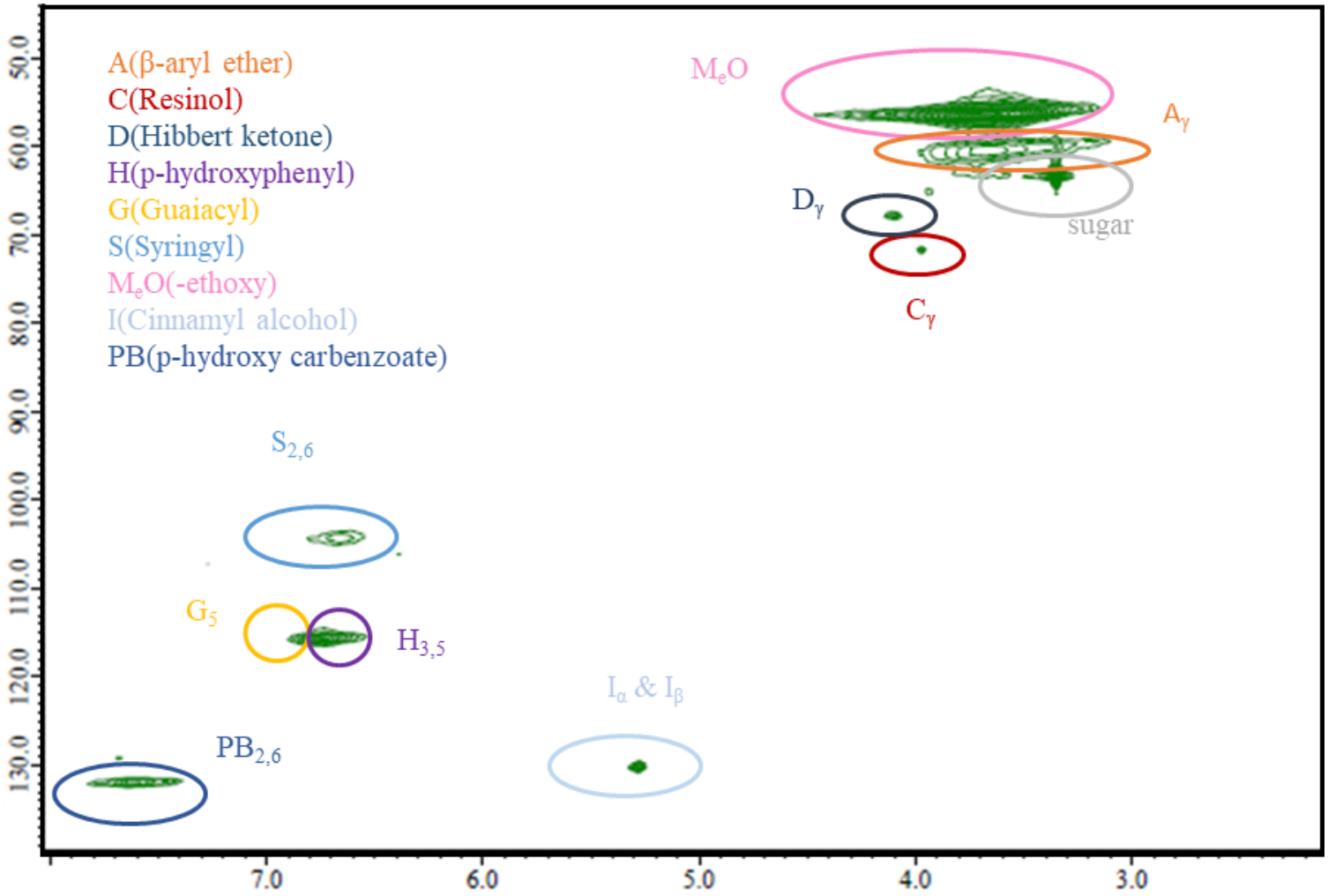

Figure 4.5 2D HSQC NMR spectra of residual lignin isolated after dilute acid pretreatment

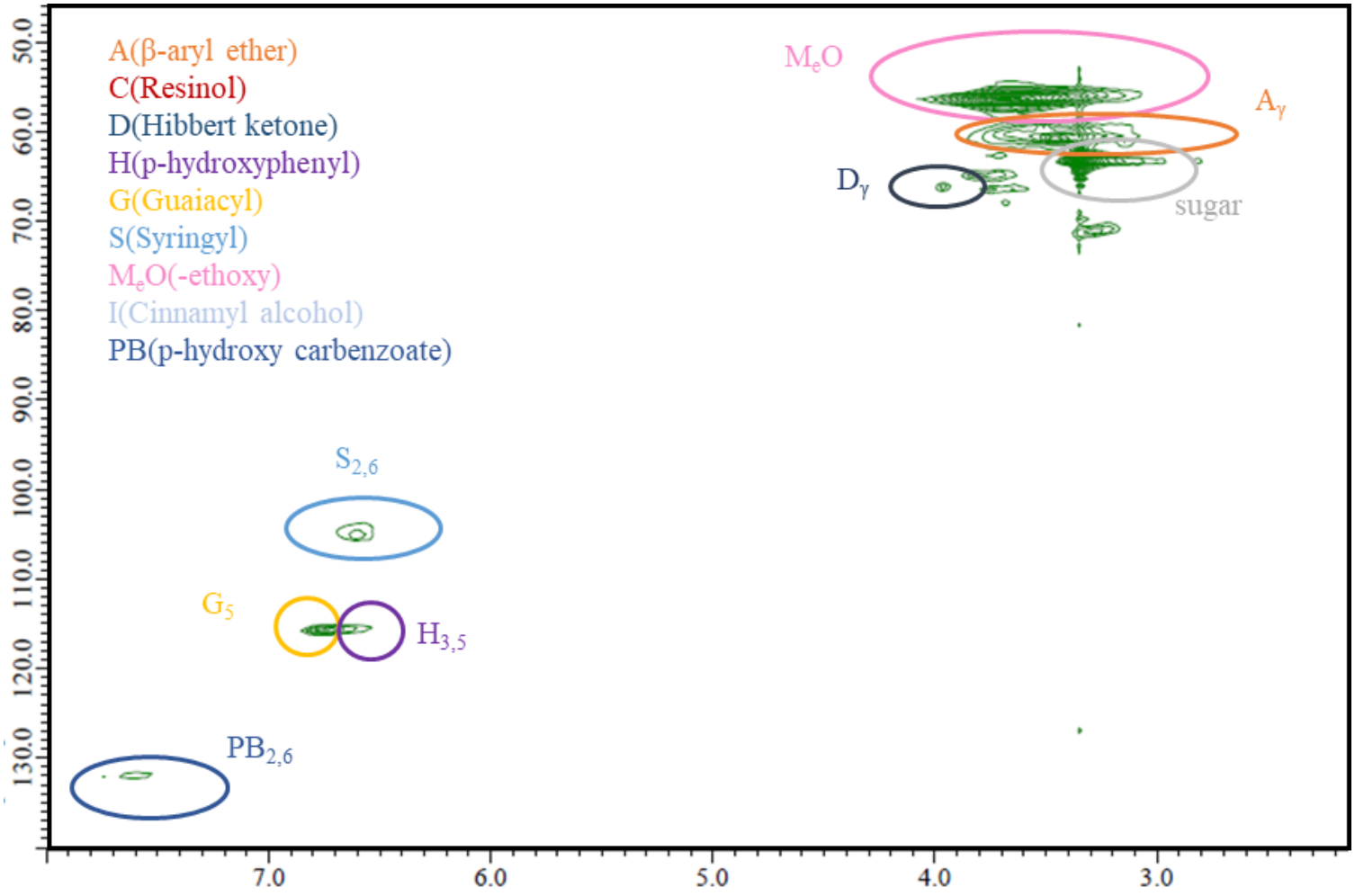

Figure 4.6 2D HSQC NMR spectra of residual lignin isolated after BDO_{60} pretreatment.

4.4.4 Kinetic simulation of pretreated substrates

The enzymatic hydrolysis model was divided into two major parts: enzyme adsorption and cellulose hydrolysis. The model includes the three ODEs and other numerical equations that described in the model development chapter including **Equation (3-1)** to (3-11). The kinetic parameters of the enzyme adsorption and hydrolysis determined by the individual experiments of enzyme adsorption of pretreated substrates and isolated lignin, and enzymatic hydrolysis of MCC with the addition so isolated lignins were used as input to the overall model structure, and the kinetic parameters of cellulose hydrolysis rate constant (k_h) and fractal exponent (h) were determined by the experimental data of enzymatic hydrolysis of pretreated substrates at 2% solid loading (w/v) and 15 mg/g substrate enzyme loading. The operation conditions were in consistent with the previous experiments. The model simulated both enzyme adsorption on the substrate and cellulose hydrolysis of each pretreated substrate and the experimental data fit well

(

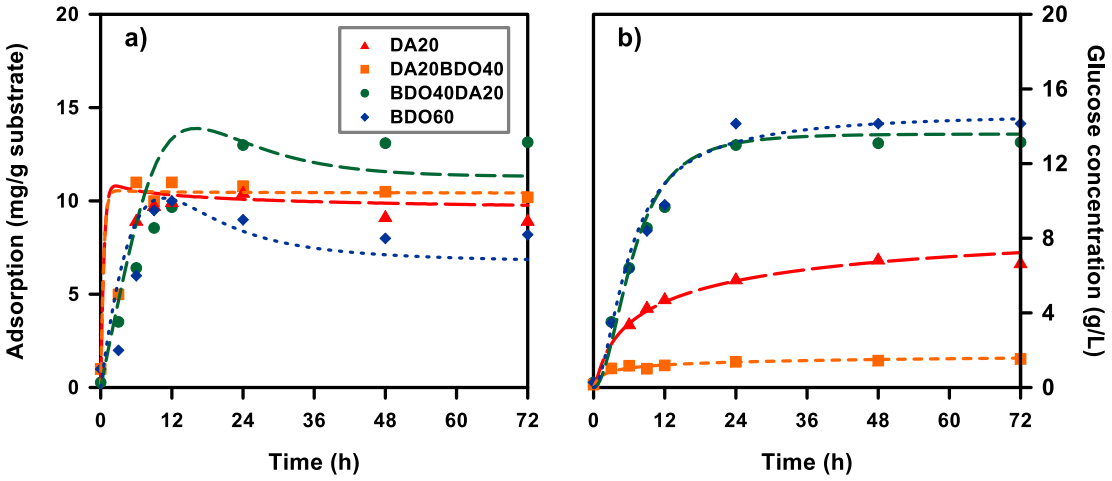

Figure 4.7). The kinetic parameters were summarized in **Table 4.4**. **Figure 4.7** illustrates the cellulose conversion yield of the pretreated substrates. The cellulose of the $BDO_{40}DA_{20}$ and BDO_{60} pretreated substrate were almost completely converted to glucose and the hydrolysis rate showed the similar trend. The enzyme adsorption of lignin correlated with decreased cellulose conversion in enzymatic hydrolysis. The adverse impact of lignin in cellulose hydrolysis not only caused by the inhibiting cellulose from enzyme adsorption, but also due to the physical/chemical properties and structural changed after pretreatment.

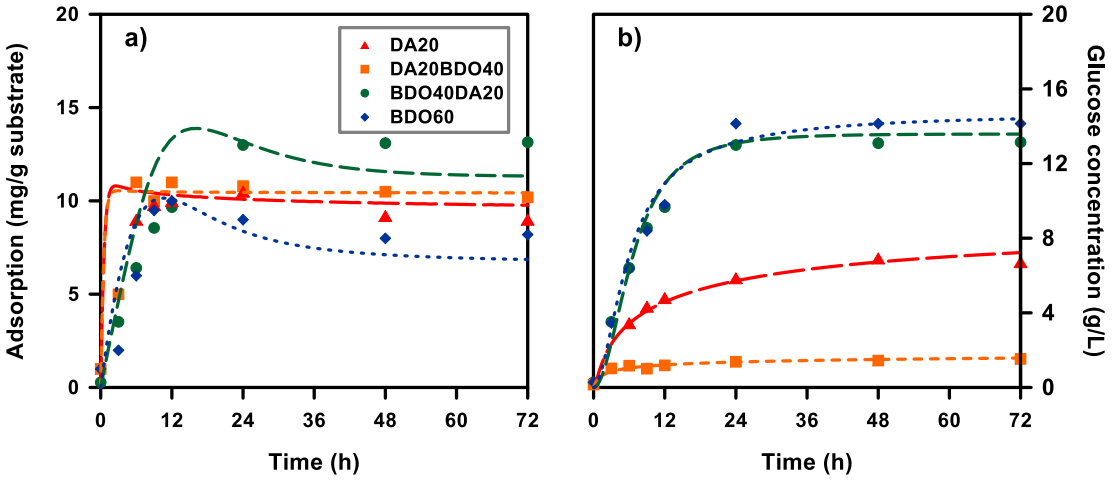

Figure 4.7 Model simulation and experimental results (symbols) of a) dynamic enzyme adsorption and b) glucose release at 50°C with 2% (w/v) solid loading and 15 mg/g substrate enzyme loading for the pretreated substrate of DA_{20}, BDO_{60}, $DA_{20}BDO_{40}$, and $BDO_{40}DA_{20}$.

Table 4.4 Kinetic parameters of enzymatic hydrolysis of the pretreated substrates

Sample	k_{ad}	h	k
DA_{20}[b]	0.7	0.46	0.72
BDO_{60}[c]	0.1	0.1	1.55
$DA_{20}BDO_{40}$[d]	0.9	1.1	0.18
$BDO_{40}DA_{20}$[e]	0.03	0.02	1.5

4.5 Conclusion

A numerical platform integrated with dynamic enzyme adsorption and cellulose hydrolysis was constructed and was successful in simulating the enzyme adsorption on various pretreated substrates of single/two-staged organosolv pretreatments. The incorporation of dynamic enzyme adsorption on substrate provided a better understanding and perspective on the cellulose hydrolysis performance with various types of residual lignins. Applying organosolv before the dilute acid treatment is an

effective way to preserve the integrity of lignin and prevent lignin condensation, and therefore reduce enzyme adsorption on lignin and improve enzymatic hydrolysis. The adsorption and hydrolysis kinetic parameter (σ_{Max}^{L} , k_{ad}, K_{IL}) confirmed that the single 1,4-BDO and 1,4-BDO first staged pretreated substrates had less adverse impact on the performance of cellulose hydrolysis.

Chapter 5 Construction of a Structural Model to Elucidate Additive Associated Lignin-Cellulase Interactions in Complex Bioconversion System

5.1 Background

Converting lignocellulosic biomass into carbonaceous polymers is a sustainable approach to reduce our reliance on fossil fuels. Lignocellulosic biomass is abundant and contains various building block chemicals for valorization. Application of the "wastes-derived biomass" can also avoid the competition between biofuel production and food supply. After tremendous efforts and breakthroughs in the key techniques, however, large scale application of lignocellulose biorefinery is still challenging, which may owe to both technical and non-technical issues. Hydrolysis is a cost intensive process to release fermentable carbon (*e.g.*, glucose and xylose) from the polysaccharides (Humbird et al., 2011). Compared to chemical conversion, enzymatic hydrolysis has attracted significant attention due to its high conversion yield, minimal byproducts formation, and mild operation conditions, but this process also suffers from the significant biomass recalcitrance against bioconversion (dos Santos et al., 2018). Cellulose is entrapped in the complicated 3-D structure of hemicelluloses and lignin,

which is difficult to reach by cellulase (Leu & Zhu, 2013). Pretreatment is an essential process to break down the recalcitrant and improve the efficiency of saccharification. The mechanism of delignification and performances of different pretreatment approaches have been reported outstandingly elsewhere (Mosier et al., 2005; Sathitsuksanoh et al., 2013). The beneficial or negative impacts of dissolved and residual lignin on the pretreated substrate have also been addressed in many publications (dos Santos et al., 2018). The existing work focuses on the development of a robust numerical method to simulate the dynamic status of enzymatic hydrolysis of lignocellulosic substrate in a complex hydrolysate.

Extensive studies of cellulose hydrolysis kinetics have been conducted in the past several decades (Jeoh et al., 2017; Liao et al., 2008; Ye & Berson, 2011). Enzymatic hydrolysis has been characterized as a two-phase heterogeneous process, comprising solid and liquid phases, which is the dynamic interaction between enzyme adsorption on the surface of cellulose and release of reducing sugars. The empirical formula can be applied to quantify the effected of substrate properties, such as specific surface area, crystallinity and lignin content; and enzyme properties like enzyme concentration, and enzyme to solid ratio. Michaelis-Menten is the typical empirical models for homogeneous reactions and is applicable for the initial rate estimation of cellulose

hydrolysis. However, the dynamic interaction and mechanism between cellulase and cellulose are not characterized in the empirical functions. Enzyme adsorption and hydrolysis product inhibition were commonly considered into the kinetic model of enzymatic hydrolysis of lignocellulosic biomass. However, most of the studies mainly focused on the effects of reducing sugar inhibition. Kadam et al. (2004) incorporated the inhibitions of cellobiose, glucose and xylose into the lignocellulose hydrolysis model. Shi et al. (2017) reported that surface morphology and structure of substrate were changed by the dynamic enzyme activities by examining Atomic Force Microscope in combination with Fourier-transform infrared and Raman spectroscopy. The altered surface features might greatly impact enzyme adsorption on the surface of cellulose and release of reducing sugars. Structural change in the lignocellulosic fibers and composition during the enzymatic hydrolysis make enzyme adsorption a dynamic process as the hydrolysis progresses. Liao et al. (2008) proposed a dynamic enzyme adsorption based on Langmuir isotherm that incorporated changes of adsorption constant as the cellulose hydrolysis progresses. Toyosawa et al. (2017) investigated the effects of non-catalytic protein addition on enzymatic hydrolysis and found that application of lysozyme reduced the non-specific adsorption of cellulase on lignin and improved enzymatic hydrolysis. However, the kinetic study has not been conducted to describe the relationship between enzyme adsorption and hydrolysis of lignocellulosic

substrate with the impacts of changed enzyme loadings and different additives.

This study aims to construct a kinetic model to simulate the dynamic status and interactions of enzyme adsorption and cellulose hydrolysis with product and lignin inhibition. As adsorption equilibrium was changed with time and during enzymatic hydrolysis, a pseudo first order adsorption kinetic was used to reflect the changing properties of enzyme-cellulose system. The specific objectives of the experimental and numerical works designed in this study are: (a) to understand the effects of different pretreatment methods and initial enzyme loadings on enzyme adsorption and hydrolysis, hence further determine the parameters that can best reflect the enzyme adsorption in the system; (b) to demonstrate the dynamic change of enzyme adsorption and enhancement of cellulose conversion in addition of Bovine Serum Albumin (BSA) and lysozyme during the entire cellulose hydrolysis process; and (c) to develop a mathematic model that incorporate the dynamic interaction among enzyme adsorption, cellulose hydrolysis, and product inhibitions for different lignocellulosic substrates.

5.2 Experiments

The basic concept of experimental design, measured parameters, and determined kinetics have been illustrated in **Figure 5.1**. Based on the designed experiment

conditions, control parameters and substrate properties were gradually applied in the model to simulate the output parameters with increasing complexity. The proposed coefficients for adsorption isotherm and reaction kinetics were then validated from the basic to more complex systems.

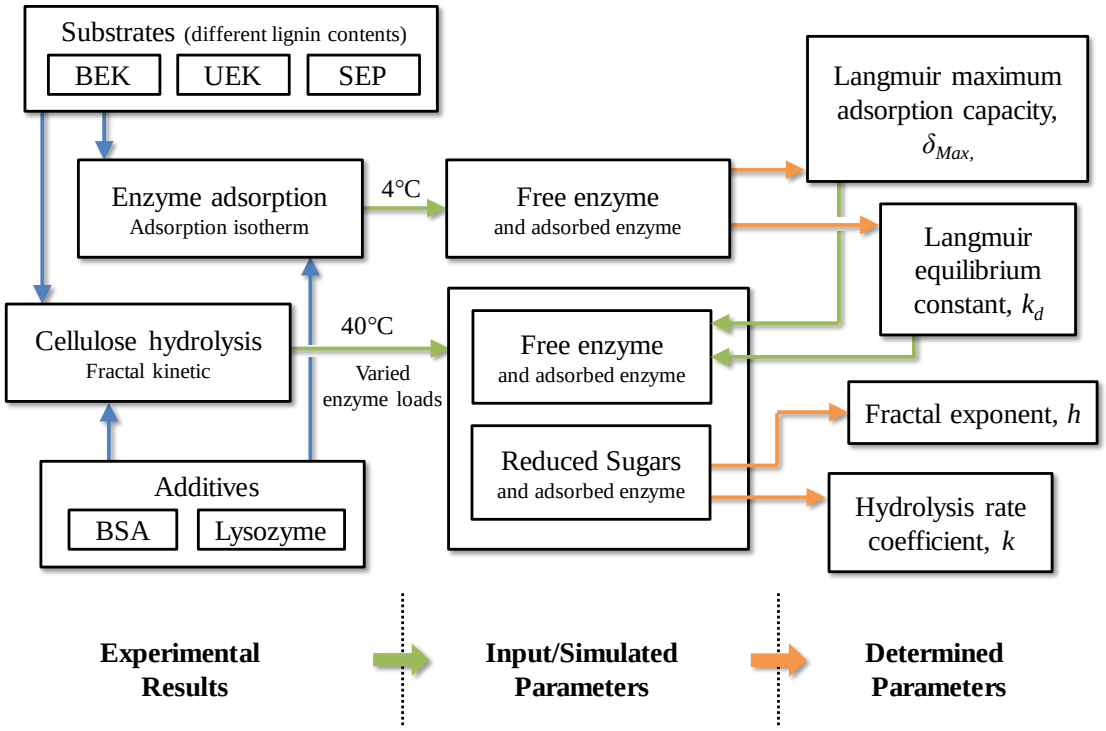

Figure 5.1 Workflow for kinetic modeling of enzymatic hydrolysis.

5.2.1 Materials/pretreatment of lignocellulosic materials

Three lignocellulosic substrates were selected in this study to investigate the impacts of lignin contents to enzyme hydrolysis. The tested Kraft pulps were produced from Australian *Eucalyptus globules* wood chips by using a M/K digester (Peabody, MA,

USA), with a liquid-to-solid ratio of 4 (w/v). The liquid involved NaOH (25% sulfidity) and Na_2S (17% active alkali). The digester was heated to 160°C at a rate of 1.5°C per min, and after that the temperature was maintained isothermally for 90 minutes (total cooking time is approximately 180 mins). The resulted unbleached Kraft pulps (UEK) were used as substrate for the experiments of cellulase adsorption and enzymatic hydrolysis. Bleached Kraft pulps (BEK) were prepared from oxygen bleached pulps by commercial DEDD bleaching sequence to completely remove lignin (Ko et al., 2011). Steam explosion pulps (SEP) were prepared from 1kg dried rice straw in 1.5% H_2SO_4 solution and saturated steam at the temperature of 190°C for 10 to 20 minutes. The solid to liquid ratio is 1:7. All the sample sizes ranged from 0.075 to 0.15 mm were selected for our experiments by fiber size fractionation with 100-mesh screen. Chemical composition analysis of the samples were performed according to the National Renewable Energy Laboratories (NREL) standard procedures (Sluiter et al., 2006; Sluiter et al., 2008). The solid samples of the pretreated substrates were grounded to powder to pass through 20-mesh sieve and treated with 72% H_2SO_4 at 30°C for 1 h and then dilute to 4% at 121°C for 1 h. The lignocellulose derived monosaccharides, including cellobiose, glucose, xylose, mannose arabinose and galactose were measured by high performance liquid chromatography (HPLC) using an HPX-87P column (Bio-Rad Laboratories) and filtered deionized water as mobile phase. The operation

temperature is 85°C and flow rate is 0.6 mL/min. The enzyme used in this study is C-Tec (Novozyme, China) with a protein concentration of 50 g/L.

5.2.2 Adsorption of cellulase

Adsorptions of cellulase on various pretreated substrates were conducted at 4 and 40˚C in sodium acetate buffer (pH 6.0). The solid loading was 0.1% (w/v) and the working volume was 15ml. The lower solid loading was used to avoid mass-transfer limitation that otherwise might confound the major findings. The enzyme dosages were 5, 10, 20, 30, 40, 50 and 60 mg/g solid for the adsorption equilibrium experiment. Samples were centrifuged at 5,000 rpm at 4˚C for 20 minutes after the solution achieving adsorption equilibrium (well mixed in shaking flask (150 rpm) for 1 h). The remaining free enzyme concentration in the supernatant was determined by Bradford method using bovine serum albumin (BSA) as standard (Bradford, 1976). Samples were mixed with Cooassie blue dye and then were measured by a UV spectrometer (PerkinElmer LAMBDA 25) at 590 nm. The absorbed enzyme was calculated from the difference between initial enzyme and measured free enzyme concentrations. The pretreated substrates underwent hydrolysis when the adsorption was conducted at 40˚C. Thus, enzyme adsorption was determined by accounting the content of solid cellulose remaining in the system at each sampling point.

5.2.3 Enzymatic hydrolysis of lignocellulose biomass

Enzymatic hydrolysis of various pretreated substrate was carried out after similar approaches as published in Ko et al. (2011). The enzyme loadings were 0.5, 5, and 50 mg/g solid. The pH was set at 6.0 and the temperatures were 4 and 40°C to investigate the adsorption and hydrolysis processes, respectively. Aliquot samples of 0.5 ml were taken at designed time intervals (1, 2, 4, 8, 12, 24 and 48h) from the mixtures and were centrifuged at 5,000 rpm at 4°C for 20 mins. Reducing sugar concentrations were measured by the dinitrosalicylic acid (DNSA) assay (Sengupta et al., 2000). Similarly, reducing sugar concentrations were determined by accounting the content of solid cellulose remaining in the system at each sampling point. Enzyme activity, protein concentration, reducing sugar concentration, reaction rate, and substrate concentration were measured at each sampling point.

5.2.4 Adsorption and hydrolysis with additives

The three pretreated substrates were mixed with excessive dosages of BSA and lysozyme for 24 hours until saturation adsorption, and then the saturated adsorbed substrates were washed twice by sodium acetate and DI water. The substrates were then resuspended in sodium acetate buffer (pH 6) for cellulase adsorption and hydrolysis as

described in the section 5.2.2 and 5.2.3.

5.3 Results and discussion

5.3.1 Lignin induced influence on adsorption isotherm

The chemical compositions of the three selected substrates for enzymatic hydrolysis experiments and simulations are presented in **Table 5.1**.

Table 5.1 Chemical compositions of pretreated substrates (wt.%)

Sample	Holocellulose	α-cellulose	Hemicellulose	Lignin	Ash
BEK	96.5	83.8	12.7	-	0.8
UEK	94.8	81.0	13.8	3.8	0.8
SEP	61.5	57.9	3.6	18.9	11.6

Table 5.2 Enzyme adsorption parameters of adsorption isotherm at 4˚C and 40˚C

Additives	Sample	σ_{max}^{S} (mg/g solid)	k_d (mg/mL)	A	R^2
T = 4˚C					
No additives	BEK	36.38	0.0207	48.40	0.9982
	UEK	25.86	0.0158	63.47	0.9908
	SEP	19.07	0.0103	96.63	0.9811
BSA	BEK	18.14	0.0760	13.17	0.9771
	UEK	7.45	0.0243	41.09	0.9659
	SEP	4.26	0.0199	50.18	0.9687
Lysozyme	BEK	8.92	0.0238	42.10	0.9999
	UEK	15.14	0.0131	76.31	0.9963
	SEP	30.80	0.0194	51.47	0.9182
T = 40˚C					
BSA	BEK	18.95	0.0744	13.44	0.99
	UEK	7.57	0.0218	45.95	0.98
	SEP	4.25	0.0199	50.34	0.97

Lysozyme	BEK	8.17	0.0149	67.31	0.9999
	UEK	12.35	0.0101	98.70	0.9997
	SEP	32.61	0.0138	72.30	0.8538

The key control parameters defined from the selected substrates is the lignin contents, of which increased from 0, 3.8, to 18.9% for BEK, UEK, and SEP, respectively. The Langmuir adsorption parameters for different pretreated lignocellulosic biomass were determined by nonlinear regression as illustrated in Error! Reference source not found., a nd the measured adsorption data were shown in **Table 5.2**. The amount of protein adsorbed on the substrates varied significantly with the types of tested substrates, pretreatment methods and additives. BEK samples showed the highest enzyme maximum adsorption capacity of 36.38 mg/g-substrate, followed by UEK sample (25.86 mg/g-substrate). SEP samples showed the lowest maximum adsorption capacity of 19.07 mg/g-substrate. This trend is consistent with the amount of lignin available in the composition of the pretreated substrates (**Figure 5.3**). SEP samples with the lowest enzyme adsorption contained the highest amount of lignin, while the lignin-free sample BEK had the highest adsorption capability. The different enzyme adsorption could be due to the higher affinity of the cellulase to the holocellulose than lignin (Nakagame et al., 2010). Steam explosion of acid-impregnated biomass resulted in high removal of the hemicellulose but not the lignin. On the other hand, bleaching using a strong oxidizing agent accelerates the ring opening of the phenolic structures and the alkaline

condition of the reaction medium assists in the extraction of the fragmented lignin. Using such an efficient alkaline-based oxidative delignification process, all lignin is eliminated and cellulose is well-exposed to enzyme, leading to higher adsorption of cellulase on the surface of cellulose.

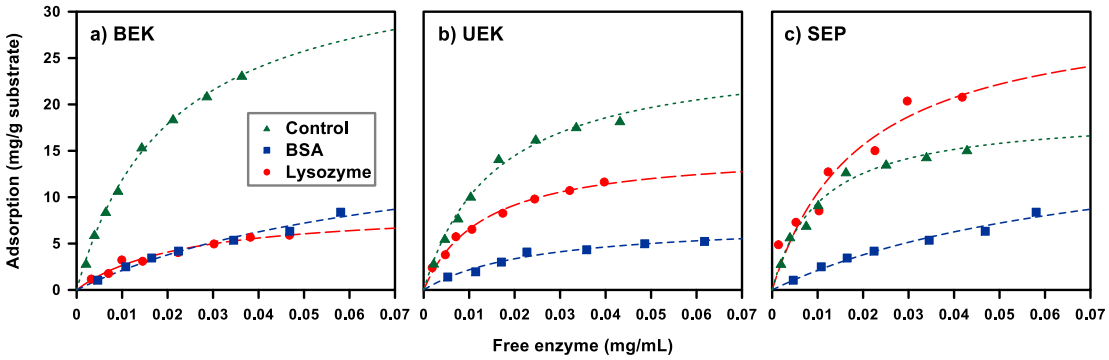

Figure 5.2 Enzyme adsorption isotherm at 4˚C with 1% (w/v) solid content. Enzyme loadings 5-60 mg/g-substrate for (a) BEK; (b) UEK; and (c) SEP with no additives (control); with BSA; and with lysozyme. Dashed lines fit with Langmuir isotherms.

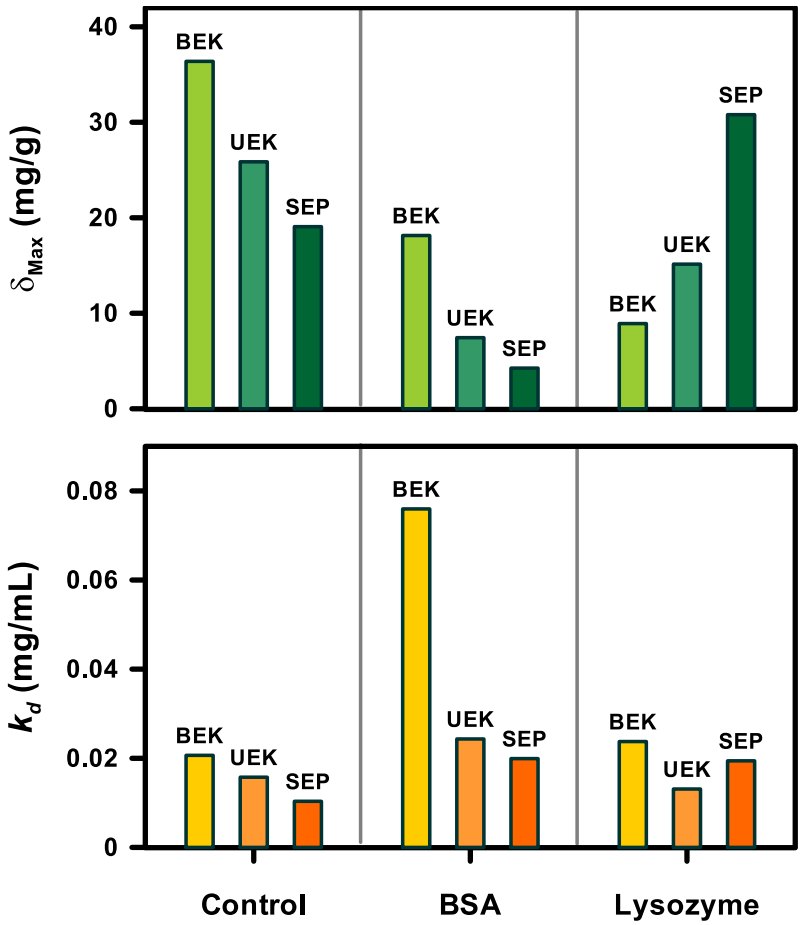

Figure 5.3 Relationships of maximun adsorption capacity (δ_{Max}) and Langmuir equilibrium constant (k_d) for three substrates at different hydrolysis conditions. Lignin and additives both play critical roles in enzymatic adsorption.

Li et al. (2016b) reported that addition of lignin caused reduction in maximum adsorption capacity of enzyme on pretreated corn stover. Lignin adsorbed onto the cellulose and sequentially reduced the surface area for enzyme adsorption. Selig et al. (2007) reported that lignin droplets produced from corn stover during pretreatment can deposit back onto the surface of celluloses, which potentially imposed adverse effects on enzyme adsorption and the efficiency of cellulose conversion. Compared to the low operation temperature, the adsorption kinetic of lignin was slower and imposed

minimal impact on enzyme activity at high and optimal operational temperature (Zheng et al., 2013). Zheng et al. (2013) reported that the enzyme adsorption on cellulose reached the adsorption peak within 0.25 hour, while adsorption on lignin took more than 12 hours to reach equilibrium at 50°C. The increasing enzyme loadings might result in enzyme crowding or competition for binding sites among the three working enzymes, impurity and other proteins that limits enzyme adsorption to cellulose.

5.3.2 Enzyme loadings and hydrolysis

The effects of different enzyme loading on enzymatic hydrolysis of the three pretreated substrates were investigated. The time course of enzyme adsorption and cellulose hydrolysis of three pretreated lignocellulosic biomass with initial enzyme loading of 0.5, 5 and 50 mg/g solid are plotted over time as shown in **Figure 5.4**. The experimental data of adsorbed enzyme and releasing sugar were fitted with the proposed model and the kinetic parameters were listed in **Table 5.3** and

Table 5.4. The enzyme absorption and glucose yield increased with the increasing enzyme loadings. The hydrolysis efficiency increased more than 16 times for BEK and UEK, and increased 11 times for SEP at the higher enzyme loading (50 mg/g). A higher

enzyme to substrate ratio effectively enhanced the hydrolysis performance as reported in many other studies (Chandra et al., 2011; Gregg & Saddler, 1996; Tengborg et al., 2001). The enzymatic hydrolysis rate was retarded with the prolonged experimental time. The hydrolysis rate coefficient and the fractal exponent increased with the increasing enzyme loading for all the three pretreated substrates. The hydrolysis rate coefficient remained the same with a further increase in the enzyme loading, which might due to statured adsorption of enzyme to cellulose (Wang et al., 2011). The excessive enzyme was presented as the free enzyme in the solution and does not react in the hydrolysis process. The increase in fractal exponent with increasing enzyme loading might be caused by overcrowding of the enzyme, which limits the enzyme diffusion on the surface of substrate at increasing enzyme loading (Xu & Ding, 2007).

Table 5.3 Kinetic parameters of fractal hydrolysis model with various enzyme loadings

Sample	Enzyme loading	k_{ad}	h	k
BEK	0.5	1	0.12	0.003
	5	1	0.3	0.005
	50	1	0.42	0.015
UEK	0.5	0.8	0.15	0.003
	5	0.8	0.38	0.005
	50	0.8	0.48	0.015
SEP	0.5	0.2	0.2	0.003
	5	0.2	0.4	0.005
	50	0.2	0.62	0.015

The hydrolysis rate coefficients were similar among three pretreated substrates, while SEP showed a higher impact on the fractal exponent, which might be ascribed to the high lignin content of SEP substrate. The fractal exponent of the cellulose hydrolysis of BEK and UEK were relatively low compared SPE, which confirmed that fractal exponent is related to the nature of the substrate. Wang et al. (2011) had performed enzymatic hydrolysis of Avicel with various loadings of isolated lignin and simulated with the fractal kinetics. The lignin inhibition on the enzymatic hydrolysis was presented by the increased fractal exponent while the hydrolysis rate coefficient was unchanged. The hydrolysis performance of substrate with high lignin could be improved by increasing of enzyme loading.

Table 5.4 Kinetic parameters of fractal hydrolysis model with BSA and lysozyme

Additives	**Sample**	k_{ad}	h	k
Control	BEK	1	0.30	0.005
	UEK	0.8	0.38	0.005
	SEP	0.2	0.40	0.005
BSA	BEK	1	0.15	0.012
	UEK	0.8	0.24	0.012
	SEP	0.2	0.35	0.012
Lysozyme	BEK	1	0.11	0.015
	UEK	0.8	0.21	0.015
	SEP	0.2	0.32	0.015

The hydrolysis rate coefficients were similar among three pretreated substrates, while SEP showed a higher impact on the fractal exponent, which might be ascribed to the high lignin content of SEP substrate. The fractal exponent of the cellulose hydrolysis of BEK and UEK were relatively low compared SPE, which confirmed that fractal exponent is related to the nature of the substrate. Wang et al. (2011) had performed enzymatic hydrolysis of Avicel with various loadings of isolated lignin and simulated with the fractal kinetics. The lignin inhibition on the enzymatic hydrolysis was presented by the increased fractal exponent while the hydrolysis rate coefficient was unchanged. The hydrolysis performance of substrate with high lignin could be improved by increasing of enzyme loading.

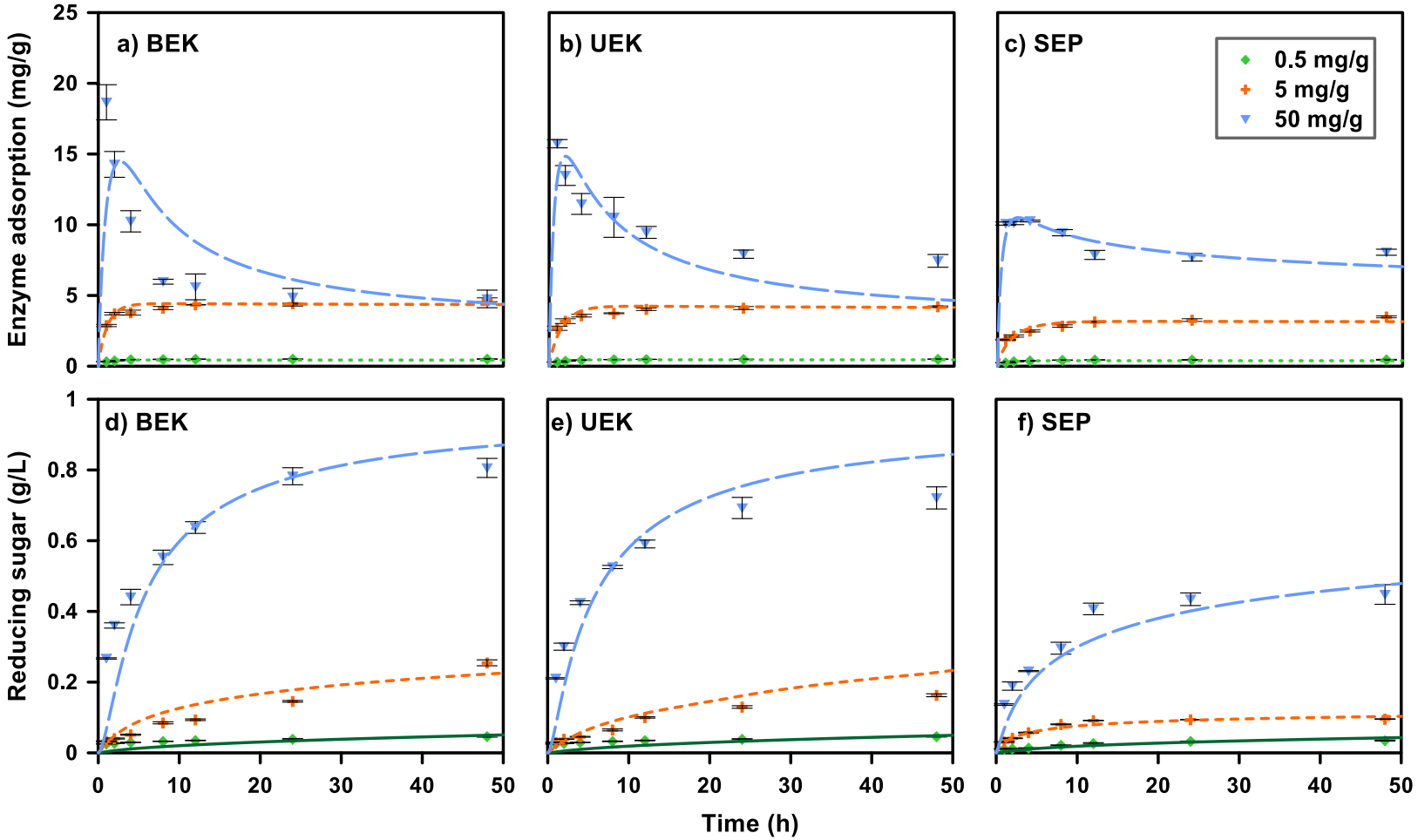

Figure 5.4 Simulation (dash lines) and experiment results (symbols) of dynamic enzyme adsorption and glucose release at 40˚C with 1% (w/v) solid content for (a) & (d) BEK, (b) & (e)UEK and (c) & (f) SEP with enzyme loadings of 0.5 mg/g, 5 mg/g, and 50 mg/g.

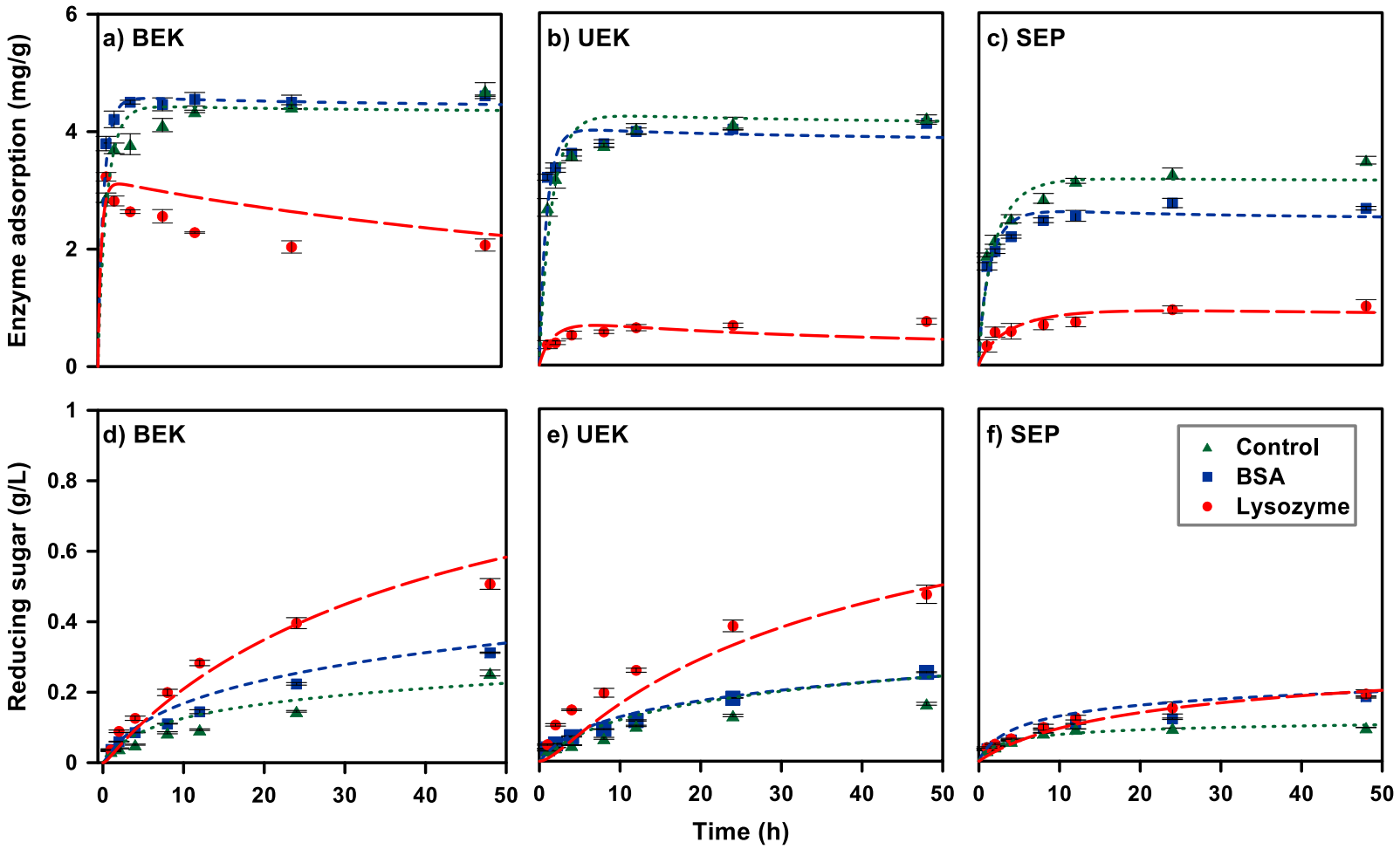

Figure 5.5 Simulation (dash lines) and experiment results (symbols) of dynamic enzyme adsorption and glucose release at 40˚C with 1% (w/v) solid content for (a) & (d) BEK, (b) & (e)UEK and (c) & (f) SEP with/without the addition of BSA/lysozyme at the enzyme loading of 5mg/g.

5.3.3 Impact of additives on adsorption and hydrolysis

Enhancement of enzymatic hydrolysis by addition of surfactants and polymers has been studies extensively. Yang and Wyman (2006) reported that only a little amount of BSA was absorbed on pure cellulose while lignin containing substrate adsorbed a significant amount of this additive. Toyosawa et al. (2017) showed that the lysozyme adsorbed only to lignin containing substrate and prevent nonproductive adsorption of cellulase by covering the surface of lignin. To improve the efficiency of cellulose conversion, BSA and lysozyme were added in attempt to block protein adsorption site of lignin and therefore reduce the nonproductive adsorption of enzyme. Kim et al. (2015) reported that the addition of BSA reduced the enzyme loading from 15 FPU/g solid to 1.3 FPU/g solid while achieving 80% of hydrolysis conversion. Ko et al. (2015) reported that a significant improvement from 17% to 72% for the liquid hot water pretreated hardwood chips with pre-incubation of 50mg/g BSA at low enzyme loading of 8 mg/g solid.

The effects of BSA and lysozyme addition on the enzyme adsorption and cellulose hydrolysis of BEK, UEK and SEP samples were investigated. The time course of enzyme adsorption and cellulose hydrolysis of three pretreated lignocellulosic biomass with and without addition of BSA and lysozyme at 5 mg/g enzyme loading are plotted over time in **Figure 5.5**. The results of BSA and lysozyme addition on the adsorption

isotherms of cellulose onto various pretreated substrates at 4˚C are showed in Error! Reference source not found.. With the addition of statured BSA, the maximum adsorption capacity of the three pretreated substrates decreased; and the maximum adsorption capacity of BEK and UEK decreased while SEP increased with the addition of lysozyme (**Figure 5.3** and **Table 5.2**). The enzyme adsorption showed the same pattern with and without BSA addition reaching equilibrium at 4.5 mg/g and 4.0 mg/g for BEK and UEK hydrolysis; while only slightly decrease of enzyme adsorption with BSA addition for SEP hydrolysis. In contrast, the enzyme adsorption reduced with the lysozyme addition for all three samples. The equilibrium enzyme adsorption was reached at approximately 1.0 mg/g for UEK and SEP samples.

While the scope of this project is to investigate the numerical relationship among the complex enzyme-cellulose-lignin interactions, the selected additives did show significant beneficial impacts to enzymatic hydrolysis at low enzyme loading (5 mg/g). With the addition of BSA and lysozyme, the glucose yield increased from 29.3% to 36.0% and 58.4% for UEK; from 19.1% to 29.6% and 55.5% for BEK; and from 17.2% to 33.2% and 34.5% for SEP, respectively. Addition of lysozyme enhanced hydrolysis yield the most for UEK (36.4%), BEK (29.1%) and SEP (18.5%), in contrast to improvement of 6.6-17.1% with BSA supplement. The two additives BSA and

lysozyme are oppositely charged at the designed pH (6.0) in this study, with acidic (4.7-5.3) and alkaline (10.7-11.3) isoelectric points, respectively (Mueller et al., 2010). Cai et al. (2018) reported that the isoelectric points of cellobiohydrolase I (CBH I) and CBH II were 3.4-4.7 and 5.3-5.6, respectively. β-glucosidase from *T. reesei* had a higher isoelectric points of 5.7 to 6.4 (Ko et al., 2015). The enzyme systems were negatively charged with and without addition of BSA in the buffer of 6.0, thus an electrostatic repulsion was formed between the enzyme and cellulose surface. Zhan et al. (2019) observed that addition of lignin carboxylate with pI around the hydrolysis pH (4.8) showed significant enhancement of hydrolysis.

Apart from the traditional and expensive BSA and lysozyme, soybean protein was used as potential lignin-blocking additive to mitigate the adverse impact of lignin and improve the cellulose hydrolysis performance. Brondi et al. (2020) reported an increase of more than one quarter and overall conversion efficiency reached 80%. in cellulose hydrolysis of sugarcane bagasse with addition of 12% (w/w) soybean concentration. Nitrogen gas was also used for displaced air to prevent enzyme deactivation by oxygen and hence improve hydrolysis performance especially at high solid loadings (Dos Santos et al., 2020).

5.3.4 Adsorption capacity and hydrolysis

Langmuir adsorption isotherm is widely used to describe and quantify enzyme adsorption (Kadam et al., 2004). However, Langmuir adsorption isotherm only described the enzyme adsorption at the equilibrium, while it is a dynamic process as it took over 12 hours to reach adsorption equilibrium (**Figure 5.4**). Especially at the high initial concentration of enzyme (50 mg/g), enzyme attached to the surface of cellulose rapidly with a peak adsorption of 15.7 mg/g, 11.7 mg/g and 9.5 mg/g for BEK, UEK and SEP within 1 hour, then followed by a desorption of enzyme caused by the initiation of hydrolysis, and eventually reached equilibrium. Enzyme adsorption on solid surface and their effectiveness are the two factors hypothesized to have a major impact on enzymatic hydrolysis. A linear relationship between enzyme adsorption and initial hydrolysis rate had been reported in previous studies (Nidetzky & Steiner, 1993). The overall patterns of enzyme adsorption matched the adsorption on pure cellulose, with an absorption peak reached within 1 hour, followed by a bounce back release of adsorbed cellulase to the solution, and eventually reached a stable adsorption (Zheng et al., 2013). The reaction rate of cellulose hydrolysis should be the same with and without lignin when the enzyme loading is above the k_d of the cellulase-cellulose adsorption. It is expected the hydrolysis rate reduced when the enzyme loading is below the value of k_d. The adsorption kinetic of cellulase regulates the distribution of cellulase between

cellulose and lignin during the dynamic adsorption-reaction process. Porosity, adsorption kinetic, binding selectivity and chemical characteristic may all have significant impacts on enzyme adsorption on lignin containing biomass (Zheng et al., 2013). Although the enzymes were considered as an enzyme complex with multiple function for the model development in this study, various enzyme components showed different degree of adsorption on lignin. β-glucosidase exhibited the strongest adsorption onto lignin (more than 80%) and indirectly lead inhibit the enzymatic hydrolysis of cellulose (Ko et al., 2015).

5.3.5 Sensitivity and validation of kinetic coefficients

Sensitivity analysis was performed to clarify the importance of the key reaction coefficients (k_{ad}, k, or h) to enzymatic hydrolysis reactions under different conditions. The base values of all parameters were obtained by solving the ODEs and presented in **Table 5.3** and **Table 5.4**. Using glucose concentration as an example, **Figure 5.6** presents the effects and significance of different kinetic parameters on the simulation results. The sensitivities of the simulation coefficients were presented in matrix form: the five experimental conductions were presented in columns for the enzyme loadings of (a) 0.5 mg/g, (b) 5 mg/g, (c) 50 mg/g, and with the addition of (d) BSA, and (e) lysozyme at the enzyme loading of 5 mg/g, respectively; and three substrates were

presented in rows for (a) BEK, (f) UEK, and (k) SEP, respectively. The relative errors between simulation results and measured data were calculated by varying the kinetic coefficients from -40% to 40% of the standard deviation, when the other parameters were fixed at the optimal values. The sensitivities of different kinetics coefficients showed no regular pattern among experimental conditions and substrates. Most of the simulation results were within ±20% relative errors if the variation of selected coefficients were limited at ±10% standard deviations of the optimal values. The adsorption coefficient k_{ad} showed a relatively small influence for all the operational conditions of the three pretreated substrates, while the fractal exponent coefficient h was the most significant parameter affecting the overall reaction.

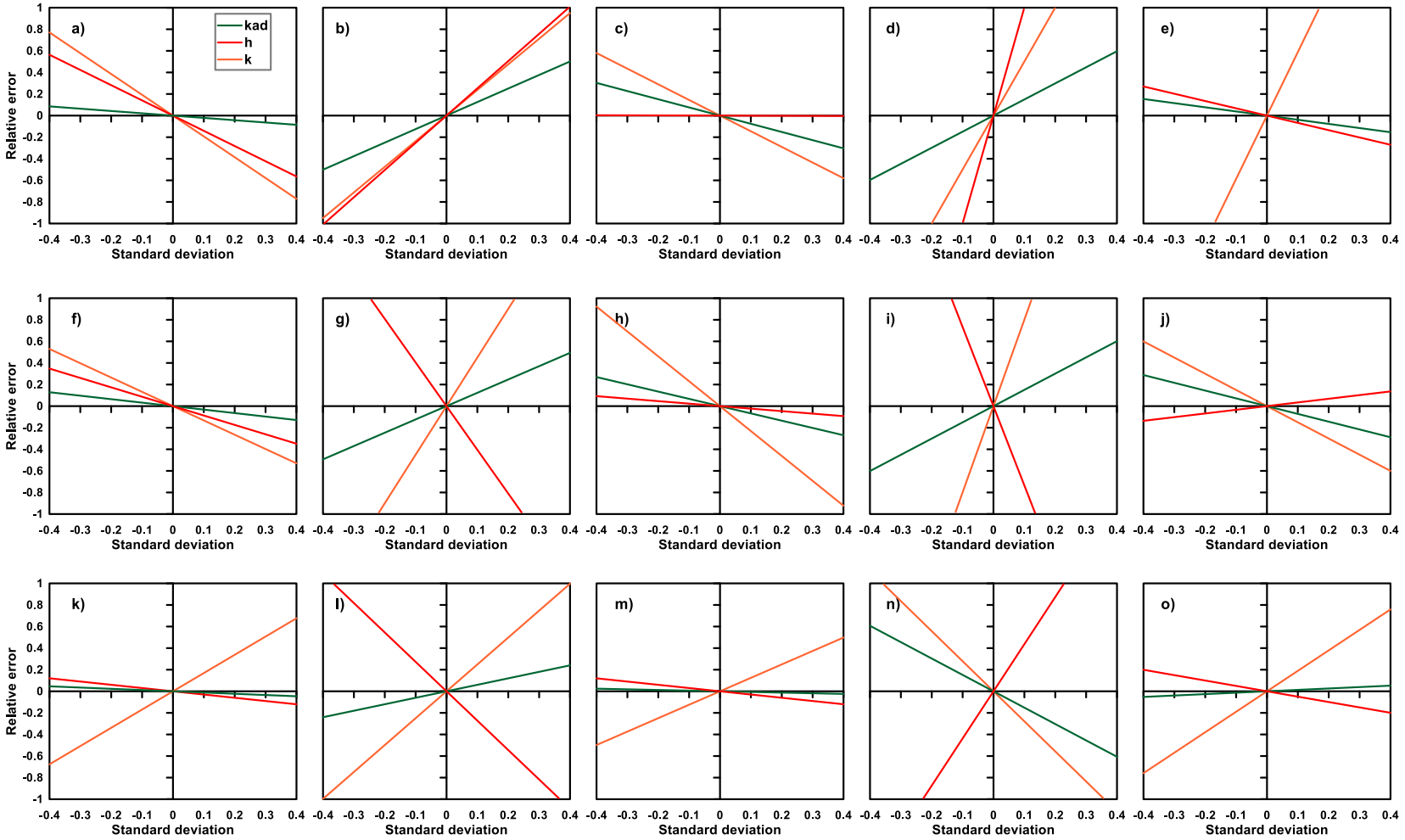

Figure 5.6 Sensitivity analysis of the kinetic parameters for the simulation model: (a-e) BEK; (f-i) UEK; (j-o) SEP with the enzyme loadings of 0.5 mg/g (a, f, & j), 5 mg/g (b, g, & k), and 50 mg/g (c, h, & m); and with the addition of BSA (d, I, & n) and lysozyme (e, j, & o) at the enzyme loading of 5mg/g.

The fractal kinetic parameters with the addition of BSA and lysozyme are summarized in **Figure 5.7**. The optimized fractal exponent coefficients *h* generally increased with the increased amount of lignin contents in the substrate, and were higher with the increases of enzyme loadings. The value of this parameter was significantly lowered when additives were introduced in the processes, of which closer to 0.5 mg/g than 5 mg/g used, implying certain impacts of the additives to enzyme activities especially for high cellulose substrates (BEK and UEK). However, addition of BSA and lysozyme increased the hydrolysis rate coefficients (**Figure 5.7b**). Compared to the fractal exponent, the hydrolysis rate coefficient increased obviously in the presence of lysozyme and BSA, for which the value (0.012 and 0.016) at 5 mg/g enzyme loadings performed nearly the same as those measured at 50 mg/g. Wang and Feng (2010) reported that the rate coefficient increased with the increases of the surfactant concentration until a saturated value was reached, while the fractal exponent decreased with the increase of the surfactant concentration. The addition of BSA and lysozyme were saturated before the enzymatic hydrolysis experiment in this study.

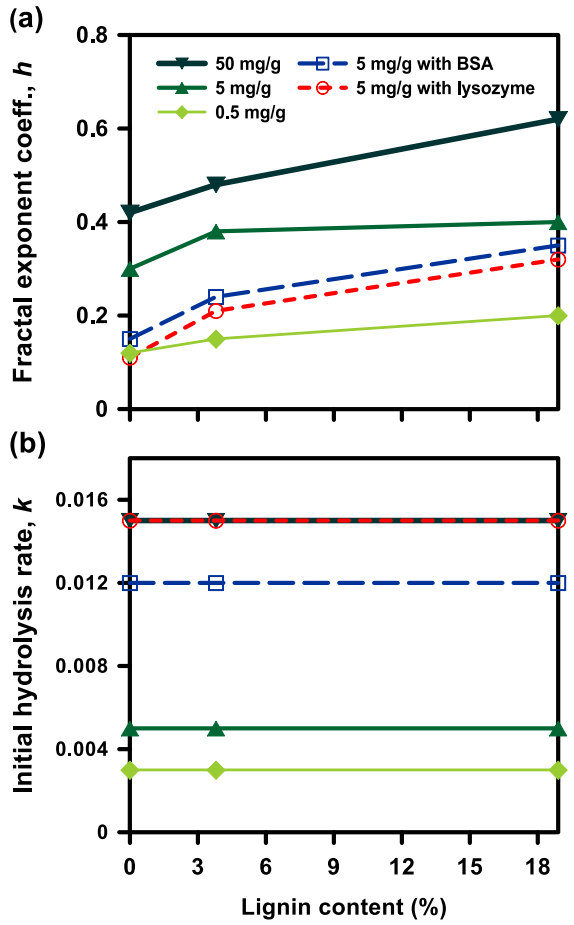

Figure 5.7 Relationship between substrate lignin contents and (a) fractal exponent and (b) hydrolysis rate coefficients.

5.4 Conclusion

Key parameters of enzyme adsorption isotherm were integrated into cellulose hydrolysis kinetics, which facilitated the simulation of dynamic enzyme adsorption and sugar release during enzymatic hydrolysis. The first order fractal model characterized quantitatively the cellulolysis rates and sugar yields at various enzyme dosages, lignin inhibition in different substrates, and the enhancement of cellulose conversion with additions of BSA and lysozyme. The two coefficients, *i.e.*, hydrolysis rate coefficient

and fractal exponent coefficients, offered both numerical and physiochemical insights toward more effective and economic pretreatment, saccharification, and enzyme recycling process in lignocellulose biorefinery. The incorporation of dynamic enzyme adsorption into the cellulose hydrolysis model, reveal the interrelationship of adsorbed enzyme and cellulose hydrolysis rate, providing new perspectives towards better understanding and future modification in the model structure.

Chapter 6 Dynamic Simulation of Continuous Mixed Sugar Fermentation with Increasing Cell Retention Time

6.1 Background

Lignocellulosic biomass in the form of agricultural residues and urban wastes represents a near-term solution for the production of biofuel and biochemicals to alleviate global climate change. Optically pure lactic acid (LA) through fermentation has attracted increasing attention for the manufacture of polylactic acid (PLA), a biodegradable and biocompatible polymer, as a substitute for petrochemical-derived plastics (Datta & Henry, 2006). Lactic acid fermentation using starch-based feedstock has been well established and commercialized, but this approach has been challenged due to the well-known competition of food *vs.* fuel (Kwan et al., 2018) and high feedstock costs (Tan et al., 2017). Applying lignocellulosic biomass for lactic acid production is environmentally preferred, but it is also a challenging task due to the increasing complexity of treatment processes, *i.e.*, pretreatment (Leu & Zhu, 2013), saccharification (Liu et al., 2016), and fermentation (Koppram et al., 2014).

Simultaneous and efficient utilization of hexoses and pentoses derived from lignocellulosic biomass is a critical bottleneck to the complete utilization of substrates

(Wang et al., 2015). Lignocellulosic hydrolysates are composed of 50-70% cellodextrins and glucose, 20-30% xylose, 0-25% lignin, some extractives (such as terpenes alkaloids, fats, and waxes), and reaction by-products, of which the types and proportion of sugars vary significantly among biomass and pretreatment methods (Islam et al., 2019; Sjostrom, 1993). Current biorefinery processes have successfully applied hexoses for lactic acid fermentation (Dong et al., 2018b), but utilization of pentoses is still challenging due to the metabolic regulation of carbon catabolite repression (CCR) (Görke & Stülke, 2008). While many strains have been discovered or engineered to use pentoses for fermentation, both natural and engineered microorganisms tend to utilize glucose preferentially when mixed sugars are provided in the process. When the glucose concentration is higher than a certain threshold, the less preferred sugars, such as xylose, may not be utilized by fermentation microorganisms, and hence are left in the fermentation broth even after the glucose is completely utilized.

Significant research efforts have been made to overcome the glucose-induced CCR in mixed sugar fermentation. Taniguchi et al. (Taniguchi et al., 2004) developed a co-cultivation process with a two-stage cultivation using two lactic acid-producing bacteria specific for glucose and xylose, and produced a high amount of lactic acid (95

g/L) from 100 g/L glucose and 50 g/L xylose (G100X50). However, no improvement in xylose consumption was achieved. Lu et al. (Lu et al., 2016) introduced an engineered *Escherichia coli* strain, JH15, in the production of D-lactic acid and obtained 83 g/L lactic acid from G50X50. The strain indeed consumed some xylose but the overall lactic acid productivity decreased to 0.87 g/L-h compared with 2.44 g/L-h using 100 g/L glucose as the substrate. Another strategy to overcome CCR is through careful adjustment of the feeding sugar combination in the fermentation process. Wang et al. (Wang et al., 2014b) discovered that complete utilization of xylose can be achieved by replacing glucose with cellobiose without inducing the CCR. In a fed-batch fermentation system with C100X60, up to 163 g/L lactic acid was produced using a xylose consuming strain (*i.e.*, *Enterococcus mundtii* QU 25, the strain used in this study), which is subjected to the CCR when isolated and characterized (Abdel-Rahman et al., 2011b). However, the productivity of 0.68 g/L-h in this process was not outstanding, and can be further improved through advanced process control and optimization.

Continuous fermentation associated with cell recycling has shown many superior features, such as increased productivity of bio-products over batch- or fed-batch processes (Li et al., 2011). The operational benefits of the continuous process are high

production rate and reduced downtime for cleaning, filling and sanitation (Ghose & Tyagi, 1979). By controlling the cell concentration and/or the cell retention time (CRT) of the process, the robustness of the continuous process can be improved to handle different substrate combinations with a higher variety of digestibilities or toxicities. The process can be operated without repeating the inoculation and may prevent significant cell decay due to sudden environmental changes (Leu & Stenstrom, 2010), which may be applied to overcome the CCR and/or growth inhibiting effects induced by pretreatment by-products, carbon sources, and end products.

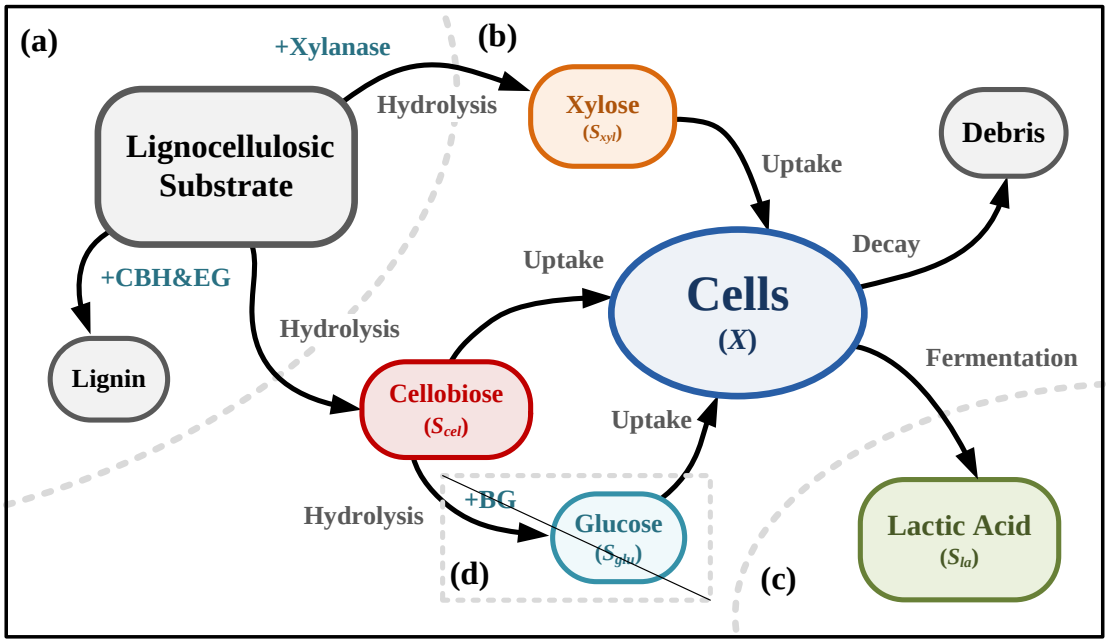

Figure 6.1 Conceptual diagram and model structure of the continuous lactic acid co-fermentation process with membrane separation and selected enzyme combination for preventing carbon catabolite repression; (a) hydrolysis system; (b) fermentation; (c) membrane separation; and (d) pathway to be cut-off to prevent carbon catabolite repression (CCR).

In this study, the potential benefits of cellobiose/xylose co-fermentation were investigated in a continuous fermentation system with a cell recycling unit and were supported by dynamic modelling. The basic concept of bioconversion process and model structure was shown in **Figure 6.1**. To better elucidate the metabolic kinetics of the fermentation strain in the specific bioreactor system, synthetic hydrolysates were applied to simulate a staged hydrolysis with reduced β-glucosidase (βG), of which the hydrolysis of cellobiose to glucose was partially prohibited. This strategy is potentially feasible through the application of commercial cellulase cocktails, while the related optimization of hydrolysis on real lignocellulosic biomass is in-progress. The lactic acid producer *E. mundtii* QU 25 used in this study was isolated by our co-authors Abdel-Rahman and Sonomoto et al. (Abdel-Rahman et al., 2011a), which was introduced in greater details in the later section. A mixture of cellobiose and xylose was fed to the system with *E. mundtii* QU 25 for continuous lactic acid fermentation. A hollow fiber microfiltration module was applied to control the CRT, and separate the residual sugars and lactic acid. The dynamic model was constructed and validated with the experimental results to simulate the growth and decay kinetics of the fermenting strain in various operations, *i.e.*, batch, continuous, and cell recycling. The sensitivity of the discussed control parameters and influent conditions were drawn to visualize the operational boundary of the overall system, and to provide insights into process control,

monitoring, and optimization.

6.2 Methods

6.2.1 Microorganism and medium

E. mundtii QU 25 was used throughout this study. This strain was found in an ovine fecal sample collected from Fukuoka Zoo, Japan by Dr. Abdel-Rahman and Prof. Sonomoto (Abdel-Rahman et al., 2011b) in our collaborative research team. It is capable to utilize glucose, xylose, and cellobiose for the production of L-(+)-lactic. The strain can produce L-(+)-lactic acid at a high optically purity in the batch (≥99.9%) (Abdel-Rahman et al., 2011a) and fed-batch system (≥99.7%) (Wang et al., 2014b), and the optimal temperature and pH for culturing were 43°C and 7.0, respectively (Abdel-Rahman et al., 2011a). It was confirmed that the strain can carry out the xylose fermentation through the PP/glycolytic pathway instead of the phosphoketolase (PK) pathway. The yield of lactic acid converted from xylose was up to 1.51 mol/mol, which was close to the maximum theoretical yield (1.67 mol/mol) in the PP/glycolytic pathway (Abdel-Rahman et al., 2011a).

The strain sample was stored at –80°C in 2-mL vials containing 15% (v/v) glycerol and refreshed annually. Cell growth, inoculum preparation, and fermentation were

conducted using a modified Man, Rogosa, and Sharpe (mMRS) medium containing the following ingredients per litre of distilled water: 10 g peptone (Becton, Dickinson and Company; Sparks, MD, USA), 8 g beef extract (Nacalai Tesque, Kyoto, Japan), 10 g yeast extract (Nacalai Tesque), 2 g K_2HPO_4 (Sigma, Tokyo, Japan), 5 g $CH_3COONa \cdot 3H_2O$ (Nacalai Tesque), 2 g tri-ammonium citrate (Nacalai Tesque), 0.2 g $MgSO_4 \cdot 7H_2O$ (Nacalai Tesque), 0.05 g $MnSO_4 \cdot 4H_2O$ (Nacalai Tesque), and 1 mL Tween 80 (Nacalai Tesque). As indicated later in each experimental description, glucose, xylose (both from Nacalai Tesque), and cellobiose (Carbosynth; Berkshire, UK) were supplemented at several concentrations as carbon sources. In all experiments, the pH of the medium was adjusted to 7.0 by 10 M NH_4OH (Wang et al., 2014b) or 10 M HCl. The medium and sugar mixtures were sterilized at 115 °C for 20 min separately to prevent heat degradation.

6.2.2 Hollow fibre microfiltration module

In continuous lactic acid production with cell recycling, a hollow fibre microfiltration module (Microza PMP-102; Asahi Kasei, Tokyo, Japan) was used to recycle cells and feed them back to the fermentor. The filtration area of this module was 0.17 m^2, every fibre had a diameter of 0.7 mm and a pore diameter of 0.25 μm. Before use, the membrane module was sterilized by 70% ethanol for >24 h and then washed with

sterilized deionized water. The module was washed with sterilized deionized water, and then stored in 1 M NaOH before next experiment.

6.2.3 Set-up of experiments

The fermentation experiments were designed by specific orders to clarify essential metabolic information of *E. mundtii* QU 25 under various conditions, especially the maximum growth rate and decay coefficient. A set of batch fermentations with various sugar combinations was conducted to study the growth kinetics of *E. mundtii* QU 25 and the kinetic parameters were defined. Continuous fermentation was performed after batch cultivation with different dilution rates. A hollow microfiltration fibre was coupled to the fermentation reactor in a closed loop configuration for cell recycling. To confirm the repeatability of the experiments, three independent experiments were carried out for each process condition in batch and continuous modes; and hence the reported data were the average of triplicates with standard deviation. The CF/CR process was conducted individually, and the reproducibility of the process was verified by three repeated measures of the dynamic change of the process conditions over well-defined frequency (3-hour intervals). More details of the experiments are provided in the following sections.

6.2.4 Batch and continuous fermentation

All continuous fermentation systems were initiated in a batch mode and then turned into continuous mode after a period of operation. This setup provided us with an opportunity to investigate the changes in microbial activities in the transition phases of the two systems. For inoculum preparation, 1 mL of strain QU 25 glycerol stock was transferred into 9 mL of mMRS medium containing ca. 15 g/L cellobiose and 15 g/L xylose and refreshed for 24 h at 43°C. For pre-culture, 4 mL of the refreshed culture was transferred to a 100-mL flask containing 36 mL of mMRS medium and cultivated for 8 h at 43°C. Main culture were obtained by inoculating 10% (v/v) pre-cultured broth into a 1-L jar fermentor (Biott; Tokyo, Japan) with a 0.4-L working volume of mMRS medium. pH was controlled at 7.0 with a pH controller (PHC-2201; Able, Tokyo, Japan) by adding 10 M NH_4OH solution (Wang et al., 2014b). The process was initiated with batch mode operation at the initial stage for 48 h in ca. 100 g/L glucose and 60 g/L xylose (G100X60), 60 h in 100 g/L cellobiose and 60 g/L xylose (C100X60), or 36 h in 50 g/L glucose and 30 g/L xylose (G50X30). The co-fermentation processes were then switched into continuous mode with designated influent conditions when the majority of the initial sugars were consumed. Samples were taken at steady state at least 4 times at every dilution rate, and analyzed in terms of cell growth and composition of sugars and fermentation products. For all continuous processes, dilution rates were changed

after steady state was achieved, or three retention times subsequently tested with the previous dilution rate. The tested dilution rates were 0.05, 0.10, 0.15, 0.20, 0.25, 0.30, and 0.35 1/h.

6.2.5 Continuous co-fermentation with cell recycling (CF/CR)

Before the continuous co-fermentation, the same refresh and pre-culture processes as previous batch and continuous fermentations were conducted; then strain QU 25 was cultivated initially in batch mode for 36 h in a 5-L jar fermentor containing a 4-L working volume. Once the cell growth reached the late logarithmic growth phase, the broth was gradually transferred to a 1-L fermentor with a pump. Cells were concentrated by recirculation through the hollow fibre module connected to a 1-L jar fermentor. Permeate from the module was collected spontaneously. The fermentation broth was therefore concentrated from 4 L to 0.4 L through this process. The CF/CR process was then initiated with feeding medium containing C50X30 at an agitation rate of 180 rpm with cell recycling. The pH of the broth was maintained at 7.0 by a pH controller with 10 M NH_4OH. Both the inflow rates of the feeding medium and alkali were balanced to the same rates of outflow of permeates from the module by pumps. Samples were taken at regular intervals.

6.2.6 Analytical methods

Cell growth was estimated in terms of optical density at a wavelength of 562 nm (OD_{562}) with spectrophotometer (UV-1600, Shimadzu). One unit of OD_{562} was equivalent to 0.218 g dry cell weight (DCW, g/L) (Abdel-Rahman et al., 2011a). The concentrations of cellobiose, xylose, glucose, and fermentation products were analysed by a high-performance liquid chromatography (HPLC) system (US HPLC-1210, JASCO, Tokyo, Japan) equipped with a refractive index detector (RID) and a SUGAR SH-1011 column (Shodex, Tokyo, Japan) (Wang et al., 2014b). The collected fermentation samples were centrifuged at 2,000 × *g* for 10 min at 4°C, and the supernatant was filtered through a 0.45 μm pore size membrane filter (Dismic-13HP, Advantec, Tokyo, Japan). HPLC analysis was conducted under the following conditions: injection volume, 20 μL; column temperature, 50°C; mobile phase, 3 mM $HClO_4$; flow rate, 1.0 mL/min (Wang et al., 2014b). The optical purity of the produced lactic acid was detected by a BF-5 biosensor (Oji, Hyogo, Japan) based on the manufacturer's protocol.

The control parameters discussed in this study were as follows: the dilution rate (h) was calculated as the feed flow rate (mL/h) of the feeding medium divided by the working volume (mL) in the fermentor. Lactic acid productivity (g/L-h) was calculated as lactic acid produced (g/L) multiplied by the dilution rate (1/h). The cell

retention time (h) was the average time the fermentation strain stayed in the system, which was equal to the hydraulic retention time (HRT) or the inverse of the dilution rate in CFSTR. When the cell was retained in the reactor, CRT increased with testing time and differed from HRT. In our study, CRT in the cell recycling CFSTR was the same as the overall testing time from the initial stage of the experiments (including the initiation phase operating at batch mode).

6.2.7 Parameter determination and model validation

The values of the kinetic parameters were determined using the numeric computing program MATLAB R2013a (MathWorks, US) as mentioned in section 3.5. The models were cross-validated against the experimental results from a separated set of single and mixed sugar fermentation. The root mean square error (RMSE), regression coefficient (R^2), bias factor (BF), and accuracy factor (AF) were calculated to evaluate and validate the flexibility of the models. The RMSE was calculated according to the following equation:

$$\mathrm{RMSE} = \sqrt{\frac{\sum_{i=1}^{n}(X_{pi} - X_{expi})^2}{n}} \qquad (6\text{-}1)$$

The BF and AF were applied to evaluate the performance of the proposed kinetic models (Germec et al., 2019; Germec et al., 2020) according to the follows Equations (**6-2**) and (**6-3**).

$$BF = 10^{\sum_{i=1}^{n} \frac{\log(X_{expi}/X_{pi})}{n}} \quad (6\text{-}2)$$

$$AF = 10^{\sum_{i=1}^{n} \frac{|\log(X_{pi}/X_{expi})|}{n}} \quad (6\text{-}3)$$

The BF and AF equal to 1 indicates a preferred match between the actual observation and model predictions. The AF value is always equal to or greater than 1, and the larger AF value, the less precise the model prediction.

The experiments in this section were conducted by Dr. Y. Wang in the Laboratory of Microbial Technology of the Kyushu University and the calculation and kinetic model development and simulation were conducted by me and presented in this study.

6.3 Results and Discussion

6.3.1 Batch fermentation

The growth kinetics of *E. mundtii* QU 25 on glucose, cellobiose, and xylose were studied by batch experiments. The batch fermentations were conducted using medium

supplemented with varying concentrations of sugars (10, 20, 50, 100 and 150 g/L) and the growth kinetic parameters were determined during the early exponential growth phase with no product inhibition. The optimized values of the kinetic parameters determined by nonlinear regression are listed in **Table 6.1**. The maximum growth rates (μ_{max}) of the studied strain were 1.20, 0.99, and 0.62 1/h for glucose, cellobiose, and xylose, respectively, which were within similar range for other lactic acid producing strains using different substrates (Ma et al., 2016; Shibata et al., 2007; Tashiro et al., 2011). The μ_{max} and K_s values for glucose were higher than xylose and cellobiose, implying that glucose is the preferred carbon source of strain QU 25, which was further confirmed by the residual sugars in CSFTR.

Table 6.1 Kinetic parameters from different batch studies and this work (*E. mundtii* QU 25)

Substrates	Microorganism	μ_{max} [a]	K_S [b]	K_{is} [c]	K_{ip} [d]	Y_{LA} [e]	Y_X [f]	Ref.
		1/h	g/L	g/L	g/L	g/g	g/g	
Glucose	*L. amylophilus*	0.32	-	-	-	0.62-0.89	-	Mercier et al. (1992)
Lactose	*L. plantarum*	0.29	45.0	-	-	0.96	0.25	Fu and Mathews (1999)
Lactose	*L. bulgaricus*	1.14	3.36	119	-	0.90	0.10	Burgos-Rubio et al. (2000)
Glucose	*Sporolactobacillus CASD*	0.13	-	-	-	-	-	Zhao et al. (2010)
Glucose	*L. lactis* NZ133	1.10	1.32	304	1.39	0.93	-	Boonmee et al. (2003)
Molasses	*E. faecealis* RKY1	1.60	0.89	167.46	-	0.9-0.99	0-0.37	Nandasana and Kumar (2008)
Glucose	*E. mundtii* QU 25	1.20	55.6	108.3	1.8	0.950	0.038	
Cellobiose	*E. mundtii* QU 25	0.99	8.9	526.8	1.5	1.015	0.028	This study
Xylose	*E. mundtii* QU 25	0.62	20.1	254.2	3.3	0.925	0.056	

[a] maximum specific growth rate; [b] half saturation concentration; [c] inhibition coefficient of substrate; [d] inhibition coefficient of product; [e] yield of lactic acid production; and [f] yield of cell production.

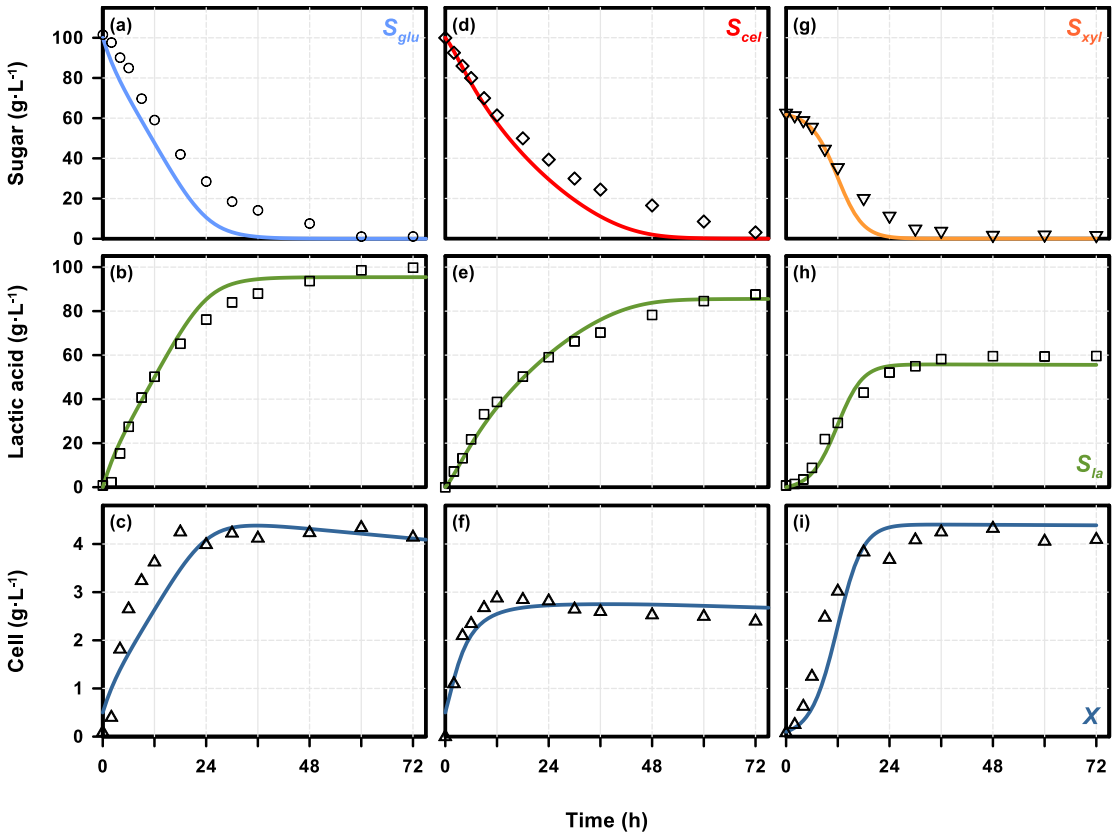

Figure 6.2 Simulation results (curves) and measurement data (symbols) for lactic acid fermentation by *E. mundtii* QU 25 with different carbon sources, *i.e.*, glucose (left), cellobiose (middle) and xylose (right). The data presented from top to bottom are residual sugars, lactic acid (*LA*), and dry cell weight (*X*). The data points represent the mean values of three independent experiments.

Cell growth and lactic acid formation were critically affected by product inhibition (K_{ip}), while the substrate inhibition (K_{is}) had relatively small adverse impacts on the studied sugars. A linear relationship was determined between substrate consumption and lactic acid formation with a yield coefficient of 1.0025 for all three sugars (details not shown); this result was similar to the calculated yield of lactic acid based on stoichiometry. The yield of lactic acid was determined from the stoichiometric

equations and batch kinetic data with values of 0.950 g/g for glucose, 1.015 g/g for xylose, and 0.925 g/g for cellobiose. The cell yields were in the low range (0.028-0.056 g/g) which could be reasonable if considering the high product yields (0.925–1.015 g/g). The model parameters were determined by fitting the simulation results with the experimental data. The results of sugar utilization, lactic acid production, and cell growth from three single sugars in the batch system are shown in **Figure 6.2**. After careful adjustment of the parameters the simulation results (lines) all fit well with the experimental results (symbols). The values of root mean square errors (RMSE), regression coefficient (R^2) bias factor (BF) and accuracy factor (AF) of the model were presented in **Table 6.2**, suggesting a high consistency between the model simulation and experimental results. The validated growth kinetics, such as the maximum growth rate and the half saturation concentrations, were applied in the other simulations for the continuous fermentation processes.

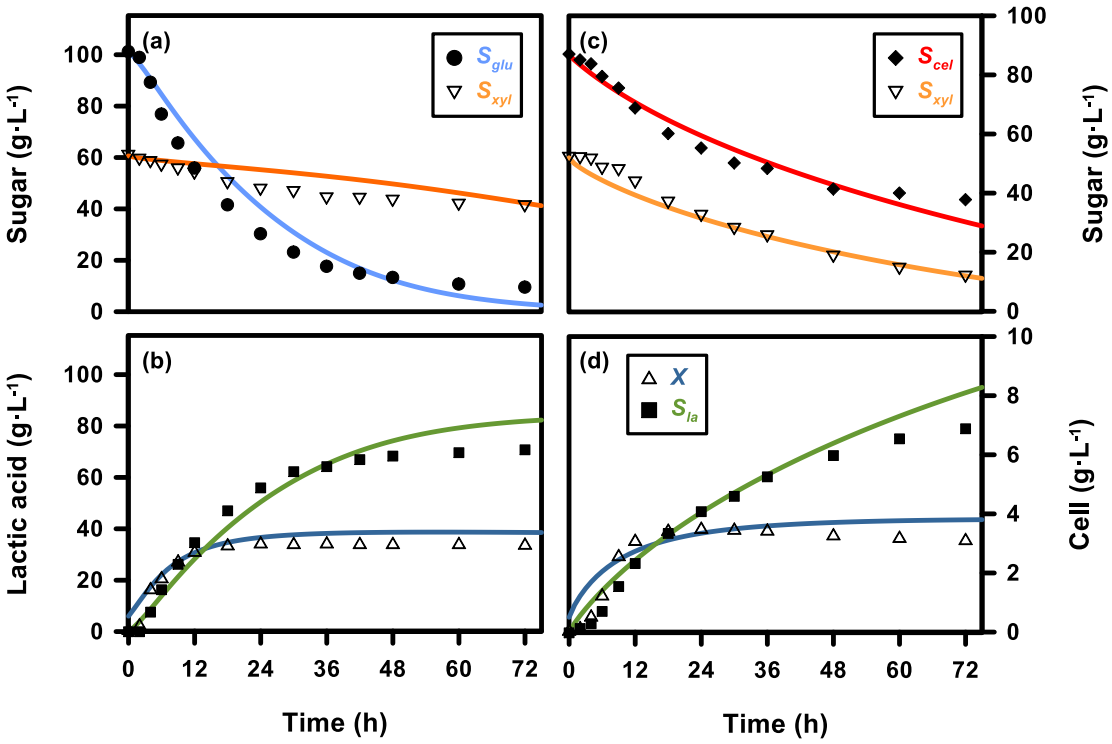

Figure 6.3 Experiment and simulation results of co-fermentation using various sugar combinations in a batch reactor; carbon catabolite repression was not observed when cellobiose with xylose was mixed. The data points represent the mean values of three independent experiments.

In addition, dynamic simulations were also carried out on batch fermentation with mixed sugars (**Figure 6.3**). The impacts of CCR were clearly shown in G100X50 (**Figure 6.3(a)**), and the majority of xylose was not consumed, as glucose was the preferential carbon source for the synthetic hydrolysate. A large amount of xylose remained in the fermentation broth even when glucose was almost completely converted into lactic acid and cell biomass. On the other hand, CCR was not observed

when C100X50 was applied (**Figure 6.3(b)**) as both sugars were utilized by the fermentation strain simultaneously during fermentation. However, a large amount of cellobiose was not utilized during the testing period when a similar amount of cells was produced in the batch system. The lactic acid concentration was slightly higher in C100X50 than in G100X50.

The simulation results of the dual sugar batch systems showed reasonable fits with the experimental results. The simulation of C100X50 was carried out by the dynamic model described in the methodology section and without the inclusion of any inhibiting factor from the co-fermenting sugars. In order to characterize CCR, the simulation of G100X50 was carried out by introducing an inhibiting coefficient from glucose to xylose in Equation (6). This simulation approach was designed only for this application, as the specific range of glucose concentrations to induce CCR was not clarified. The sensitivity of the inhibiting functions needs to be validated with more comprehensive experiments, which is beyond the scope of this study. As the main focus of this work is to investigate the fermentation of cellobiose and xylose, we tend to study the inhibiting kinetics of CCR in greater detail elsewhere.

6.3.2 Continuous co-fermentation

This feature of the continuous co-fermentation process for the complete utilization of hexose and pentose were investigated. G100X60 and C100X50 were initially tested at a dilution rate of 0.2 1/h for process control and comparison (**Table 6.3**). For G100X60, when continuous fermentation reached a steady state, a cell concentration of 1.99 g/L was achieved, and a much higher amount of glucose was consumed than xylose (27.5 g/L over 2.64 g/L, respectively). The ratio of consumed xylose to consumed glucose (X/G) was 0.096, which exhibited an obvious CCR for xylose utilization. *E. mundtii* QU 25 growing on G100X60 produced 24.2 g/L lactic acid with a yield of 0.803 g/g and productivity of 4.84 g/L-h, and a small amount of by-product (0.151 g/L acetic acid) was detected. When glucose was replaced by cellobiose (C100X60) at the same dilution rate of 0.20 1/h, the cell concentration increased to 2.42 g/L at steady state. A cellobiose consumption of 21.8 g/L was achieved with a higher xylose consumption of 11.7 g/L, than with G100X50. The ratio of consumed xylose to the consumed cellobiose (X/C) increased to 0.538, suggesting the relief of CCR for xylose consumption. The continuous fermentation process with C100X60 demonstrated a homofermentative lactic acid production of 27.5 g/L with a yield of 0.820 g/g and productivity of 5.49 g/L-h.

To confirm the beneficial effects of co-fermentation with C100X60 over that with

G100X60, the sugar mixture was changed back to G100X60 after C100X50 was tested. Similar parameters were obtained comparing with the first cycle (**Table 6.3**). The sugar combination should be the decisive factor in continuous co-fermentation. Feeding with C100X60 achieved simultaneous sugar utilization in continuous co-fermentation with a high productivity.

Table 6.2 Validation of mathematical models for sugar consumption, product formation and cell growth.

Substrates	Sugar consumption				Production formation				Cell growth			
	RMSE[a]	R^{2b}	BF[c]	AF[d]	RMSE	R^2	BF	AF	RMSE	R^2	BF	AF
Glucose	12.6	0.964	1.20	1.20	5.29	0.981	0.88	1.26	0.71	0.865	1.05	1.27
Cellobiose	7.99	0.967	1.08	1.08	3.17	0.992	1.04	1.09	0.21	0.930	1.03	1.08
Xylose	4.40	0.990	1.23	1.23	3.83	0.995	1.01	1.11	0.23	0.978	0.93	1.20

[a] root mean square error; [b] regression coefficient; [c] bias factor; [d] accuracy factor.

Table 6.3 Continuous L-lactic acid production by *E. mundtii* QU 25 using different sugar mixtures in feeding media (G100X60 or C100X60) at dilution rate of 0.2 1/h

Mixed sugars[a]	X[b] g/L	S_{glu}[c] g/L	S_{cel}[d] g/L	S_{xyl}[e] g/L	X/H[f] ratios	S_{LA}[g] g/L	S_{aa}[h] g/L	Y_{LA}[i] g/g	P_{LA}[j] g/L·h
G100X60	1.99 ± 0.05	75.4 ± 1.5	-	57.7 ± 1.3	0.096	24.2 ± 1.8	0.151 ± 0.068	0.803	4.84
C100X60	2.42 ± 0.11	-	79.4 ± 1.7	49.7 ± 0.8	0.538	27.5 ± 0.5	0.383 ± 0.022	0.820	5.49
G100X60	2.06 ± 0.14	72.7 ± 1.0	-	57.6 ± 0.6	0.103	25.4 ± 1.3	0.134 ± 0.017	0.812	5.08

[a]composition of fed medium, *i.e.*, G100X60, 100 g/L glucose and 60 g/Lxylose; C100X60, 100 g/L cellobiose and 60 g/Lxylose; [b]cell concentration; [c]effluent glucose concentration; [d]effluent cellobiose concentration; [e]effluent xylose concentration; [f]the ratio of consumed xylose to consumed hexoses (glucose or cellobiose); [g] lactic acid concentration; [h]acetic acid concentration; [i]yield of lactic acid production; and [j] lactic acid productivity.

6.3.3 Effects of dilution rates on continuous co-fermentation

The dilution rate is a critical control parameter for maximizing productivity in continuous fermentation process. In this study, continuous co-fermentation of C100X60 was performed at dilution rates increasing from 0.05 to 0.25 1/h (0.05 1/h, intervals), and the results are presented in **Table 6.4** (top). The cell formation increased when the dilution rate was between 0.05 1/h to 0.20 1/h, and a maximum value of 2.57 g/L was achieved at 0.201/h. Further increasing in the dilution rate to 0.25 1/h decreased cell concentration to 1.74 g/L. Total sugar consumption ranged from 28.5-33.7 g/L, and lactic acid production was 20.8-27.9 g/L at all dilution rates. The X/C ratio was higher than 0.508, among which it increased to 0.543 at a dilution rate of 0.20 1/h. The highest productivity of 5.37 g/L-h with 26.9 g/L lactic acid was obtained at a dilution rate of 0.20 1/h, which was considered optimal for C100X60 utilization by *E. mundtii* QU 25 in continuous mode. The highest productivity obtained in this study was much higher than 0.635 g/L-h in batch experiments (Wang et al., 2014b). However, high residual cellobiose of 77.2 g/L and xylose of 50.3 g/L were observed, and hence, further investigations were carried out to decrease the residual sugars.

Table 6.4 Effect of dilution rates on lactic acid production in CSFTR

	D[b] 1/h	X[c] g/L	S_{cel}[d] g/L	S_{xyl}[e] g/L	X/C ratio[f]	S_{LA}[g] g/L	S_{aa}[h] g/L	Y_{LA}[i] g/g	P_{LA}[j] g/L-h
C100X60[a] – CFSTR									
D1	0.05	1.03 ± 0.01	86.6 ± 4.1	44.8 ± 1.4	0.980	25.5 ± 0.3	0.381 ± 0.080	0.887	1.28
D2	0.10	1.43 ± 0.01	82.5 ± 3.8	46.7 ± 2.2	0.671	24.1 ± 0.8	0	0.780	2.41
D3	0.15	2.53 ± 0.03	79.0 ± 1.1	48.1 ± 0.8	0.508	27.9 ± 0.7	0.260 ± 0.039	0.844	4.18
D4	0.20	2.57 ± 0.02	77.2 ± 3.7	50.3 ± 2.5	0.543	26.9 ± 1.2	0.201 ± 0.031	0.823	**5.37**
D5	0.25	1.74 ± 0.05	83.4 ± 1.9	48.2 ± 1.7	0.575	20.8 ± 0.9	0.116 ± 0.023	0.730	5.21
C50X30[a] – CFSTR									
D1	0.05	1.06 ± 0.03	29.3 ± 0.4	20.9 ± 0.4	0.441	32.7 ± 0.5	0.559 ± 0.018	1.09	1.64
D2	0.10	1.43 ± 0.05	28.1 ± 0.5	21.5 ± 0.5	0.412	27.1 ± 1.3	0.380 ± 0.043	0.881	2.71
D3	0.15	1.52 ± 0.08	30.9 ± 1.2	20.7 ± 0.7	0.465	22.1 ± 1.5	0.276 ± 0.058	0.770	3.31
D4	0.20	2.18 ± 0.16	31.3 ± 0.9	22.7 ± 0.2	0.461	22.9 ± 0.9	0.415 ± 0.011	0.871	4.57
D5	0.25	2.42 ± 0.02	26.7 ± 0.4	22.9 ± 0.6	0.304	23.4 ± 0.5	0.651 ± 0.064	0.763	5.85
D6	0.30	2.29 ± 0.08	29.5 ± 0.7	23.7 ± 0.1	0.303	21.7 ± 0.9	0.650 ± 0.031	0.798	**6.52**
D7	0.35	2.16 ± 0.12	30.4 ± 0.5	23.9 ± 0.3	0.312	18.0 ± 0.7	0.570 ± 0.032	0.695	6.29
C50X30[a] – CF/CR									
D0	0.20	33.6 ± 1.9	0.32 ± 0.2	4.71 ± 0.9	0.521	**65.2 ± 3.5**	1.97 ± 0.21	0.854	**13.03**

[a] compositions of fed medium, *i.e.*, C100X60, 100g/L cellobiose and 60 g/L xylose; C50X30, 50g/L cellobiose and 30 g/L xylose; [b] dilution rates; [c] cell concentration; [d] effluent cellobiose concentration; [e] effluent xylose concentration; [f] ratios of consumed xylose over consumed cellobiose; [g] lactic acid concentration; [h] acetic acid concentration; [i] yields of lactic acid production; and [j] lactic acid productivity

C50X30 was investigated in similar fashion as continuous co-fermentation for increasing dilution rates of 0.05-0.35 1/h, as presented in **Table 6.4** (bottom). The cell concentration increased with the dilution rate from 1.06 g/L (at *D*=0.05 1/h) to 2.42 g/L (at *D*=0.25 1/h), but a further increase in the dilution rates to 0.30 1/h and 0.35 1/h resulted in lower cell concentrations of 2.29 and 2.16 g/L, respectively. The limiting cell retention time (inverse of the dilution rates) of the strain in the CFSTR, or the CRT for zero cell production may be lower than 2 hours. The X/C ratios were almost similar at dilution rates of 0.05-0.20 1/h ranged 0.412-0.465, respectively. When the dilution rate was higher than 0.20 1/h, the X/C ratio decreased dramatically from 0.461 (at *D*=0.20 1/h) to 0.303 (at *D*=0.251/h), implying a critical condition among cell concentration, sugar compositions, and increased CCR for xylose utilization. The lactic acid productivity increased with the increasing dilution rate until *D*=0.30 1/h, and a maximum value of 6.52 g/L-h was reached.

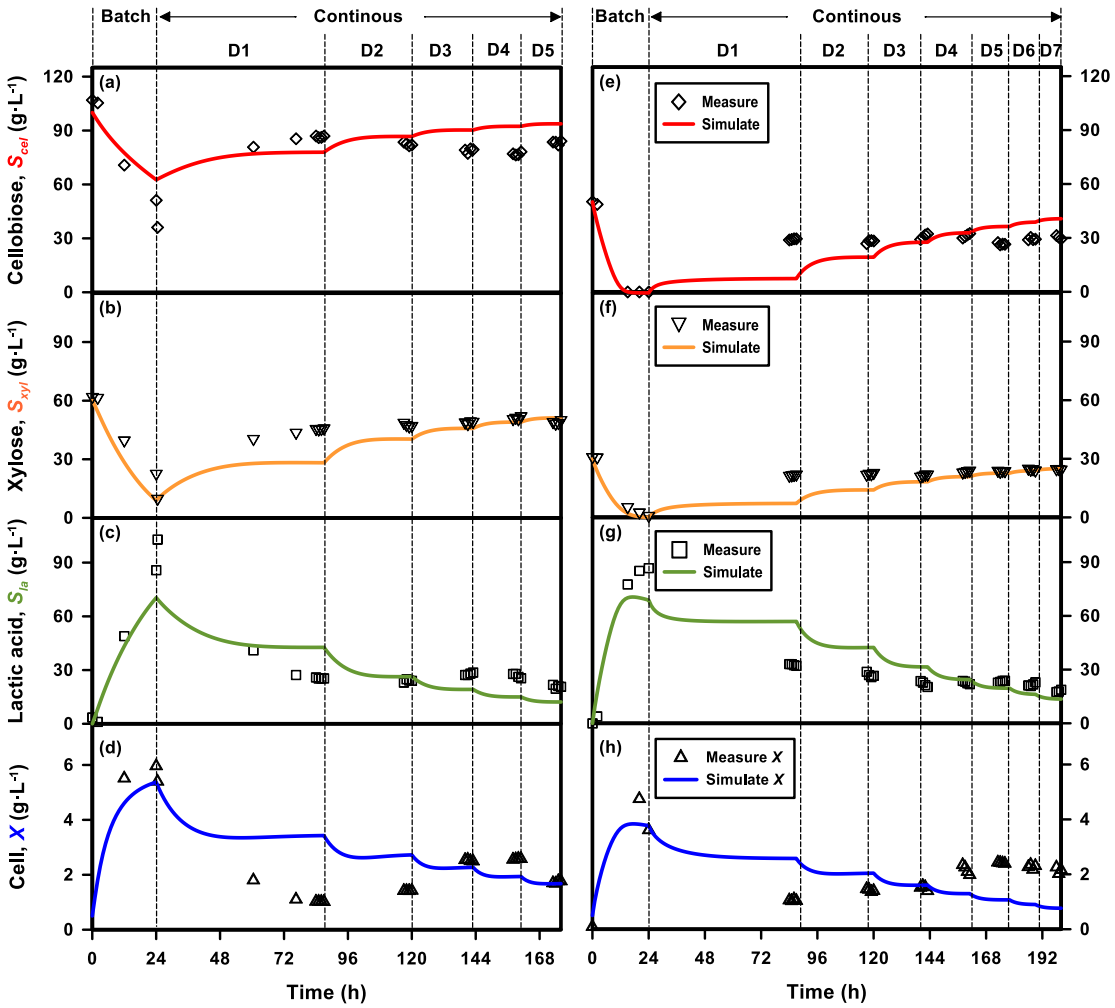

Figure 6.4 Continuous fermentation to produce lactic acid using *E. mundtii* QU 25 with combined cellobiose and xylose. The designed feeding sugar combinations were: cellobiose 100 g/L and xylose 60 g/L (C100X60, left); and cellobiose 50 g/L and xylose 30 g/L (C50X30, right). Both reactors started with batch mode and then transferred to continuous mode after achieving state-state. The color coded curves show the simulation results and the symbols indicate the experimental results. At least three analyses were carried out before the transition of different operational conditions in the process.

As the co-fermentation experiments were carried out continuously, and the influent conditions were adjusted over well-controlled retention time, the experimental results served well as examples of dynamic simulations of the mathematical model. The

dynamic records of the experiments and the corresponding simulation results are presented in **Figure 6.4**. Effluent cellobiose, xylose, lactic acid, and cell concentrations are shown in four different rows of the subfigures; and the two columns represent the influent sugars combinations of C100X50 (left) and C50X30 (right). D1 - D7 represent the tested dilution rates (0.05 – 0.35 1/h) and the multiple symbols represent the experimental data when steady state was achieved at the tested dilution rates.

In general, the model described reasonably well the dynamic status of the measured parameters, especially on the predictions of immediate changes of substrate and product concentrations between batch and continuous modes. However, some limitations were also discovered for further improvement of the experiments and model structure. In the experiments, cellobiose, xylose, and lactic acid concentrations were at relatively constant levels after the first dilution rate (D1), but obvious increases of cell concentration were observed from D1 to D4 (onward) for both experiments. Before the cell started to be diluted, regional peaks could be found at specific dilution rates, *i.e.*, at the end of D4 for C100X50 and D5 for C50X30. In fact, sugar consumption and lactic acid production also followed this pattern, but the covered ranges were less significant. The changes in cell concentrations over dilution rates were not predicted by the simulation.

Based on Monod kinetics, cell concentrations increase with the related consumption of the substrate. This increase is compensated by cell decay and “wash-out” effects due to high dilution rates in CSFTR. As the cell yield coefficients determined in the batch system were quite low, the simulated cell concentration in the process should be a continuously decrease with the increase in dilution rate. This uncertainty between the model and experimental results may be due to the incomplete cell suspension in the fermentation broth or other uncharacterized factors in the model. The fermentor used in this study is a typical cylindrical column container with a mechanical stirrer installed through the reactor from the top. The CSFTR was controlled by pumping the same amount of liquid in and out of the system. The cell samples were collected through a sampling pipe extending to the bottom of the reactor. When performing long-term continuous experiments, the fermenting cells may not be completely suspended in the fermentation broth, or consistently discharged with the liquid effluent. A slightly higher cell concentration may exist in the bottom part of the jar, which results in inconsistency. Regardless, clarification of this issue requires further investigation and was not significant when the fermentation cells were completely retained in the fermentation process, as detailed in the next section.

6.3.4 Continuous fermentation with cell recycling (CF/CR)

Controlling cell concentration through cell recycling has been demonstrated to be an efficient technique to obtain high cell density and lactic acid productivity in continuous fermentation with a single carbon source, *i.e.*, glucose (Tashiro et al., 2011) and starch (Shibata et al., 2007). The CF/CR process was performed after receiving concentrated cell concentration from a 4-L reactor, with mMRS medium containing C50X30 at pH 7.0 (Abdel-Rahman et al., 2015; Wang et al., 2014b) and a dilution rate of 0.2 h^{-1} (**Figure 6.5**). Approximately 15-fold higher cells (33.6 g/L) and 2-fold lower residual xylose concentration (4.71 g/L) in the fermentation broth were achieved in comparison to the processes without cell recycling. The X/C ratio was 0.521 in the CF/CR process compared to 0.461 in the conventional mode under the same dilution rate. A high optically pure (≥99.8%) L-lactic acid concentration of 65.2 g/L and productivity of 13.03 g/L-h were obtained with slightly lower lactic acid yield over the consumed sugars (0.854 g/g), compared to 22.9 g/L, 4.57 g/L-h, and 0.871 g/g without cell recycling, respectively. Only minimal by-products of 0.02-1.97 g/L acetic acid, 0.26-1.93 g/L formic acid, and 0-1.65 g/L ethanol produced from the undesirable pK pathway were measured (Wang et al., 2015), further confirming our hypothesis in model development. The significant benefits of cell recycle were further clarified when the lactic acid yields were expressed based on the

feeding sugars instead of the consumed sugars. In the CF/CR process, almost all the feeding sugars were utilized by the fermentation strain, and the lactic acid yield was 0.801 g/g -feeding sugars; while in the process without cell recycling, the yield of lactic acid was 0.285 g/g -feeding sugars at the same dilution rate of 0.2 1/h. The fermentation strategy demonstrated outstanding productivity, end-product concentration, and consumption of mixed sugars for more feasible applications.

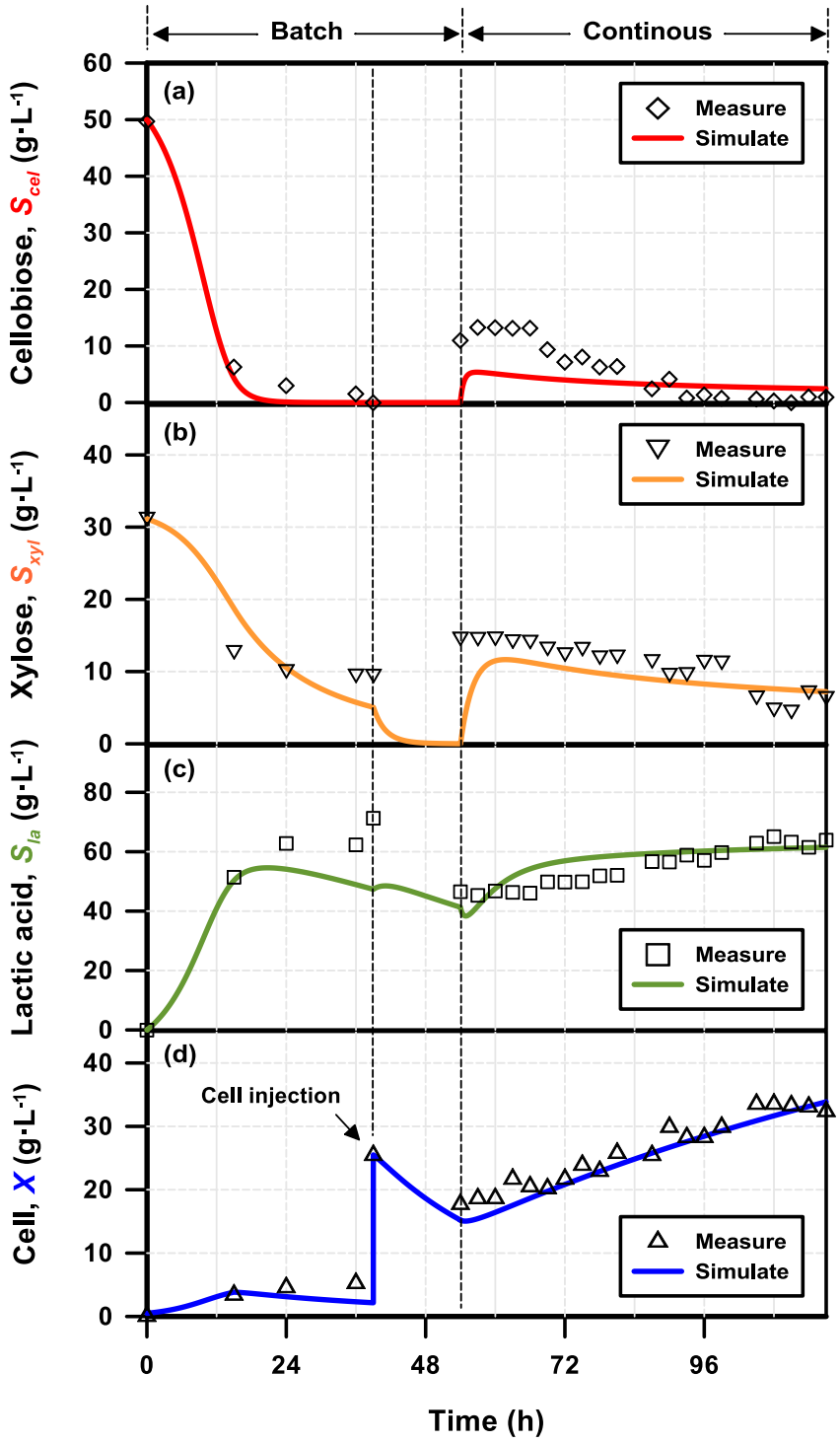

Figure 6.5 Continuous fermentation with cell recycling to produce lactic acid using *E. mundtii* QU 25 with a combination of cellobiose and xylose. The designed feeding sugar combination was cellobiose 50 g/L and xylose 30 g/L. The reactor started with batch mode and then transferred to continuous mode after achieving steady-state. The cells were concentrated before transfer. The color coded curves show the simulation results and the points show the averages of three measurements.

Table 6.5 Comparison of lactic acid production by different continuous fermentation systems.

Fermentation Mode	Substrates	Microorganism	S_{LA}[a] (g/L)	Y_{LA}[b] (g/g)	P_{LA}[c] (g/L-h)	Isomer (optical purity, %)	D[d] (1/h)	Ref.
Free cells	Corn stover hydrolysate	*B. coagulans* strain AD	42	0.95	3.69	ND[e]	0.167	Ahring et al. (2016)
Free cells	Lactose: 60 g/L	*Lb. bulgaricus* ATCC 8001	30	0.72	7.2	ND[e]	0.24	Taleghani et al. (2014)
Free cells	Xylose: 50 g/L	*E. mundtii* QU 25	21.7	0.855	3.14	L (-)	0.15	Abdel-Rahman et al. (2016)
Free cells	C50X30[f]	*E. mundtii* QU 25	21.7	0.801	6.52	L (99.8)	0.3	This work
Immobilization	Glucose: 45 g/L	*Lc. lactis* IO-1	8.91	0.89	4.46	ND[e]	0.5	Sirisansaneeyakul et al. (2007)
Immobilization	Lactose: 100 g/L	*Lb. helveticus* ATCC 15009	75.6	0.96	3.90	ND[e]	0.056	Tango and Ghaly (2002)
Cell recycling	Glucose: 20 g/L	*Lb. delbrueckii subsp. lactis* QU 41	20.7	1.03	18.0	D (99.9)	0.87	Tashiro et al. (2011)
Cell recycling	Corn steep: 30 g/L	*Lactobacillussp.* RKY2	42.0	0.95	6.7	ND[e]	0.16	Wee and Ryu (2009)
Cell recycling	Tapioca hydrolysate	*B. coagulans* A107	50.3	0.80	10.1	L (+)	0.2	López-Gómez et al. (2019)
Cell recycling	Acid whey: 90 g/L	*L. coryniformissubsp. torquens*	45.9	0.92	9.2	L (-)	0.2	López-Gómez et al. (2019)
Cell recycling	Molasses	*B. coagulans* A40	59.6	0.85	5.9	L (+)	0.1	López-Gómez et al. (2019)
Cell recycling	Corn stover hydrolysate	*B. coagulans* NBRC 12714	92	0.91	13.8	L (99.5)	0.15	Ma et al. (2016)
Cell recycling	Glucose: 50 g/L	*B. coagulans* PS5	42	0.84	8.6	L (-)	0.2	Fan et al. (2017)
Cell recycling	Glucose: 100 g/L	*E. faecalis* RKY1 KCTC 8890P	≥90	0.95	3.72	L (+)	0.04	Lee et al. (2014)
Cell recycling	Xylose: 50 g/L	*E. mundtii* QU 25	41.0	1.01	6.15	L (-)	0.155	Abdel-Rahman et al. (2016)
Cell recycling	C50X30[f]	*E. mundtii* QU 25	65.2	0.854	13.03	L (99.8)	0.2	This work

[a]Lactic acid concentration. [b]Yield of lactic acid production. [c]Lactic acid productivity. [d]Dilution rate. [e]Not determined. *Lb., Lactobacillus*; *Lc., Lactococcus*；*E., Enterococcus; B., Bacillus;* and [f]Cellobiose 50 g/L and xylose 30 g/L.

The experiment results of the CF/CR process for lactic acid production were compared with the data of the most recent publications in **Table 6.5.** Lactic acid fermentation is a product- and substrate- specific process, and the applied microorganisms and operation conditions play significant roles. The target of the lignocellulosic biomass biorefinery is to increase the product conversion yield from various carbon sources. Continuous fermentation is an attractive concept toward industrialization, and hence has been widely studied recently. The CFSTR operation with free cells suffers from the unbalanced limiting growth rate and metabolic characteristics over short HRTs (high dilution rates), and hence are not feasible in continuous fermentation. Immobilization and cell recycling using hollow fiber microfiltration module have been widely applied to increase the cell density in the bioreactor, and hence further improve the productivity and stability of the process. This concept was confirmed by the experimental results in this study, as the productivity of lactic acid and fermentation titer were both at the high range compared to other studies. Among the references, Tashiro (Tashiro et al., 2011) and Ma et al. (Ma et al., 2016) provided the only two cases with higher productivities than this work. With similar experimental set-up, the former study was conducted at an extremely low influent sugar concentration (glucose 20 g/L); and the later one used an outstanding thermophilic strain (*B. coagulans* NBRC 12714) in a well-constructed

biorefinery process, *i.e.*, modified pretreatment process and solid background of sequencing fermentation data.

In addition to the productivity, other critical information shown in the table of process performance (**Table 6.5**) is the inconsistent relationship between the dilution rate and the production yield. It is widely known that the strain characteristics and experimental set-ups both play important roles in the fermentation processes, therefore many quantitative measures, *i.e*., product concentration, yield, productivity, and dilution rate, have been introduced in the studies to support the cross-comparison. However, it should be also noted that the CRT is also a critical parameter but has not been reported throughout the cited literatures. Theoretically, the cell activity is a function of many parameters including the cell aging in the reactor. With the cell metabolism, the productivity and the final product should increase rapidly at the beginning of fermentation, and then reach a plateau before the final decline over time. However, since there is no discharge control of the excessive cells, the CRTs of the reported CF/CR experiments are equal to the running time, which may not directly reflect to this process condition. A standardized index and operational procedure may be needed to support the comparison among the CF/CR studies.

The dynamic change in cellobiose, xylose, lactic acid, and cell concentrations in the CF/CR process (symbols, including the operation in batch mode) and the simulation results (lines) are presented in **Figure 6.5(a)** through **Figure 6.5(d)**, respectively. Significant consumptions of cellobiose and xylose were shown at the beginning phase of the batch system (from 0 to 24^{th} hour), which was associated with the corresponding increase in lactic acid production and a slightly increase in cell concentration. Xylose was not completely utilized, and approximately 10 g/L residual sugar in the effluent of the system from 24^{th}-36^{th} hour before cell injection. The concentrated cells were introduced 15 hours before the process was changed to continuous mode. The CF/CR functioned properly with consistent reduction in residual sugars and increase in lactic acid/cell concentrations.

The simulation results showed outstanding characterization of the process conditions over the whole experiment. It accurately predicted the consumption of cellulose at batch mode and the overall statuses of the components in continuous mode. While no measurements were conducted during the transition period (from the 39^{th} to the 54^{th} hours), the model simulated the degradation of sugars due to a significant increase in cells, as no additional sugars were introduced in the reactor. During the transition period, the cell concentration declined considerably due to decay, and then increased

again in the continuous process when sugars were again introduced in the CF/CR process. Although the CCR on the xylose consumption during the batch mode was not simulated (**Figure 6.5(b)**, hours 24-36), this model showed high sensitivity in handling the flow condition changes, cell growth, and cell retention problems.

6.3.5 Importance of cell retention time (CRT)

In summary of all the experimental results collected in this study for C50X30, including the relationships of cellobiose, xylose, lactic acid, and cell concentrations, are plotted in **Figure 6.6**. CRTs did show critical impacts on the continuous process. With the increase in CRT, the fermentation strain with a high density was more effective in utilizing the sugars and may be more robust, reflecting the changing properties of the hydrolysate. The benefits of the high cell density fermentation and the CRT control have been demonstrated in many biological systems, *i.e.*, increase in xylose utilization for high biofuel productivity (Sarks et al., 2014), regulation of the consumption rates of various carbon sources (Leu et al., 2009), and real-time gas phase monitoring for optimal cells metabolism (Leu et al., 2010).

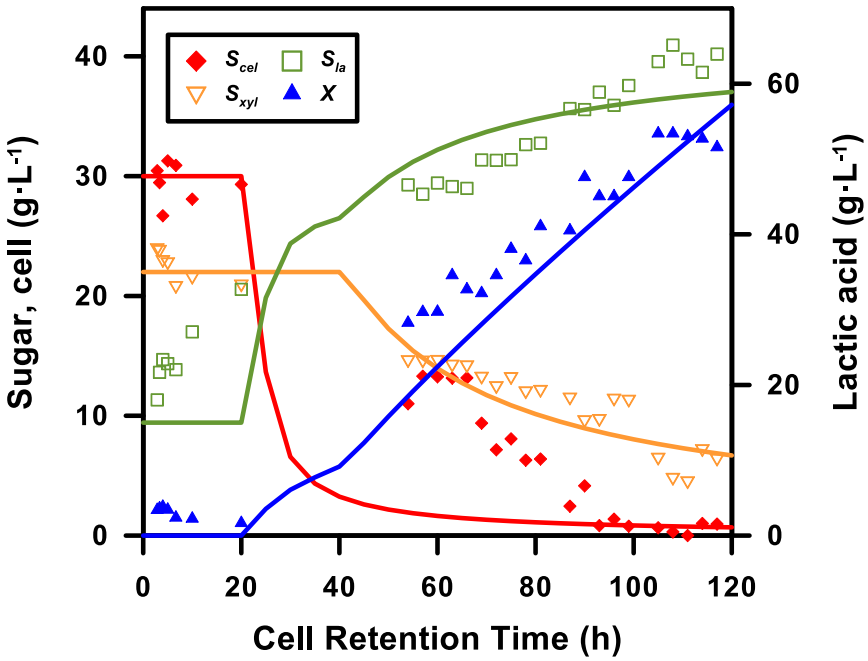

Figure 6.6 Performances of co-fermentation over different cell retention times (in hours) and two attempted numerical fits: (a) linear regressions; and (b) steady state expression based on the proposed simulation model.

Meanwhile, the difference in the commonly applied control parameter dilution rate (1/HRT) used in the conventional fermentation process over the factor for cell retention (1/CRT) should be emphasized. As the cells have been recovered from the liquid stream, the CRT of the CF/CR must be longer than the HRT, and this expression applies to all other biological systems such as bioaugmentation or fed-batch fermentation.

To better visualize the potential applications of the long CRT operation, the dynamic model was simplified to steady state expressions as the numerical strategy used in Leu

et al. (Leu et al., 2009). The expressions were derived by eliminating the accumulation terms (*i.e.*, *dX/dt* and *dS/dt*) in Equations (3-18) and (3-19), and followed by a series of algebraic operations as presented in supplementary information (Equations (3-21) to (3-32)). The sugar and cell concentrations as functions of the key control parameters are presented in the following equations:

$$S_{sug} = \frac{K_S \cdot \left(1 + CRT \cdot K_D\right)}{CRT \cdot \left(\mu_{max} - K_D\right) - 1} \tag{6-4}$$

$$X = Y_{sug}^{X} \cdot \frac{CRT}{HRT} \cdot \frac{S_{sug}^{in} - S_{sug}}{K_D \cdot CRT + 1} \tag{6-5}$$

The results of the steady state expressions were plotted against the experimental results in **Figure 6.6**, which also summarizes the potential benefits and issues of the model. The model clearly demonstrated the possibility of CF/CR operation for process control and optimization. For instance, the important wash-out period at low CRT operation on residual sugars and delayed cell growth was shown in the model, suggesting a potential issue of continuous operation that was not observed in the batch experiments. As the fermentation experiments at short CRT were prepared with the well-inoculated seed strains, the challenges of low CRT operation were not observed in this work. The cell bleeding and complete consumption of xylose at extremely long CRT has not been

characterized because the study have targeted and designed experiments for a high productivity. The experiments were discontinued after 117 hours of operation when the maximum lactic acid concentration 65.15 g/L was reached at 108 hours and the cell concentration was at the maximum at 105 hours. In the simulation model, the cell bleeding and endogenous respiration were all included in the decay term through the first-order reaction kinetics, which may be recorded more clearly if longer and well-controlled CRTs are conducted. The impacts of rapid sugar uptake and delayed growth, or CCR were not characterized due to the current model structure and limited simulation parameters. These uncertain points require further investigations of the system in the future works.

6.4 Conclusion

Continuous co-fermentation was demonstrated to be a feasible strategy to improve the productivity of lactic acid production using a cellobiose/xylose mixture and *Enterococcus mundtii* QU 25. The high productivity 13.03 g/L-h and product concentration (65.2 g/L) were contributed by a significant fraction of xylose conversion (34.2%) over cellobiose (65.7%), implying the feasibility of the conversion of lignocellulosic substrates. The kinetic model developed based on the experimental results provided further understanding of the process conditions with

various reactor modes, dilution rates, and cell retention times. Further experiments can be designed based on the model structure to clarify the beneficial effects of a long CRT operation for the reduction in CCR and cell decay in the presence of growth inhibiting substrates.

.

Chapter 7 Conclusion

The derived model structure integrating dynamic enzyme adsorption, cellulose hydrolysis and fermentation was successfully constructed and validated with experimental results. The model might be able to provide a new perspective toward better understanding of lignin-induced nonproductive adsorption of cellulase and impacts on cellulose hydrolysis performance. The model was able to apply to various pretreated substrates accounting the impacts of residual lignin and surfactants. Mixed sugars co-fermentation of pentose and hexose was conducted in batch, fed-batch and continuous model of fermentation and model simulation was applied for process optimization. Key kinetic parameters were identified and optimized. Further experiments on simultaneous saccharification and fermentation for lignocellulose biomass can be designed based on the model structure to clarify the beneficial effects of cell retention time in a continuous operation with cell recycle using organosolv pretreated substrates.

The numerical model platform showed a great flexibility of capturing the dynamic interactions between enzyme adsorption, cell growth and production formation and t in the enzymatic hydrolysis and fermentation. It can be further expanded to

investigate the impacts other substrate properties or operation factors, such as operation temperature, pH, and functional groups of the lignin. It can also apply to different type of feedstock, such as food waste, with a different composition of carbohydrates and different types of applied enzymes. The model structure provides a solid foundation for future model modification/development for other hydrolysis and fermentation system or biomass pretreatment.

References

Abdel-Rahman, M. A., Tashiro, Y., Zendo, T., Hanada, K., Shibata, K., & Sonomoto, K. (2011a). Efficient homofermentative L-(+)-lactic acid production from xylose by a novel lactic acid bacterium, Enterococcus mundtii QU 25. *Applied and Environmental Microbiology, 77*(5), 1892-1895.

Abdel-Rahman, M. A., Tashiro, Y., Zendo, T., Sakai, K., & Sonomoto, K. (2016). Highly efficient L-lactic acid production from xylose in cell recycle continuous fermentation using Enterococcus mundtii QU 25. *RSC Advances, 6*(21), 17659-17668.

Abdel-Rahman, M. A., Tashiro, Y., Zendo, T., Shibata, K., & Sonomoto, K. (2011b). Isolation and characterisation of lactic acid bacterium for effective fermentation of cellobiose into optically pure homo L-(+)-lactic acid. *Applied Microbiology and Biotechnology, 89*(4), 1039-1049.

Abdel-Rahman, M. A., Tashiro, Y., Zendo, T., & Sonomoto, K. (2013). Improved lactic acid productivity by an open repeated batch fermentation system using Enterococcus mundtii QU 25. *RSC Advances, 3*(22), 8437-8445.

Abdel-Rahman, M. A., Xiao, Y., Tashiro, Y., Wang, Y., Zendo, T., Sakai, K., & Sonomoto, K. (2015). Fed-batch fermentation for enhanced lactic acid production from glucose/xylose mixture without carbon catabolite repression. *Journal of Bioscience and Bioengineering, 119*(2), 153-158.

Ahring, B. K., Traverso, J. J., Murali, N., & Srinivas, K. (2016). Continuous fermentation of clarified corn stover hydrolysate for the production of lactic acid at high yield and productivity. *Biochemical Engineering Journal, 109*, 162-169. doi:https://doi.org/10.1016/j.bej.2016.01.012

Alfani, F., Gallifuoco, A., Saporosi, A., Spera, A., & Cantarella, M. (2000). Comparison of SHF and SSF processes for the bioconversion of steam-exploded wheat straw. *Journal of Industrial Microbiology and Biotechnology, 25*(4), 184-192.

Atalla, R. H., & VanderHart, D. L. (1984). Native cellulose: a composite of two distinct crystalline forms. *Science, 223*, 283-286.

Bajpai, P. (2016). Structure of lignocellulosic biomass *Pretreatment of Lignocellulosic Biomass for Biofuel Production* (pp. 7-12): Springer.

Ballesteros, M. (2010). Enzymatic hydrolysis of lignocellulosic biomass. *Bioalcohol Production: Biochemical Conversion of Lignocellulosic Biomass, Woodhead Publishing Series in Energy*, 159-177.

Bilal, M., & Iqbal, H. M. (2020). Recent advancements in the life cycle analysis of

lignocellulosic biomass. *Current Sustainable/Renewable Energy Reports*, 1-8.

Boonmee, M., Leksawasdi, N., Bridge, W., & Rogers, P. L. (2003). Batch and continuous culture of Lactococcus lactis NZ133: experimental data and model development. *Biochemical Engineering Journal, 14*(2), 127-135.

Bradford, M. M. (1976). A rapid and sensitive method for the quantitation of microgram quantities of protein utilizing the principle of protein-dye binding. *Analytical Biochemistry, 72*(1-2), 248-254.

Brondi, M. G., Elias, A. M., Furlan, F. F., Giordano, R. C., & Farinas, C. S. (2020). Performance targets defined by retro-techno-economic analysis for the use of soybean protein as saccharification additive in an integrated biorefinery. *Scientific Reports, 10*(1), 1-13.

Brower, J. E., Zar, J. H., & von Ende, C. (1998). Field and laboratory methods for general ecology.

Burgos-Rubio, C. N., Okos, M. R., & Wankat, P. C. (2000). Kinetic study of the conversion of different substrates to lactic acid using Lactobacillus bulgaricus. *Biotechnology Progress, 16*(3), 305-314.

Cai, C., Zhan, X., Lou, H., Li, Q., Pang, Y., Qian, Y., Zhou, H., & Qiu, X. (2018). Recycling cellulase by a pH-responsive lignin-based carrier through electrostatic interaction. *ACS Sustainable Chemistry & Engineering, 6*(8), 10679-10686.

Chandel, A. K., Silva, S., & Singh, O. V. (2011). Detoxification of lignocellulosic hydrolysates for improved bioethanol production. *Biofuel Production-Recent Developments and Prospects*, 225-246.

Chandra, R. P., Au-Yeung, K., Chanis, C., Roos, A. A., Mabee, W., Chung, P. A., Ghatora, S., & Saddler, J. N. (2011). The influence of pretreatment and enzyme loading on the effectiveness of batch and fed-batch hydrolysis of corn stover. *Biotechnology Progress, 27*(1), 77-85.

Chen, H. (2014). Chemical composition and structure of natural lignocellulose *Biotechnology of lignocellulose* (pp. 25-71): Springer.

Datta, R., & Henry, M. (2006). Lactic acid: recent advances in products, processes and technologies—a review. *Journal of Chemical Technology and Biotechnology, 81*(7), 1119-1129.

Ding, S.-Y., Liu, Y.-S., Zeng, Y., Himmel, M. E., Baker, J. O., & Bayer, E. A. (2012). How does plant cell wall nanoscale architecture correlate with enzymatic digestibility? *Science, 338*(6110), 1055-1060.

Dong, C., Meng, X., Yeung, C. S., Ho-Yin, T., Ragauskas, A. J., & Leu, S.-Y. (2019). Diol pretreatment to fractionate a reactive lignin in lignocellulosic biomass

biorefineries. *Green Chemistry, 21*(10), 2788-2800.

Dong, C., Wang, Y., Chan, K., Akanksha, B., & Leu, S. (2018a). Temperature profiling to maximize energy yield with reduced water input in a lignocellulosic ethanol biorefinery. *Applied Energy, 214*, 63-72.

Dong, C., Wang, Y., Zhang, H., & Leu, S.-Y. (2018b). Feasibility of high-concentration cellulosic bioethanol production from undetoxified whole Monterey pine slurry. *Bioresource Technology, 250*, 102-109.

dos Santos, A. C., Ximenes, E., Kim, Y., & Ladisch, M. R. (2018). Lignin–enzyme interactions in the hydrolysis of lignocellulosic biomass. *Trends in Biotechnology*.

Dos Santos, A. C. F., Ximenes, E., N Thompson, D., Ray, A. E., Szeto, R., Erk, K., Dien, B. S., & Ladisch, M. R. (2020). Effect of using a nitrogen atmosphere on enzyme hydrolysis at high corn stover loadings in an agitated reactor. *Biotechnology Progress, 36*(6), e3059.

Fan, L., & Lee, Y. h. (1983). Kinetic studies of enzymatic hydrolysis of insoluble cellulose: Derivation of a mechanistic kinetic model. *Biotechnology and Bioengineering, 25*(11), 2707-2733.

Fan, R., Ebrahimi, M., Quitmann, H., & Czermak, P. (2017). Lactic acid production in a membrane bioreactor system with thermophilic Bacillus coagulans: Online monitoring and process control using an optical sensor. *Separation Science and Technology, 52*(2), 352-363.

Fu, W., & Mathews, A. (1999). Lactic acid production from lactose by Lactobacillus plantarum: kinetic model and effects of pH, substrate, and oxygen. *Biochemical Engineering Journal, 3*(3), 163-170.

Görke, B., & Stülke, J. (2008). Carbon catabolite repression in bacteria: many ways to make the most out of nutrients. *Nature Reviews Microbiology, 6*(8), 613-624.

Gan, Q., Allen, S., & Taylor, G. (2003). Kinetic dynamics in heterogeneous enzymatic hydrolysis of cellulose: an overview, an experimental study and mathematical modelling. *Process Biochemistry, 38*(7), 1003-1018.

Germec, M., Cheng, K.-C., Karhan, M., Demirci, A., & Turhan, I. (2019). Application of mathematical models to ethanol fermentation in biofilm reactor with carob extract. *Biomass Conversion and Biorefinery*, 1-16.

Germec, M., Karhan, M., Demirci, A., & Turhan, I. (2020). Implementation of flexible models to bioethanol production from carob extract–based media in a biofilm reactor. *Biomass Conversion and Biorefinery*, 1-17.

Ghose, T. K., & Tyagi, R. (1979). Rapid ethanol fermentation of cellulose hydrolysate. I. Batch versus continuous systems. *Biotechnology and Bioengineering, 21*(8),

1387-1400.

Gregg, D. J., & Saddler, J. N. (1996). Factors affecting cellulose hydrolysis and the potential of enzyme recycle to enhance the efficiency of an integrated wood to ethanol process. *Biotechnology and Bioengineering, 51*(4), 375-383.

Guo, F., Shi, W., Sun, W., Li, X., Wang, F., Zhao, J., & Qu, Y. (2014). Differences in the adsorption of enzymes onto lignins from diverse types of lignocellulosic biomass and the underlying mechanism. *Biotechnology for Biofuels, 7*(1), 1-10.

HKEPD. (2020). *Monitoring of Solid Waste in Hong Kong - Waste Statistics for 2019*. Hong Kong.

HKHCSBG. (2009). *Hong Kong Herbarium and South China Botanical Garden (HKHCSBG). Flora of Hong Kong*. Hong Kong: Agriculture, Fisheries and Conservation Department.

Horn, S. J., & Eijsink, V. G. (2010). Enzymatic hydrolysis of steam-exploded hardwood using short processing times. *Bioscience, Biotechnology, and Biochemistry, 74*(6), 1157-1163.

Humbird, D., Davis, R., Tao, L., Kinchin, C., Hsu, D., Aden, A., Schoen, P., Lukas, J., Olthof, B., & Worley, M. (2011). *Process design and economics for biochemical conversion of lignocellulosic biomass to ethanol: dilute-acid pretreatment and enzymatic hydrolysis of corn stover*. Retrieved from United State:

Islam, M. K., Thaemngoen, A., Lau, C. Y., Guan, J., Yeung, C. S., Chaiprapat, S., & Leu, S.-Y. (2021). Staged organosolv pretreatment to increase net energy and reactive lignin yield in whole oil palm tree biorefinery. *Bioresource Technology, 326*, 124766.

Islam, M. K., Wang, H., Rehman, S., Dong, C., Hsu, H.-Y., Lin, C. S. K., & Leu, S. Y. (2019). Sustainability metrics of pretreatment processes in a waste derived lignocellulosic biomass biorefinery. *Bioresource Technology*, 122558.

Jørgensen, H., Kristensen, J. B., & Felby, C. (2007). Enzymatic conversion of lignocellulose into fermentable sugars: challenges and opportunities. *Biofuels, Bioproducts and Biorefining, 1*(2), 119-134.

Jeoh, T., Cardona, M. J., Karuna, N., Mudinoor, A. R., & Nill, J. (2017). Mechanistic kinetic models of enzymatic cellulose hydrolysis–A review. *Biotechnology and Bioengineering*.

Kadam, K. L., Rydholm, E. C., & McMillan, J. D. (2004). Development and validation of a kinetic model for enzymatic saccharification of lignocellulosic biomass. *Biotechnology Progress, 20*(3), 698-705.

Ketterings, Q. M., Coe, R., van Noordwijk, M., & Palm, C. A. (2001). Reducing

uncertainty in the use of allometric biomass equations for predicting above-ground tree biomass in mixed secondary forests. *Forest Ecology and Management, 146*(1), 199-209.

Kim, S., & Holtzapple, M. T. (2006). Effect of structural features on enzyme digestibility of corn stover. *Bioresource Technology, 97*(4), 583-591.

Kim, Y., Kreke, T., Ko, J. K., & Ladisch, M. R. (2015). Hydrolysis-determining substrate characteristics in liquid hot water pretreated hardwood. *Biotechnology and Bioengineering, 112*(4), 677-687.

Ko, C.-H., Chaiprapat, S., Kim, L.-H., Hadi, P., Hsu, S.-C., & Leu, S.-Y. (2017). Carbon sequestration potential via energy harvesting from agricultural biomass residues in Mekong River basin, Southeast Asia. *Renewable and Sustainable Energy Reviews, 68*, 1051-1062.

Ko, C.-H., Chen, F.-J., Lee, J. J., & Tzou, D.-L. M. (2011). Effects of fiber physical and chemical characteristics on the interaction between endoglucanase and eucalypt fibers. *Cellulose, 18*(4), 1043-1054.

Ko, J. K., Ximenes, E., Kim, Y., & Ladisch, M. R. (2015). Adsorption of enzyme onto lignins of liquid hot water pretreated hardwoods. *Biotechnology and Bioengineering, 112*(3), 447-456.

Kohyama, T. (1993). Size-structured tree populations in gap-dynamic forest--the forest architecture hypothesis for the stable coexistence of species. *Journal of Ecology*, 131-143.

Koppram, R., Tomás-Pejó, E., Xiros, C., & Olsson, L. (2014). Lignocellulosic ethanol production at high-gravity: challenges and perspectives. *Trends in Biotechnology, 32*(1), 46-53.

Kumar, L., Arantes, V., Chandra, R., & Saddler, J. (2012). The lignin present in steam pretreated softwood binds enzymes and limits cellulose accessibility. *Bioresource Technology, 103*(1), 201-208.

Kumar, P., Barrett, D. M., Delwiche, M. J., & Stroeve, P. (2009). Methods for pretreatment of lignocellulosic biomass for efficient hydrolysis and biofuel production. *Industrial and Engineering Chemistry Research, 48*(8), 3713-3729.

Kumar, R., & Wyman, C. E. (2009). Cellulase adsorption and relationship to features of corn stover solids produced by leading pretreatments. *Biotechnology and Bioengineering, 103*(2), 252-267.

Kwan, T. H., Hu, Y., & Lin, C. S. K. (2018). Techno-economic analysis of a food waste valorisation process for lactic acid, lactide and poly (lactic acid) production. *Journal of Cleaner Production, 181*, 72-87.

López-Gómez, J. P., Alexandri, M., Schneider, R., & Venus, J. (2019). A review on the

current developments in continuous lactic acid fermentations and case studies utilising inexpensive raw materials. *Process Biochemistry, 79*, 1-10.

Lawrence, A. W., & McCarty, P. L. (1970). Unified basis for biological treatment design and operation. *Journal of the Sanitary Engineering Division, 96*(3), 757-778.

Lee, R.-K., Ryu, H.-W., Oh, H., Kim, M., & Wee, Y.-J. (2014). Cell-recycle continuous fermentation of Enterococcus faecalis RKY1 for economical production of lactic acid by reduction of yeast extract supplementation. *Journal of Microbiolog and Biotechnology, 24*(5), 661-666.

Leu, S.-Y., Libra, J. A., & Stenstrom, M. K. (2010). Monitoring off-gas O2/CO2 to predict nitrification performance in activated sludge processes. *Water Research, 44*(11), 3434-3444.

Leu, S.-Y., & Stenstrom, M. K. (2010). Bioaugmentation to improve nitrification in activated sludge treatment. *Water Environment Research, 82*(6), 524-535.

Leu, S.-Y., & Zhu, J. (2013). Substrate-related factors affecting enzymatic saccharification of lignocelluloses: our recent understanding. *Bioenergy Research, 6*(2), 405-415.

Leu, S. Y., Babcock, R. W., Tzeng, C. J., & Stenstrom, M. K. (2009). Modeling the performance of hazardous wastes removal in bioaugmented activated sludge processes. *Water Environment Research, 81*(11), 2309-2319.

Li, F., Liu, X., Zhang, X., Zhao, D., Liu, H., Zhou, C., & Wang, R. (2016a). Urban ecological infrastructure: an integrated network for ecosystem services and sustainable urban systems. *Journal of Cleaner Production, 30*, 1e7.

Li, S.-Y., Srivastava, R., Suib, S. L., Li, Y., & Parnas, R. S. (2011). Performance of batch, fed-batch, and continuous A–B–E fermentation with pH-control. *Bioresource Technology, 102*(5), 4241-4250.

Li, Y., Sun, Z., Ge, X., & Zhang, J. (2016b). Effects of lignin and surfactant on adsorption and hydrolysis of cellulases on cellulose. *Biotechnology for Biofuels, 9*(1), 20.

Liao, W., Liu, Y., Wen, Z., Frear, C., & Chen, S. (2008). Kinetic modeling of enzymatic hydrolysis of cellulose in differently pretreated fibers from dairy manure. *Biotechnology and Bioengineering, 101*(3), 441-451.

Liu, H., Sun, J., Leu, S. Y., & Chen, S. (2016). Toward a fundamental understanding of cellulase-lignin interactions in the whole slurry enzymatic saccharification process. *Biofuels, Bioproducts and Biorefining*.

Liu, Z., Slininger, P., Dien, B., Berhow, M., Kurtzman, C., & Gorsich, S. (2004). Adaptive response of yeasts to furfural and 5-hydroxymethylfurfural and new

chemical evidence for HMF conversion to 2, 5-bis-hydroxymethylfuran. *Journal of Industrial Microbiology and Biotechnology, 31*(8), 345-352.

Liu, Z. L. (2011). Molecular mechanisms of yeast tolerance and in situ detoxification of lignocellulose hydrolysates. *Applied Microbiology and Biotechnology, 90*(3), 809-825.

Liu, Z. L., Slininger, P. J., & Gorsich, S. W. (2005). *Enhanced biotransformation of furfural and hydroxymethylfurfural by newly developed ethanologenic yeast strains.* Paper presented at the Twenty-Sixth Symposium on Biotechnology for Fuels and Chemicals.

Lu, H., Zhao, X., Wang, Y., Ding, X., Wang, J., Garza, E., Manow, R., Iverson, A., & Zhou, S. (2016). Enhancement of D-lactic acid production from a mixed glucose and xylose substrate by the Escherichia coli strain JH15 devoid of the glucose effect. *BMC Biotechnology, 16*(1), 19.

Luedeking, R., & Piret, E. L. (1959). A kinetic study of the lactic acid fermentation. Batch process at controlled pH. *Journal of Biochemical and Microbiological Technology and Engineering, 1*(4), 393-412.

Ma, K., Hu, G., Pan, L., Wang, Z., Zhou, Y., Wang, Y., Ruan, Z., & He, M. (2016). Highly efficient production of optically pure l-lactic acid from corn stover hydrolysate by thermophilic Bacillus coagulans. *Bioresource Technology, 219*, 114-122.

Mercier, P., Yerushalmi, L., Rouleau, D., & Dochain, D. (1992). Kinetics of lactic acid fermentation on glucose and corn by Lactobacillus amylophilus. *Journal of Chemical Technology and Biotechnology, 55*(2), 111-121.

Mosier, N., Wyman, C., Dale, B., Elander, R., Lee, Y., Holtzapple, M., & Ladisch, M. (2005). Features of promising technologies for pretreatment of lignocellulosic biomass. *Bioresource Technology, 96*(6), 673-686.

Mueller, B., Zacharias, M., & Rezwan, K. (2010). Bovine serum albumin and lysozyme adsorption on calcium phosphate particles. *Advanced Engineering Materials, 12*(1-2), B53-B61.

Mutturi, S., & Lidén, G. (2014). Model-based estimation of optimal temperature profile during simultaneous saccharification and fermentation of Arundo donax. *Biotechnology and Bioengineering, 111*(5), 866-875.

Nakagame, S., Chandra, R. P., & Saddler, J. N. (2010). The effect of isolated lignins, obtained from a range of pretreated lignocellulosic substrates, on enzymatic hydrolysis. *Biotechnology and Bioengineering, 105*(5), 871-879.

Nandasana, A. D., & Kumar, S. (2008). Kinetic modeling of lactic acid production from molasses using Enterococcus faecalis RKY1. *Biochemical Engineering Journal,*

38(3), 277-284.

Nidetzky, B., & Steiner, W. (1993). A new approach for modeling cellulase–cellulose adsorption and the kinetics of the enzymatic hydrolysis of microcrystalline cellulose. *Biotechnology and Bioengineering, 42*(4), 469-479.

Olofsson, K., Bertilsson, M., & Lidén, G. (2008). A short review on SSF–an interesting process option for ethanol production from lignocellulosic feedstocks. *Biotechnology for Biofuels, 1*(1), 7.

Palmqvist, E., & Hahn-Hägerdal, B. (2000). Fermentation of lignocellulosic hydrolysates. II: inhibitors and mechanisms of inhibition. *Bioresource Technology, 74*(1), 25-33.

Parawira, W., & Tekere, M. (2011). Biotechnological strategies to overcome inhibitors in lignocellulose hydrolysates for ethanol production: review. *Critical Reviews in Biotechnology, 31*(1), 20-31.

Peres, A. P. G., Lunelli, B., & Fllho, R. (2013). Application of biomass to hydrogen and syngas production. *Chemical Engineering Transactions*.

Philippidis, G. P., & Hatzis, C. (1997). Biochemical Engineering Analysis of Critical Process Factors in the Biomass-to-Ethanol Technology. *Biotechnology Progress, 13*(3), 222-231.

Philippidis, G. P., Smith, T. K., & Wyman, C. E. (1993). Study of the enzymatic hydrolysis of cellulose for production of fuel ethanol by the simultaneous saccharification and fermentation process. *Biotechnology and Bioengineering, 41*(9), 846-853.

Robak, K., & Balcerek, M. (2018). Review of second generation bioethanol production from residual biomass. *Food technology and Biotechnology, 56*(2), 174-187.

Sadhu, S., & Maiti, T. K. (2013). Cellulase production by bacteria: a review. *Microbiology Research Journal International*, 235-258.

Sarker, M., & Rahman, L. (2010). *Estimation of forest biomass using remote sensing.* The Hong Kong Polytechnic University.

Sarks, C., Jin, M., Sato, T. K., Balan, V., & Dale, B. E. (2014). Studying the rapid bioconversion of lignocellulosic sugars into ethanol using high cell density fermentations with cell recycle. *Biotechnology for Biofuels, 7*(1), 73.

Sathitsuksanoh, N., George, A., & Zhang, Y. H. P. (2013). New lignocellulose pretreatments using cellulose solvents: a review. *Journal of Chemical Technology and Biotechnology, 88*(2), 169-180.

Selig, M. J., Viamajala, S., Decker, S. R., Tucker, M. P., Himmel, M. E., & Vinzant, T. B. (2007). Deposition of lignin droplets produced during dilute acid pretreatment of maize stems retards enzymatic hydrolysis of cellulose.

Biotechnology Progress, 23(6), 1333-1339.

Sengupta, S., Jana, M., Sengupta, D., & Naskar, A. (2000). A note on the estimation of microbial glycosidase activities by dinitrosalicylic acid reagent. *Applied Microbiology and Biotechnology, 53*(6), 732-735.

Shafiei, M., Kumar, R., & Karimi, K. (2015). Pretreatment of lignocellulosic biomass *Lignocellulose-based Bioproducts* (pp. 85-154): Springer.

Shahzadi, T., Mehmood, S., Irshad, M., Anwar, Z., Afroz, A., Zeeshan, N., Rashid, U., & Sughra, K. (2014). Advances in lignocellulosic biotechnology: A brief review on lignocellulosic biomass and cellulases. *Advances in Bioscience and Biotechnology, 2014*.

Shi, J., Wu, D., Zhang, L., Simmons, B. A., Singh, S., Yang, B., & Wyman, C. E. (2017). Dynamic changes of substrate reactivity and enzyme adsorption on partially hydrolyzed cellulose. *Biotechnology and Bioengineering, 114*(3), 503-515.

Shibata, K., Flores, D. M., Kobayashi, G., & Sonomoto, K. (2007). Direct l-lactic acid fermentation with sago starch by a novel amylolytic lactic acid bacterium, Enterococcus faecium. *Enzyme and Microbial Technology, 41*(1), 149-155. doi:https://doi.org/10.1016/j.enzmictec.2006.12.020

Sirisansaneeyakul, S., Luangpipat, T., Vanichsriratana, W., Srinophakun, T., Chen, H. H.-H., & Chisti, Y. (2007). Optimization of lactic acid production by immobilized Lactococcus lactis IO-1. *Journal of Industrial Microbiology and Biotechnology, 34*(5), 381.

Sjostrom, E. (1993). *Wood chemistry: fundamentals and applications*: Gulf professional publishing.

Sluiter, A., Hames, B., Ruiz, R., Scarlata, C., Sluiter, J., & Templeton, D. (2006). Determination of sugars, byproducts, and degradation products in liquid fraction process samples. *Golden: National Renewable Energy Laboratory*.

Sluiter, A., Hames, B., Ruiz, R., SCarlata, C., Sluiter, J., TempletOn, D., & Crocker, D. (2008). Determination of structural carbohydrates and lignin in biomass. *Laboratory analytical procedure, 1617*(1), 1-16.

Smith, P. e., Krohn, R. I., Hermanson, G. T., Mallia, A. K., Gartner, F. H., Provenzano, M., Fujimoto, E. K., Goeke, N. M., Olson, B. J., & Klenk, D. (1985). Measurement of protein using bicinchoninic acid. *Analytical Biochemistry, 150*(1), 76-85.

South, C., Hogsett, D., & Lynd, L. (1995). Modeling simultaneous saccharification and fermentation of lignocellulose to ethanol in batch and continuous reactors. *Enzyme and Microbial Technology, 17*(9), 797-803.

Sun, Y., & Cheng, J. (2002). Hydrolysis of lignocellulosic materials for ethanol

production: a review. *Bioresource Technology, 83*(1), 1-11.

Taherzadeh, M. J., & Karimi, K. (2007). Acid-based hydrolysis processes for ethanol from lignocellulosic materials: a review. *BioResources, 2*(3), 472-499.

Taleghani, H. G., Najafpour, G. D., & Ghoreyshi, A. (2014). Batch and continuous production of lactic acid using Lactobacillus bulgaricus (ATCC 8001). *Pakistan Journal of Biotechnology, 11*(1), 1-12.

Tan, J., Abdel-Rahman, M. A., & Sonomoto, K. (2017). Biorefinery-Based Lactic Acid Fermentation: Microbial Production of Pure Monomer Product *Synthesis, Structure and Properties of Poly (lactic acid)* (pp. 27-66): Springer.

Tango, M., & Ghaly, A. (2002). A continuous lactic acid production system using an immobilized packed bed of Lactobacillus helveticus. *Applied Microbiology and Biotechnology, 58*(6), 712-720.

Taniguchi, M., Tokunaga, T., Horiuchi, K., Hoshino, K., Sakai, K., & Tanaka, T. (2004). Production of l-lactic acid from a mixture of xylose and glucose by co-cultivation of lactic acid bacteria. *Applied Microbiology and Biotechnology, 66*(2), 160-165. doi:10.1007/s00253-004-1671-x

Tashiro, Y., Kaneko, W., Sun, Y., Shibata, K., Inokuma, K., Zendo, T., & Sonomoto, K. (2011). Continuous d-lactic acid production by a novelthermotolerant Lactobacillus delbrueckii subsp. lactis QU 41. *Applied Microbiology and Biotechnology, 89*(6), 1741-1750.

Tengborg, C., Galbe, M., & Zacchi, G. (2001). Influence of enzyme loading and physical parameters on the enzymatic hydrolysis of steam-pretreated softwood. *Biotechnology Progress, 17*(1), 110-117.

Toyosawa, Y., Ikeo, M., Taneda, D., & Okino, S. (2017). Quantitative analysis of adsorption and desorption behavior of individual cellulase components during the hydrolysis of lignocellulosic biomass with the addition of lysozyme. *Bioresource Technology, 234*, 150-157.

Wang, R., Koppram, R., Olsson, L., & Franzén, C. J. (2014a). Kinetic modeling of multi-feed simultaneous saccharification and co-fermentation of pretreated birch to ethanol. *Bioresource Technology, 172*, 303-311.

Wang, Y., Abdel-Rahman, M. A., Tashiro, Y., Xiao, Y., Zendo, T., Sakai, K., & Sonomoto, K. (2014b). L-(+)-Lactic acid production by co-fermentation of cellobiose and xylose without carbon catabolite repression using Enterococcus mundtii QU 25. *RSC Advances, 4*(42), 22013-22021.

Wang, Y., Tashiro, Y., & Sonomoto, K. (2015). Fermentative production of lactic acid from renewable materials: Recent achievements, prospects, and limits. *Journal of Bioscience and Bioengineering, 119*(1), 10-18.

Wang, Z., & Feng, H. (2010). Fractal kinetic analysis of the enzymatic saccharification of cellulose under different conditions. *Bioresource Technology, 101*(20), 7995-8000.

Wang, Z., Lv, Z., Du, J., Mo, C., Yang, X., & Tian, S. (2014c). Combined process for ethanol fermentation at high-solids loading and biogas digestion from unwashed steam-exploded corn stover. *Bioresource Technology, 166*, 282-287.

Wang, Z., Xu, J.-H., Feng, H., & Qi, H. (2011). Fractal kinetic analysis of polymers/nonionic surfactants to eliminate lignin inhibition in enzymatic saccharification of cellulose. *Bioresource Technology, 102*(3), 2890-2896.

Wee, Y.-J., & Ryu, H.-W. (2009). Lactic acid production by Lactobacillus sp. RKY2 in a cell-recycle continuous fermentation using lignocellulosic hydrolyzates as inexpensive raw materials. *Bioresource Technology, 100*(18), 4262-4270.

Wingren, A., Galbe, M., & Zacchi, G. (2003). Techno-economic evaluation of producing ethanol from softwood: Comparison of SSF and SHF and identification of bottlenecks. *Biotechnology Progress, 19*(4), 1109-1117.

Ximenes, E., Kim, Y., Mosier, N., Dien, B., & Ladisch, M. (2011). Deactivation of cellulases by phenols. *Enzyme and Microbial Technology, 48*(1), 54-60.

Xu, F., & Ding, H. (2007). A new kinetic model for heterogeneous (or spatially confined) enzymatic catalysis: contributions from the fractal and jamming (overcrowding) effects. *Applied Catalysis A: General, 317*(1), 70-81.

Yang, B., Dai, Z., Ding, S.-Y., & Wyman, C. E. (2011). Enzymatic hydrolysis of cellulosic biomass. *Biofuels, 2*(4), 421-449.

Yang, B., & Wyman, C. E. (2006). BSA treatment to enhance enzymatic hydrolysis of cellulose in lignin containing substrates. *Biotechnology and Bioengineering, 94*(4), 611-617.

Yang, Q., & Pan, X. (2016). Correlation between lignin physicochemical properties and inhibition to enzymatic hydrolysis of cellulose. *Biotechnology and Bioengineering, 113*(6), 1213-1224.

Ye, Z., & Berson, R. E. (2011). Kinetic modeling of cellulose hydrolysis with first order inactivation of adsorbed cellulase. *Bioresource Technology, 102*(24), 11194-11199.

Yu, Z., Gwak, K. S., Treasure, T., Jameel, H., Chang, H. m., & Park, S. (2014). Effect of lignin chemistry on the enzymatic hydrolysis of woody biomass. *ChemSusChem, 7*(7), 1942-1950.

Zhan, X., Cai, C., Pang, Y., Qin, F., Lou, H., Huang, J., & Qiu, X. (2019). Effect of the isoelectric point of pH-responsive lignin-based amphoteric surfactant on the enzymatic hydrolysis of lignocellulose. *Bioresource Technology, 283*, 112-119.

Zhang, J., Shao, X., & Lynd, L. R. (2009). Simultaneous saccharification and co-fermentation of paper sludge to ethanol by Saccharomyces cerevisiae RWB222. Part II: Investigation of discrepancies between predicted and observed performance at high solids concentration. *Biotechnology and Bioengineering, 104*(5), 932-938.

Zhao, B., Wang, L., Li, F., Hua, D., Ma, C., Ma, Y., & Xu, P. (2010). Kinetics of D-lactic acid production by Sporolactobacillus sp. strain CASD using repeated batch fermentation. *Bioresource Technology, 101*(16), 6499-6505.

Zhao, Y., Man, Y., Wen, J., Guo, Y., & Lin, J. (2019). Advances in imaging plant cell walls. *Trends in Plant Science, 24*(9), 867-878.

Zheng, Y., Zhang, S., Miao, S., Su, Z., & Wang, P. (2013). Temperature sensitivity of cellulase adsorption on lignin and its impact on enzymatic hydrolysis of lignocellulosic biomass. *Journal of Biotechnology, 166*(3), 135-143.